UNIVERSIDAD DE CONCEPCIÓN
FACULTAD DE CIENCIAS FÍSICAS Y MATEMÁTICAS

Evolutionary Constraints on Physical Parameters and Magnetic Activity in Double Periodic Variables (DPVs)

Understanding the dynamo mechanism in binary systems through the perspective of V1001 Cen and HD 170582

Por: Paúl Calderón

Profesor Guía:

Dr. Ronald Mennickent.

Profesor Co-Guía:

Dr. Dominik Schleicher.

Comisión Evaluadora:

Dr. Ronald Mennickent, Dr. Dominik Schleicher,
Dr. Jaime Rosales, Dr. Douglas Geisler, Dr. Rodrigo Reeves

Tesis presentada a la Dirección de Postgrado de la Universidad de Concepción para optar al grado académico de Doctor en Ciencias con Mención en Física.

Abril 2026

Concepción, Chile.

Se declara que en la presente tesis se utilizó inteligencia artificial generativa únicamente para apoyar la redacción y traducción del texto. Los cálculos, gráficos, tablas, análisis y resultados constituyen trabajo original de los autores.

Dedicated to all those who look at the night sky and realize that it's not enough to see, but that they need to know!

ACKNOWLEDGEMENTS

I give thanks to all those who, moved by their faith, become instruments of good deeds; for me, it is there where the true manifestation of God resides.

I thank my mother for giving me life and for guiding me onto the right path. Without her constant love and support, I would not have reached this goal. Thank you, mother, for your infinite patience during my long years of study.

To my beautiful wife, thank you for making me so happy and for being the pillar that sustains me during the difficult times. Your unwavering faith in my abilities, even when all seemed lost, is the engine that drives me to strive for a better life for both of us.

I am deeply grateful to Dr. Ronald Mennickent Cid for proposing this challenge and for his fundamental guidance; without his patience, this work would not have seen the light of day. My gratitude extends to all my undergraduate and graduate professors. In particular, I would like to thank Professor Jeanette Stock, my “astronomical mother,” and Dr. Claudio Mendoza, whom we will always remember with gratitude.

To my colleagues in the Astronomy and Physics departments at UdeC: thanks to Dr. Jaime Rosales for his support with the calculations and scientific guidance, and to Mgtr. José Ilić García for his invaluable help with LaTeX formatting. You made this difficult journey much kinder and more pleasant.

To my family, who with their unique and "Macondiana" personality, provided the necessary support to keep me going. I also thank the Department of Physical and Mathematical Sciences at UdeC for the academic training I received.

Finally, I thank the stars that shine every night; they awakened my curiosity and are the reason for my passion for science.

Contents

List of Tables

List of Figures

Resumen

Las Variables Periódicas Dobles (DPV) constituyen una clase de sistemas binarios interactuantes, cuya variabilidad de ciclo largo sigue siendo uno de los fenómenos más intrigantes de la astrofísica estelar. Esta tesis doctoral presenta una investigación sobre la naturaleza de las DVP mediante un enfoque dual: la determinación precisa de parámetros fundamentales mediante análisis fotométrico y espectroscópico, y la reconstrucción de su historia evolutiva mediante modelado numérico avanzado.

Para delimitar las propiedades físicas de estos sistemas, realizamos un estudio detallado de múltiples longitudes de onda de V1001 Cen. Mediante el empleo de los modelos de síntesis de curvas de luz de Djurašević y datos espectroscópicos del espectrómetro CHIRON, derivamos las dimensiones de los componentes estelares y las propiedades del disco de acreción circumbinario. El desenredo espectroscópico mediante la técnica Gonzalez Levato permitió una estimación precisa de las temperaturas efectivas ($T_d = 8,750 \pm 250\,K$; $T_g = 20,000 \pm 2,000\,K$) y las semiamplitudes de la velocidad radial. Nuestros resultados identifican a V1001 Cen como un sistema en su segunda fase de transferencia de masa (edad ~ 190 Myr) con una razón de masas de $q \approx 0.15$, donde la estrella ganadora se rejuvenece significativamente por la acreción de material.

Para complementar este marco observacional, utilizamos el código MESA (Módulos para Experimentos en Astrofísica Estelar) para explorar las vías evolutivas y la viabilidad física de los mecanismos de dinamo magnéticos. Centrándonos en el sistema HD 170582, implementamos el formalismo de Tayler-Spruit para modelar el transporte de momento angular interno y la generación del campo magnético. Mediante una minimización multiparamétrica de χ^2, se reprodujo con éxito el estado actual del sistema, sugiriendo masas iniciales de $M_{d,i} = 6.0\,M_\odot$ y $M_{g,i} = 5.0\,M_\odot$ en un régimen casi conservativo ($\dot{M} \approx 9.6 \times 10^{-7}\,M_\odot yr^{-1}$).

Una contribución clave de esta investigación es el análisis de la influencia del parámetro de longitud de mezcla (α_{MLT}) en la activación de la dinamo estelar dentro de la envoltura del donante. Mediante la construcción de diagramas de diagnóstico y la variación de α_{MLT} de 0.5 a 4.0, demostramos una fuerte correlación entre la eficiencia convectiva y el índice de ley de potencia de la dinamo (α). Nuestros hallazgos revelan

que, para mantener el índice de la dinamo dentro del rango teóricamente consistente ($0.33 \leq \alpha \leq 0.83$) y reproducir con éxito los ciclos largos observados, la longitud de mezcla debe limitarse a $\alpha_{\rm MLT} \lesssim 2.0$. Los valores que superan este umbral resultan en velocidades convectivas no físicas que inhiben el mecanismo de la dinamo de Schleicher y Mennickent. Este trabajo proporciona un marco para comprender la interacción entre la transferencia de masa, la convección estelar y el magnetismo en la evolución de sistemas binarios de interacción de masa intermedia.

Palabras Clave – Estrellas Binarias, Variables Periódicas Dobles, Mecanismo de Dínamo Magnético

Abstract

Double Periodic Variables (DPVs) constitute a class of interacting binaries whose long-cycle variability remains one of the most intriguing phenomena in stellar astrophysics. This doctoral thesis presents a investigation into the nature of DPVs through a dual approach: the precise determination of fundamental parameters via photometric and spectroscopic analysis, and the reconstruction of their evolutionary history using advanced numerical modeling.

To constrain the physical properties of these systems, we conducted a detailed multi-wavelength study of V1001 Cen. By employing Djurašević's light curve synthesis models and spectroscopic data from the CHIRON spectrometer, we derived the dimensions of the stellar components and the properties of the circumbinary accretion disk. Spectroscopic disentangling via the Gonzalez & Levato technique allowed for an accurate estimation of effective temperatures ($T_d = 8,750 \pm 250\,K$; $T_g = 20,000 \pm 2,000\,K$) and semi-amplitudes of radial velocity. Our results identify V1001 Cen as a system in its second phase of mass transfer (age $\sim$ 190 Myr) with a mass ratio of $q \approx 0.15$, where the gainer star is significantly rejuvenated by the accretion of material.

Complementing this observational framework, we utilized the `MESA` (Modules for Experiments in Stellar Astrophysics) code to explore the evolutionary pathways and the physical viability of magnetic dynamo mechanisms. Focusing on the system HD 170582, we implemented the Tayler-Spruit formalism to model internal angular momentum transport and magnetic field generation. Through a multiparametric χ^2 minimization, the system's current state was successfully reproduced, suggesting initial masses of $M_{d,i} = 6.0\,M_\odot$ and $M_{g,i} = 5.0\,M_\odot$ in a nearly conservative regime ($\dot{M} \approx 9.6 \times 10^{-7}\,M_\odot yr^{-1}$).

A key contribution of this research is the analysis of the influence of the mixing length parameter (α_{MLT}) on the activation of the stellar dynamo within the donor's envelope. By constructing diagnostic diagrams and varying α_{MLT} from 0.5 to 4.0, we demonstrate a strong correlation between convective efficiency and the dynamo power-law index (α). Our findings reveal that to maintain the dynamo index within

the theoretically consistent range ($0.33 \leq \alpha \leq 0.83$) and successfully reproduce the observed long cycles, the mixing length must be constrained to $\alpha_{\rm MLT} \lesssim 2.0$. Values exceeding this threshold result in unphysical convective velocities that inhibit the Schleicher & Mennickent dynamo mechanism. This work provides a framework for understanding the interplay between mass transfer, stellar convection, and magnetism in the evolution of intermediate-mass interacting binaries.

Keywords – Binary stars, Double Periodic Variables, Magnetic Dynamo Mechanism

Chapter 1

Introduction

1.1 Motivation

Most stars do not evolve in isolation, but rather as members of multiple systems. In particular, close binaries constitute privileged astrophysical laboratories, since their evolution is governed by nonlinear processes that do not appear (or are negligible) in single stars: tidal interaction, rotational synchronization, angular momentum loss, mass transfer, and the formation of circumstellar structures. When the more evolved component of the two expands until it fills its Roche lobe, the volume within which orbiting material is gravitationally bound to the star (more about this in chapter 2), Roche lobe overflow (RLOF) begins, triggering an interaction phase capable of completely transforming both the internal structure of the stars and the orbital dynamics. It is precisely in this regime that characteristic observational phenomena emerge (complex light curves, perturbed spectral lines, continuum excesses), which allow physical hypotheses related to internal transport, magnetism, and dissipation in accretion flows to be tested against real data.

Within interacting intermediate mass binaries, Double Periodic Variables (DPVs) are distinguished by exhibiting two simultaneous photometric timescales: an orbital period associated with the eclipsing geometry, and a quasi periodic long cycle, typically of the order of ~ 33 times the orbital period. In Galactic DPVs, the long cycle manifests as an additional modulation superimposed on the orbital light curve and

is interpreted, under the dominant hypothesis, as an indirect consequence of cyclic variations in the mass transfer rate. These variations reconfigure the structure of the accretion disk and, consequently, the observed radiative output. The role of the disk is central: in DPVs, the accretor is usually surrounded by an optically thick disk that can contribute a non negligible fraction of the total flux, and whose geometry (thickness, outer rim, hot regions) changes with the interaction state.

The underlying physical question is which mechanism can impose an additional clock (the long cycle) on a system whose orbital period remains stable. A particularly appealing scenario is one in which the tidally synchronized donor develops a magnetic activity cycle within its convective envelope; this cycle modifies the quadrupole moment and/or the effective radius of the donor, thereby modulating Roche lobe overflow and, consequently, the mass transfer rate. Within this framework, the observed long cycle can be quantitatively linked to hydrodynamic properties of the donor (radius and maximum convective velocity) through relations of the Schleicher & Mennickent type, in which the exponent α (power law index) must remain within a physically consistent range ($1/3 \lesssim \alpha \lesssim 5/6$) (Schleicher and Mennickent, 2017). This allows one to move from a qualitative idea (*"magnetism modulates mass transfer"*) to a quantitative test: if an evolutionary model reproduces the current masses, radii, and periods, it must also yield a convective regime compatible with a physically admissible α and with the observed P_l.

The motivation of this thesis, therefore, is to construct a unified framework (observational, evolutionary, and diagnostic) that connects: (a) the photometric/spectroscopic characterization and the role of the accretion disk (which defines what is actually observed), (b) the evolutionary reconstruction including mass transfer (which fixes the physical state of the stars), and (c) the physical consistency of the dynamo mechanism (which is associated with the second period). To maximize the discriminating power of the analysis, two Galactic DPVs with contrasting properties are studied jointly: V1001 Cen and HD 170582. On the one hand, V1001 Cen allows the validation of the simultaneous reproduction of fundamental parameters, disk properties, and the long cycle in a system that is currently in a second mass transfer phase and has an age of $\sim$ 190 Myr. While

on the other hand, HD 170582 represents a more massive and younger system undergoing rapid mass transfer at ~ 81.8 Myr, where it is also possible to quantify how $\alpha_{\rm MLT}$ regulates the activation of the dynamo and to delimit the convective regime compatible with the long cycle. This comparison makes it possible to address an interesting question: does the dynamo mechanism proposed for DPVs operate robustly across different evolutionary regimes and, at the same time, can it be used to constrain internal convection parameters?

1.2 Objectives

General Objective: To construct an analysis combining observational techniques and evolutionary models of DPVs that links the photometric/spectroscopic characterization and the role of the accretion disk with evolutionary reconstruction using `MESA`, in order to quantitatively assess the viability of the proposed dynamo mechanism as an explanation for the long cycle and, based on this, to impose constraints on internal physical parameters (in particular, the convective efficiency parametrized by $\alpha_{\rm MLT}$).

To accomplish this objective, the following specific objectives are necessary:

- To perform a consistent photometric and spectroscopic characterization of V1001 Cen, determining the fundamental parameters of the system (e.g., mass ratio, temperatures, radii) and establishing a geometric solution that includes an optically thick accretion disk, in order to describe the current state of the system.
- To reconstruct the evolutionary history of V1001 Cen and HD 170582 from ZAMS using binary models with `MESA`, adjusting the initial parameters (masses and initial orbital period) to reproduce the current state under quasi conservative mass transfer scenarios; in particular, to identify the evolutionary phase of each system.
- To evaluate the consistency of the Schleicher & Mennickent dynamo mechanism as an explanation for the long cycle in both systems, using internal donor

quantities extracted from `MESA` (radius and maximum convective velocity) within the $P_{\rm cycle}$–$P_{\rm rot}$ relation and verifying that the index α remains within the physically admissible range.

- To quantify, in HD 170582, the impact of convective efficiency on the viability of the dynamo through a parametric exploration of $\alpha_{\rm MLT}$ and a diagnostic framework R_2–v_c–α, with the goal of delimiting the range of $\alpha_{\rm MLT}$ compatible with a physically consistent dynamo index.
- To explore whether dynamo activation and the reproduction of the long cycle are robust across different evolutionary windows, and to discuss whether a characteristic scenario emerges for DPVs at different stages of interaction.

1.3 Hypothesis

Central hypothesis (falsifiable): *The long photometric cycle observed in Double Periodic Variables is produced by a cyclic magnetic dynamo operating in the donor star, which induces a periodic modulation of the mass transfer rate.*

This hypothesis is evaluated under the premise that the proposed mechanism must be physically self consistent, reproducible across different evolutionary stages, and compatible with both the observed long periods and the internal stellar structure of the donor.

Necessary physical conditions

For the hypothesis to be viable, the following conditions must be simultaneously satisfied:

1. The donor star must possess a sufficiently extended convective envelope capable of sustaining a magnetic dynamo during the interacting phase of binary evolution.
2. Binary evolutionary models starting from the zero age main sequence must reproduce the current observed configuration of the system (masses, radii, temperatures, orbital period) under a physically plausible mass transfer scenario.

3. The internal convective properties predicted by the evolutionary models (in particular the convective velocity v_c and donor radius R_2) must yield dynamo parameters consistent with a cyclic magnetic regime.

4. The resulting dynamo power law index α must remain within the theoretically admissible interval ($1/3 \leq \alpha \leq 5/6$), which imposes an upper limit on the convective efficiency of the donor star, constraining the mixing length parameter to solar like values.

Violation of any of these conditions renders the hypothesis physically inconsistent and therefore falsified.

Observational and evolutionary predictions

If the hypothesis is correct, the following predictions must hold:

1. The observed long photometric period P_l can be quantitatively reproduced using donor stellar parameters (R_2, v_c) derived from evolutionary models, without requiring unphysical dynamo indices.

2. Systems at different evolutionary stages (e.g., V1001 Cen and HD 170582) should display long cycle behaviour consistent with a common dynamo driven mechanism, despite differences in mass transfer rate and evolutionary phase.

3. The inferred convective efficiency of the donor star must be compatible with independent stellar constraints; values of α_{MLT} that imply unrealistically high convective velocities should be excluded by the requirement of dynamo self consistency.

4. The presence and stability of an accretion disk, when observed, should be consistent with magnetically modulated mass transfer rather than requiring ad hoc variability mechanisms.

1.3.1 Application of the hypothesis

The hypothesis is tested through a structured and potentially falsifiable procedure:

1. **Observational anchoring:** a consistent photometric and spectroscopic solution, including accretion disk modelling when required, must yield reliable fundamental parameters for the system.
2. **Evolutionary reconstruction:** evolutionary tracks computed with `MESA` must reproduce the observed state from plausible initial conditions.
3. **Dynamo consistency test:** the observed long cycle must be reproducible using the donor's internal properties extracted from the evolutionary models, without driving the dynamo index outside its physical range.
4. **Robustness to internal uncertainties:** the mechanism must remain viable under reasonable variations of the mixing length parameter; if only extreme or unphysical values of $\alpha_{\rm MLT}$ allow reproduction of the long cycle, the hypothesis is weakened or falsified.

Within the structure of this thesis, the hypothesis is examined through: (i) observational characterization and disk modelling (V1001 Cen), (ii) evolutionary reconstruction using `MESA` (both systems), and (iii) dynamo diagnostics and convective parameter exploration (particularly for HD 170582).

Chapter 2

Theoretical Framework

2.1 Binary Systems

Most stars in the Universe exist as binaries or multiple systems, making the study of binary star evolution crucial for understanding stellar populations. Binary star systems provide information about stellar masses and radii, parameters used to constrain theoretical models of stellar evolution. The conceptual framework for describing orbital motion is based on Kepler's and Newton's laws, initially assuming that the stars are point masses. This approximation is valid as long as the stars are not too close together, allowing for the derivation of relationships between stellar masses, orbital velocities, and the geometry of their orbits in their mutual gravitational field. (Hilditch, 2001).

The motion of the components in these systems is defined through two key descriptions: the relative orbit and the barycentric (or absolute) orbits. On one hand, the relative orbit describes the path of one component with respect to the other and is an ellipse in which the more massive component occupies one of the foci. The concept of reduced mass is fundamental to the analysis of relative motion. $\mu = M_1 M_2/(M_1 + M_2)$ (Hilditch, 2001). On the other hand, barycentric orbits describe the motion of each star relative to the common center of mass (barycenter). These orbits are ellipses that share the same eccentricity (e) and period (P) as the relative orbit. The distance between the components, the semi major axis of the relative orbit (a), is the sum of

the barycentric semi major axes. ($a = a_1 + a_2$) (Hilditch, 2001; Tauris and van den Heuvel, 2023).

The geometry and orientation of the orbit in three dimensional space are defined by six orbital elements:

1. **The semi major axis**(a): Defines the size of the orbit.
2. **The eccentricity** (e): Defines the shape of the ellipse. The distances of closest approach and furthest approach are periastron ($r_p = a(1 - e)$) and apastron ($r_a = a(1 + e)$).
3. **The inclination** (i): Is the angle of the orbital plane with respect to the plane of the sky tangent to the system. A value of $i = 90°$ implies that the observer's line of sight coincides with the orbital plane, an essential characteristic of eclipsing binaries.
4. **The length of periastron** ($\bar{\omega}$): Indicates the orientation of the major axis within the orbital plane.
5. **The angle of the ascending node** (ω): Indicates the orientation of the line of nodes (intersection of the orbital plane with the plane of the sky).
6. **The time of passage through periastron** (T): Establishes the temporary position of the star in the orbit (Hilditch, 2001; Tauris and van den Heuvel, 2023).

In addition to these geometric elements, orbital dynamics are governed by conservation laws. Kepler's Third Law (modified by Newton) relates the orbital period, the semi major axis, and the sum of the masses ($M_1 + M_2$) by the expression $G(M_1 + M_2) = 4\pi^2 a^3/P^2$. Kepler's Second Law states that the radius vector sweeps out equal areas in equal times, which is equivalent to the conservation of specific angular momentum. This implies that the orbital velocity (V) varies continuously in eccentric orbits, reaching its maximum at periastron (Hilditch, 2001; Tauris and van den Heuvel, 2023).

Finally, the total angular momentum (J) and total energy (C) of the system are fundamental conserved quantities for an isolated two body binary system and

intrinsically determine the shape and size of the relative orbit. These concepts are crucial, as variations in C and J are used to investigate the evolution of binary systems, particularly during mass exchange and loss processes (Hilditch, 2001; Eggleton, 2006).

2.1.1 Roche Potential

Describing the dynamics and evolution of close binary systems those whose orbital separation is comparable to stellar radii requires the theoretical framework of the Roche potential Φ_R. This model is based on the treatment of two point masses orbiting in circles around their common center of mass, analyzing equipotential surfaces in a co-rotating reference frame (Hilditch, 2001; Eggleton, 2006).

The total potential experienced by a test particle in this co-rotating system is the sum of the gravitational potentials of the two stellar masses and the centrifugal potential. The geometry of these equipotential surfaces depends crucially on the mass ratio $q = M_2/M_1$, where M_1 and M_2 are the masses of the primary and secondary stars, respectively (Hilditch, 2001; Eggleton, 2006; Tauris and van den Heuvel, 2023).

The fundamental application of the Roche potential in binary astrophysics lies in the fact that the surface of a star in hydrostatic equilibrium in a co-rotating, circular system corresponds to an equipotential Roche surface. The most relevant configuration is defined by the critical surface that passes through the interior Lagrange point, L_1, a saddle point where the spatial gradient of the potential is zero.

This critical surface encloses the two Roche lobes (RL), which represent the maximum volume a stellar component can occupy before its surface matter, upon crossing L_1, falls under the gravitational influence of the companion star (Hilditch, 2001; Eggleton, 2006).

To quantify the confinement volume, the effective Roche lobe radius (r_L) is used, defined as the radius of a sphere with a volume equivalent to the RL. This radius is expressed in terms of the orbital separation a and the mass ratio q. A widely used analytical approximation for the RL radius is the formula of Eggleton (1983):

$$r_L = \frac{R_L}{a} \approx \frac{0.49q^{2/3}}{0.6q^{2/3} + \ln(1 + q^{1/3})} \tag{2.1.1}$$

This formulation is used to determine whether a binary system is classified as detached, semi detached, or contact, depending on whether one or both stars fill their respective Roche lobes. Thus, the evolutionary dynamics of close binary systems are dominated by Roche Lobe Overflow (RLOF), the process by which matter flows from the donor star filling its lag lobe to the gainer through the L_1 point (Hilditch, 2001; Tauris and van den Heuvel, 2023).

The classification of RLOF cases (Case A, B, or C) depends on the evolutionary stage of the donor star when the overflow occurs, with Cases A, B, and C being those initiated during the main sequence, the giant transition, or the supergiant/AGB phase, respectively. These processes are relevant for explaining phenomena such as Algol's Paradox, where the least massive star is the most evolved, resulting from a reversal of the mass ratio due to RLOF (Hilditch, 2001; Tauris and van den Heuvel, 2023).

The mass transfer process can be conservative (total mass and angular momentum are conserved) or non conservative (the system loses mass and angular momentum). The stability of the mass transfer on dynamic, thermal, or nuclear timescales is determined by comparing how the donor star's radius reacts to mass loss (ζ^*) with the response of the RL radius to mass changes (ζ_L). If $\zeta^* < \zeta_L$, the transfer is generally stable. The modification of the orbital angular momentum during the RLOF not only affects the stability of the process, but also dictates the expansion or contraction of the orbit, a determining factor in the subsequent evolution of the binary (Eggleton, 2006; Tauris and van den Heuvel, 2023).

2.1.2 Eclipsing Binary

Eclipsing binary stars are systems in which the orbital plane is oriented such that, from the observer's line of sight, the components periodically occult each other. This phenomenon produces variations in the system's luminous intensity, known as light curves, which allow for the determination of fundamental parameters such as stellar radii, relative temperatures, and orbital inclination (Hilditch, 2001). Geometrically, these systems are classified into three main categories based on the filling of their Roche lobes: detached binaries, where both stars lie well within their respective lobes;

semidetached binaries, where one component has filled its Roche lobe and initiates mass transfer toward its companion; and contact binaries, in which both components fill or overfill their lobes and share a common envelope (Hilditch, 2001).

Within this classification, DPVs are predominantly identified as Algol type eclipsing binary systems in a semidetached stage (Mennickent, 2017). In these systems, the donor star (less massive and more evolved) transfers material through the L_1 Lagrange point toward the gainer star (typically a B-type spectral star), which is usually surrounded by an optically thick accretion disk (Rosales Guzmán et al., 2018). Most studied DPVs exhibit light curves characteristic of eclipsing binaries or ellipsoidal variations, with the short period modulation being attributed exclusively to the orbital motion of the interacting system (Poleski et al., 2010).

The taxonomic classification of eclipsing binary systems is primarily based on the morphology of their light curves, distinguishing three essential phenomenological categories:

- **Algol type (EA)**, characterized by well defined eclipse events and negligible brightness variations outside eclipses, indicating spherical or only moderately distorted stellar components.
- β **Lyrae type (EB)**, which exhibit continuous flux variations attributable to strong ellipsoidal distortions of the stellar components, with significant differences between the depths of the primary and secondary minima.
- **W Ursae Majoris type (EW)**, which display continuous variability with minima of comparable depth, typical of contact configurations.

Nevertheless, from an astrophysical and evolutionary perspective, it is imperative to complement this photometric classification with the Kopal scheme, which categorizes systems according to the physical configuration of the stars with respect to their critical equipotential surfaces (Roche lobes), dividing them into detached systems, semi detached systems (where one component fills its Roche lobe, initiating mass transfer processes), and contact systems (Hilditch, 2001).

2.1.3 Double Periodic Variables (DPVs)

Double Periodic Variables constitute a crucial class of intermediate mass interacting binary systems, generally classified as hot Algols[1], which exhibit a dual photometric phenomenology. These systems are defined by two temporal variabilities:

1. **An Orbital Period** (P_o): This is defined as the time interval required for the stellar components of a binary system to complete one revolution around their common center of mass, or barycenter.

2. **A Long Cycle** (P_l): This constitutes an intrinsic low frequency photometric modulation, typically quasi sinusoidal, whose duration scales empirically with the orbital period following the approximate relation $P_l \approx 33 \times P_o$. Although the nature of the long cycle remains a subject of debate, the main hypothesis suggests that it is due to a cyclic modulation in the mass transfer rate, possibly driven by the magnetic dynamo mechanism in the evolved donor star (Schleicher and Mennickent, 2017).

Double periodic variables are distinguished by their interacting binary behavior, manifesting a photometric variability that occurs on two time scales, a short orbital period associated with eclipses between stars and a long photometric cycle, approximately 33 times the orbital period, the origin is a topic under investigation (García et al., 2021). This relation was originally established empirically through observational measurements following the discovery of the first DPVs in the Large Magellanic Cloud, where a linear correlation between the orbital period and the long cycle was identified (Mennickent et al., 2003a). Subsequent studies based on larger samples, particularly those drawn from the OGLE catalogs, refined this value to an average ratio of approximately 33 ((Mennickent et al., 2003b) established as $P_l = 35.17(75)P_o$), albeit with a significant intrinsic dispersion, with the $P_{\rm long}/P_{\rm orb}$ ratio typically ranging between 27 and 39 (Poleski et al., 2010; Celedón et al., 2025)

(Mennickent and Kolaczkowski, 2010) and (Mennickent, 2022) describe DPVs as intermediate mass binaries with optically thick disks around the accretor star. The primary more massive component is referred to as the gainer, and the less massive

[1]Algol type stars are interacting binary systems in a semi detached mass transfer stage.

one as the donor. The interest of DPVs lies in their potential as natural laboratories for the study of the evolution of binary systems and the interaction between stellar components.

While the orbital period remains remarkably stable, the long cycle variability is not strictly periodic and exhibits significant fluctuations in duration and amplitude over decadal timescales, as evidenced by systematic period decreases in systems such as OGLE-LMC-DPV 065 and OGLE-BLG-ECL-157529 (Mennickent et al., 2019, 2020). Photometrically, this cycle manifests as a quasi sinusoidal (or occasionally double humped) modulation that is more prominent in redder bands, typically reaching amplitudes of $\Delta I \sim 0.2$ mag (Michalska et al., 2010).

Physically, the long cycle variability is driven by structural modifications of the accretion disk in response to variations in the mass transfer rate ($\dot{\mathrm{M}}$) (Garcés et al., 2018). Light curve synthesis indicates that during the long cycle maximum, the disk tends to be geometrically thinner and hotter, whereas at the minimum, an increased $\dot{\mathrm{M}}$ leads to vertical inflation and partial obscuration of the accreting star (Mennickent and Djurašević, 2021; Mennickent et al., 2025). These transitions are accompanied by changes in the position and temperature of impact regions at the disk edge, suggesting that the long period is an observational manifestation of magnetically modulated mass transfer cycles that periodically reshape the circumbinary environment (Mennickent et al., 2025).

To explain the physical origin of this variability, Schleicher and Mennickent (2017) proposed a magnetic dynamo model operating within the donor star, a mechanism distinct from the Tayler Spruit dynamo typically integrated into `MESA` models. In these systems, tidal locking ensures synchronous rotation of the donor, which, coupled with the presence of an extended convective zone, facilitates the generation of an efficient magnetic dynamo. This activity cycle induces periodic variations in the star's quadrupole moment that, via the Applegate mechanism, lead to cyclic fluctuations in its equatorial radius (Applegate, 1992; Mennickent et al., 2018). Since the donor is in a Roche lobe overflow regime, these radial variations directly modulate the mass transfer rate toward the accreting star, providing a coherent physical basis for the observed photometric long cycle and its characteristic period ratio (Schleicher and

Mennickent, 2017; Rosales et al., 2024).

In this context, an open and still largely unexplored question concerns the extent to which the efficiency of convection, parametrized through the mixing length parameter $\alpha_{\rm MLT}$, affects the physical viability of the magnetic dynamo mechanism proposed for DPVs. Since the generation and modulation of magnetic activity in the donor star critically depend on the properties of its convective envelope, variations in $\alpha_{\rm MLT}$ may lead to substantially different internal velocity fields and, consequently, to distinct dynamo regimes.

2.1.3.1 Magnetic Dynamo

Observational studies of systems such as DQ Vel and OGLE-LMC-DPV-065 have reported cyclic structural changes in the accretion disk (radius, temperature, and thickness) and in the intensity of spectral lines, which are consistent with a variable mass transfer rate modulated by the Applegate mechanism (Mennickent and Djurašević, 2025). In this way, the dynamo hypothesis not only offers a causal explanation for the secondary photometric periodicity, predicting the relationship between the long cycle and the orbital period, but also coherently integrates stellar evolution with the accretion disk hydrodynamics in these interacting binaries.

Recent research based on stellar evolution models has reinforced the feasibility of this scenario through detailed numerical simulations. The use of the MESA code to model specific systems, such as V495 Cen and V4142 Sgr, has allowed for the implementation of the dynamo formalism from Spruit (2002), demonstrating that differential rotation and internal stratification in the donor star can generate significant toroidal and poloidal magnetic fields (Rosales et al., 2019a, 2024).

2.1.3.2 Operating mechanism in the DPVs

In the field of astrophysics of binary star systems, specifically in DPVs, Equation 7 from the (Schleicher and Mennickent, 2017) study emerges as a fundamental pillar for understanding the relationship between the dynamo cycle and the rotation period in these systems. This equation is instrumental in unraveling the complex magnetic interactions inherent to DPVs.

The starting point is the empirical and theoretical relationship that links the dynamo cycle period to the stellar rotation period through the dynamo number (D), following the form proposed by Soon et al. (1993) and Baliunas et al. (1996):

$$P_{cycle} = D^{\alpha} P_{rot} \tag{2.1.2}$$

where α is a power law index whose typical values range between 1/3 and 5/6. In the context of DPVs, synchronous rotation is assumed due to tidal coupling, so that $P_{rot} = P_{orb}$ (Schleicher and Mennickent, 2017).

The dynamo number is expressed as a function of the Rossby number (Ro) as $D = Ro^{-2}$. The Rossby number is defined using the expression of Soker (2000):

$$Ro = 9 \left(\frac{v_c}{10\,\mathrm{km\,s^{-1}}} \right) \left(\frac{H_p}{40 R_2} \right)^{-1} \left(\frac{\omega}{0.1 \omega_{Kep}} \right)^{-1} \left(\frac{P_{Kep}}{\mathrm{yr}} \right) \tag{2.1.3}$$

where v_c is the convective velocity, H_p is the pressure scale height, ω is the angular velocity of the donor star, ω_{Kep} is the Keplerian angular velocity at the surface of the donor, and P_{Kep} is the orbital period of a test particle at the donor's surface. For a donor star filling its Roche lobe, one may approximate $\omega = 0.31\,\omega_{Kep}$ (Schleicher and Mennickent, 2017).

The convective velocity is derived from the mixing length theory (MLT). Assuming convective energy transport conditions, one has:

$$v_c = v_s \sqrt{\nabla - \nabla_{ad}} \tag{2.1.4}$$

where v_s is the sound speed in the stellar interior. Using scaling relations for the convective flux, the density ρ, and the surface gravity g as functions of the donor mass (M_2), radius (R_2), and luminosity (L_2), (Schleicher and Mennickent, 2017) obtained:

$$\nabla - \nabla_{ad} = \left(\frac{2\sqrt{2}}{15} \right)^{2/3} L_2^{2/3} R_2^{5/3} (G M_2)^{-5/3} \left(\frac{l_m}{H_p} \right)^{-4/3} \tag{2.1.5}$$

Combining this expression with the sound speed $v_s = \sqrt{GM_2/R_2}$, one obtains an expression for v_c in terms of the fundamental stellar parameters.

By substituting the expression for v_c and the orbital relations into the definition of the Rossby number, and subsequently into the activity cycle equation, one obtains the final expression that relates the long cycle (identified as the dynamo cycle) to the orbital period and the physical parameters of the donor star (Schleicher and Mennickent, 2017; Mennickent et al., 2018):

$$P_{cycle} = P_{rot}\left[11.5\left(\frac{2\sqrt{2}}{15}\right)^{1/3}\frac{R_\odot}{\mathrm{yr}}\right]^{-2\alpha} \times \left[L_2^{2/3}R_2^{2/3}M_2^{-2/3}\left(\frac{l_m}{H_p}\right)^{-4/3}\left(\frac{P_{Kep}}{\epsilon_H R_2}\right)^2\right]^{-\alpha} \tag{2.1.6}$$

where the pressure scale height has been parametrized as a fraction of the stellar radius, $H_p = \epsilon_H R_2$ (typically assuming $\epsilon_H = 1$ for simplicity), and l_m is the mixing length (Schleicher and Mennickent, 2017).

By compactifying some expressions like v_c other values, the equation is expressed as follows:

$$P_{\mathrm{cycle}} = \left(\frac{11.5\, v_c P_{\mathrm{Kep}} R_\odot}{\epsilon_H R_2[\ \mathrm{kms}^{-1}\ \mathrm{yr}]}\right)^{-2\alpha} P_{\mathrm{rot}}. \tag{2.1.7}$$

In this expression, $\mathrm{P_{cycle}}$ represents the dynamo cycle period, and $\mathrm{P_{rot}}$ is the donor's rotation period (P_o) (Schleicher and Mennickent, 2017). Key physical parameters, typically derived from stellar evolution models MESA, include the convective velocity ($\mathrm{v_c}$), defined as the maximum value in the donor's convective regions, and the donor's radius ($\mathrm{R_2}$) (Calderón et al., 2025; Rosales et al., 2024). Additional terms are: $\mathrm{P_{Kep}}$, the Keplerian orbital period of a test particle at the donor's surface (Schleicher and Mennickent, 2017); ϵ_H, a parameter linking the pressure scale height ($\mathrm{H_p}$) and the Roche radius ($\mathrm{R_{Roche}}$); and α, the power law index relating the cycle period to the dynamo number (D) (Schleicher and Mennickent, 2017).

Recently, an alternative dynamical mechanism based on the nodal precession of a

tilted accretion disk driven by tidal torques has been explored to explain the long cycle variability in Double Periodic Variables (Jiao et al., 2026). Although this model is able to morphologically reproduce some photometric variations, the analytical framework still requires thorough testing, since it relies on a physical simplification that treats the three dimensional structure of the accretion disk by approximating it to the limiting case of a rigid precessing ring. Theoretically, this formulation establishes a strong mathematical and kinematic dependence between the outer radius of the disk and the resulting precession period.

This analytical constraint is in direct contradiction with recent photometric and tomographic modeling of systems such as OGLE-LMC-DPV-065, which demonstrate that the geometric dimensions of the disk—particularly its radius and vertical thickness undergo drastic structural variations while the long cycle period behaves as an underlying clock that remains constant or exhibits a temporal evolution completely decoupled from the radial extent (Mennickent and Djurašević, 2025; Garcés et al., 2025).

Given these dynamical limitations, the hypothesis of a stellar magnetic dynamo operating within the donor component (Schleicher and Mennickent, 2017) remains the most plausible theoretical scenario in light of the observational evidence. Within this framework, the structural alterations observed in the circumstellar disk do not constitute the origin of the long photometric cycle, but instead arise as a natural hydrodynamic response to a mass transfer rate that is cyclically modulated by fluctuations in the equatorial radius of the donor star, driven by the redistribution of internal angular momentum according to the mechanism proposed by Applegate (1992).

2.2 Astrophysics Modeling

Numerical modeling constitutes a fundamental pillar of modern stellar astrophysics, as it enables the inference of intrinsic physical parameters and evolutionary states that are not directly accessible through observations. In the regime of interacting binary systems, the application of theoretical models is indispensable for disentangling the

photometric and spectroscopic contributions of stellar components distorted by the Roche potential and by complex circumstellar structures. Specifically for the study of DPVs, the light curve synthesis code developed by Djurašević (1992b, 1996) has been extensively employed. Complementarily, to understand the evolutionary history and the dynamics of mass transport, stellar evolution codes such as `MESA` are used, as they allow the simulation of binary interactions from the main sequence to advanced evolutionary phases (Paxton et al., 2011, 2013, 2015, 2018b; Jermyn et al., 2023).

2.2.1 Light curve synthesis Djurašević model

Djurašević models constitute an advanced numerical methodology for the synthesis and analysis of light curves in close binary systems, particularly those exhibiting strong interaction and complex accretion structures, such as W Serpentis variables and DPVs (Djurašević, 1992a, 1996). These models are based on Roche geometry to describe the equipotential surfaces of the stellar components, incorporating the effects of rotational and tidal distortion in both synchronous and asynchronous systems.

A fundamental feature of this formalism is the inclusion of an accretion disk around the mass gaining star. Unlike simple two dimensional approximations, the Djurašević model treats the disk as an optically and geometrically thick physical structure. The disk's morphology is defined by its radius and vertical thickness (at both the inner and outer edges), allowing for conical, concave, or convex configurations. The radial temperature distribution of the disk is usually parameterized by a power law, accounting for deviations from the theoretical steady state (Mennickent et al., 2015; Mennickent and Djurašević, 2021).

To reproduce the asymmetries frequently observed in the light curves of interacting systems (such as the O'Connell effect or unequal quadrature maxima), the model incorporates active regions ("spots") on the disk edge:

- **Hot Spot:** Represents the impact region of the gas stream originating from the L_1 Lagrange point onto the disk edge.
- **Bright Spot:** Simulates additional shock regions or spiral structures in the disk, often located on the opposite side of the hot spot, consistent with hydrodynamic

simulations (Garcés et al., 2018; Rosales et al., 2023b).

The determination of orbital and stellar parameters is achieved by solving the inverse problem. The code employs the Simplex optimization algorithm Nelder and Mead (1965) to iteratively minimize the sum of the squared residuals between the observed photometry and the synthetic light curve generated by the model (Djurašević, 1992b; Mennickent et al., 2025).

2.2.2 Modules for Experiments in Stellar Astrophysics (MESA)

MESA code has been established as a fundamental open source suite, enabling detailed simulations of stellar evolution through a modular architecture that incorporates state of the art microphysics, such as updated equations of state and opacities (Paxton et al., 2011, 2013). Specifically, the implementation of the MESA-binary module allows for the simultaneous evolution of two interacting stellar components, solving the internal structure equations together with the evolution of the orbital parameters, which is critical for systems in which the thermal and nuclear timescales are modified by mass exchange (Paxton et al., 2015).

The standard methodology for the study of DPVs initiates the simulations from the zero age main sequence (ZAMS), tracing the complete evolutionary tracks of intermediate mass binary systems. These simulations incorporate key physical processes, such as Roche lobe overflow, which is treated through implicit schemes (e.g., Ritter or Kolb prescriptions) that compute the mass transfer rate $\dot{M}$ as a function of the excess of the stellar radius over the Roche lobe radius (Paxton et al., 2015). In the specific case of DPVs, a quasi conservative mass loss scenario is frequently assumed, in which the accretion efficiency is limited by the Eddington rate; this approach mimics the formation of an accretion disk around the gainer star when the mass flow exceeds the star's direct assimilation capacity (Rosales et al., 2019b; Mennickent et al., 2025). In addition, the code self consistently handles the orbital angular momentum balance ($J_{\rm orb}$), accounting for losses due to stellar winds, magnetic braking, and, crucially, the transport of angular momentum associated with non conservative mass transfer (Paxton et al., 2015).

Finally, the validation of the evolutionary simulations is established through a rigorous

statistical analysis, by minimizing the χ^2 parameter to ensure that the fundamental physical parameters derived from the models (current masses, radii, orbital periods, effective temperatures, and luminosities) are consistent with the spectroscopic and photometric observations of the present day DPV systems. This methodology has been successfully applied to reconstruct the evolutionary history of specific systems such as V4142 Sgr, V495 Cen, and V1001 Cen, revealing that these objects are typically found in a thermal timescale mass transfer stage (Case B) and have, in many instances, experienced a reversal of the mass ratio (Rosales et al., 2024, 2019b; Calderón et al., 2025).

2.2.2.1 Mass transfer

The mass transfer process begins when the donor star overflows its critical volume (Hilditch, 2001; Eggleton, 2006; Frank et al., 2002). `MESA` calculates the geometry of the Roche Lobe using analytical approximations, such as the Eggleton formulation (Hilditch, 2001; Eggleton, 2006).

`MESA` incorporates both explicit and implicit methods to calculate the RLOF mass transfer rate ($\dot{M}_{RLOF}$) (Paxton et al., 2011, 2015). Explicit schemes include the Ritter model (Paxton et al., 2011, 2015) and the Kolb & Ritter scheme. In implicit computation, the solver iteratively adjusts the transfer rate until the stellar radius (R) matches the Roche Lobe radius (R_{RL}) within a predefined tolerance (Paxton et al., 2011, 2015).

The code ensures the consistency of the chemical composition and entropy of the transferred material. The composition of the accreted material is defined as identical to the current surface composition of the donor star (Paxton et al., 2011, 2015). Furthermore, the specific entropy of the accreted material is adjusted to be consistent with the surface of the accreting star (Paxton et al., 2011, 2015). `MESA` also employs criteria such as the von Zeipel stability criterion and the thermal stability criterion to ensure the consistency and stability of the stellar mass during the process (Paxton et al., 2011, 2015).

The modeling of binary evolution must account for mass and angular momentum loss, leading to quasi conservative evolution. `MESA` offers multiple stellar wind formalisms,

such as the Reimers model for red giants (Paxton et al., 2011, 2015) and the Blöcker scheme for AGB stars (Asymptotic Giant Branch) (Reimers, 1975; Blöcker, 1995). Parametric fractions are also utilized to control mass distribution. The parameter α is associated with spherically symmetric outflow (fast wind or Jeans mode) from the donor, and β describes the isotropic re-emission or ejection of material from the accretor in the form of a fast wind (Paxton et al., 2015). The binary module includes the modeling of stellar rotation, tidal interaction, and spin up due to accretion (Paxton et al., 2015). Angular momentum redistribution within the star is handled with a diffusion approximation. In systems where the accreting star cannot accumulate mass at a high rate, such as in DPVs, `MESA` allows for imposing a limitation, typically the Eddington accretion rate ($\dot{M}_{\rm Edd}$). This restriction is crucial for simulating the formation of an accretion disk (Frank et al., 2002).

2.2.2.2 Mass loss

`MESA` manages mass loss ($\dot{M}$) by routinely calculating it at each time step before solving the coupled structure and composition equations (Paxton et al., 2011, 2018a). For wind driven mass loss in single stars, the code integrates various formalisms that depend on the evolutionary phase and mass of the star.

For stars on the Red Giant Branch (RGB), the Reimers formalism (Reimers, 1975) is commonly used, this formalism is useful for the case of DPVs because it is based on the premise that mass loss is driven primarily by convection processes and mechanical activity in the outer layers of the star. For stars reaching the AGB, the Blöcker model is implemented, based on dynamical calculations of Mira type star atmospheres (Blöcker, 1995). For massive stars or those with transitional hot winds, `MESA` allows the use of the Dutch scheme (which includes recipes like Vink et al. (2001); Nugis and Lamers (2000)) or the functions by de Jager et al. (1988). Additionally, a prescription for rotationally enhanced mass loss is incorporated, which increases as the surface rotational velocity approaches the critical velocity (Paxton et al., 2018a).

In the modeling of DPVs with `MESA`, the choice of the mass loss formalism for the donor star during its RGB evolution is based on physical rigor. Rosales et al. (2024) argue that the Reimers scheme is more appropriate than the de Jager scheme, as the

Reimers model is based on the premise that mass loss is driven by convection processes in the star's outer layers (Reimers, 1975; Rosales et al., 2024). This perspective aligns more realistically with the condition of DPVs, where the donor star is filling its Roche Lobe due to its evolutionary expansion and convection plays a dominant role. In contrast, the de Jager scheme, which links mass loss to a combination of radiation, convection, and thermal pulses, is not compatible with the observed characteristics of DPV donor stars (de Jager et al., 1988; Rosales et al., 2024). For more advanced phases, such as the AGB, the Blöcker formalism is used (Blöcker, 1995; Rosales et al., 2024).

Additionally, with `MESA`, the mass transfer is quasi-conservative. Rosales and collaborators (Rosales et al., 2024), following the formalism of Soberman et al. (1997), define the mass and angular momentum loss from the system using parametric fractions of the transferred mass, which allows for tracing the evolutionary history and validating the models against current observational parameters (Rosales et al., 2019b; Calderón et al., 2025).

2.2.2.3 The stellar dynamo in the `MESA`

The Tayler–Spruit (ST) dynamo mechanism, implemented in the `MESA` stellar evolution code (Paxton et al., 2015, 2018a), is a theoretical tool for modeling the generation of magnetic fields in stable, radiative regions of differentially rotating stars.

The ST dynamo, proposed by Spruit (2002), addresses the transport of angular momentum and the amplification of magnetic fields in radiative zones, where convection is inefficient. This formalism assumes that the stellar rotation is a function of the radial coordinate (Spruit, 2002; Rosales et al., 2024). The process begins by assuming an initial magnetic field weak enough that the initial magnetic forces are negligible. The differential rotation winds up the radial component (B_r) of the magnetic field, amplifying it predominantly into the azimuthal (toroidal) component (B_ϕ), such that $B_\phi > B_r$. If the differential rotation is sufficiently strong, a dynamo process is sustained (Rosales et al., 2019b, 2021).

The generated azimuthal field must be intense enough to trigger the Tayler instability (Spruit, 2002; Rosales et al., 2019b). This instability, along with differential rotation

and stratified layers, provides an ideal ingredient for angular momentum transport. In stratified regions, thermal diffusion reduces the stabilizing effect of the entropy gradient, facilitating the onset of magnetic instabilities (Rosales et al., 2019b).

The `MESA` model implements the ST dynamo following seminal works (Paxton et al., 2013; Spruit, 2002). For characterization, parameters such as the angular velocity (Ω), magnetic diffusivity (η), the Brunt-Väisälä frequency (N), and the differential rotation gradient ($q = \partial \ln \Omega / \partial \ln r$) are considered (Paxton et al., 2013). The parameter q has two forms, q_0 (without thermal diffusion) and q_1 (with thermal diffusion). q_0 and q_1 represent the minimum threshold of the shear rate necessary to generate the critical magnetic field intensity that activates the Tayler instability and, in the case of q_1, convective currents (Paxton et al., 2013; Spruit, 2002).

The ST model in `MESA` provides estimates for the magnetic field components (B_r and B_ϕ) based on dynamo processes that consider stable stratification. In DPV simulations, the toroidal component (B_ϕ) has been observed to be dominant, as expected (Rosales et al., 2019b). In the models by Rosales et al. (2024), the inclusion of differential rotation is fundamental for simulating the ST dynamo in the donor. The activation and amplification of the magnetic fields are influenced by the mixing diffusivity (D_{ST}) outside the overshooting zone (Rosales et al., 2024).

The `MESA` model developed by Rosales et al. (2023b) for the DPV V4142 Sgr showed that the system is in a thermal timescale mass transfer phase. The analysis of the ST dynamo in this system supports the role of differential rotation in field generation, with the diffusivity D_{ST} being active outside the overshooting zone influencing the amplification of the magnetic fields (Rosales et al., 2024). In the study of V495 Cen, (Rosales et al., 2019b), implemented the ST dynamo and concluded that the presence of magnetic fields within the donor is justified. The results suggest that the predicted magnetic field intensities are in agreement with the intensities observed in evolved and late type stars (Rosales et al., 2019b). `MESA`'s capability to model the dynamo and quasi conservative mass transfer allows for predicting the magnetic cycles that could help in understanding the second photometric variability of DPVs (Rosales et al., 2019b).

Recent investigations have evaluated the quantitative feasibility of the coupling

between magnetic activity and orbital dynamics in the context of DPVs, using stellar evolution models specifically applied to the OGLE-LMC-ECL-14413 system (Mennickent et al., 2025). Through numerical simulations based on the `MESA` code and employing the Tayler Spruit prescription for magnetic field generation, it was determined that the field intensities in the subsurface of the donor star are weak, generally below 1 kG. Applying the Applegate formalism to link these intensities with structural variations yields fractional changes in the stellar radius (ΔR/R) on the order of 10^{-6}, which translates into negligible fluctuations in the mass flux through the L_1. Consequently, under the current premises of the Tayler Spruit model, the predicted magnetic intensities are insufficient to drive the significant changes in the mass transfer rate necessary to explain the amplitude of the observed long photometric cycles in these systems (Mennickent et al., 2025).

It is important to emphasize that the ST dynamo formalism implemented in `MESA` and the dynamo model employed to interpret the long photometric cycle in DPVs play fundamentally different and complementary roles in this thesis. These two mechanisms are not identified with each other, nor are they assumed to describe the same physical process.

The ST dynamo provides a prescription for the generation of internal magnetic fields in stably stratified, radiative regions of differentially rotating stars. Its primary role is to account for angular momentum transport, internal magnetic stresses, and the redistribution of rotation within the stellar interior. In the context of this work, the ST dynamo is used as an internal transport mechanism that contributes to shaping the donor's rotational and structural profile during binary evolution, thereby influencing the internal conditions under which convection develops. The magnetic fields predicted by the ST formalism are predominantly internal and subsurface, and their associated amplitudes are not expected to directly modulate the mass transfer rate at the L_1 point on secular timescales.

By contrast, the dynamo mechanism, following the Schleicher & Mennickent formalism, invoked to explain the long photometric cycle in DPVs is explicitly associated with the convective envelope of the donor star and operates on longer, cyclic timescales. This dynamo is not implemented in `MESA` as a transport prescription, but is instead

evaluated a posteriori using donor stellar properties (radius, convective velocity, and rotation) extracted from the evolutionary models. Its role is to provide a physically motivated clock capable of modulating the mass transfer rate through magnetic activity cycles, thereby producing the observed long period variability.

Therefore, within the framework of this thesis, the ST dynamo and the Schleicher & Mennickent dynamo are used in a complementary manner: the former governs internal angular momentum transport and magnetic field generation in radiative regions during stellar evolution, while the latter provides an external, observationally testable mechanism for secular mass transfer modulation driven by donor star convection. The use of both formalisms does not imply their equivalence, but rather reflects the multi scale nature of magnetic processes operating in interacting binaries.

2.2.2.4 Mixing length theory

In the stellar evolution code `MESA`, the phenomenon of convective overshooting is modeled by extrapolating the mixing diffusion coefficient beyond the formal boundary of the convective region through an exponential decay scheme (Paxton et al., 2011; Herwig, 2000). Mathematically, the diffusion coefficient in the adjacent radiative region is expressed as

$$D_{\mathrm{OV}} = D_{\mathrm{conv},0} \exp\left(-\frac{2z}{f\lambda_{P,0}}\right), \tag{2.2.1}$$

where $D_{\mathrm{conv},0}$ is the diffusion coefficient derived from mixing length theory (MLT) and evaluated near the Schwarzschild boundary, z is the spatial distance measured from this boundary into the radiative layer, $\lambda_{P,0}$ is the local pressure scale height, and f is a dimensionless free parameter that governs the efficiency and spatial extent of the extra mixing (Paxton et al., 2011). Since the mixing coefficient derived from MLT drops to zero exactly at the geometric boundary of the convective zone, evaluating overshooting directly from this exact limit is numerically suboptimal. To remedy this limitation, the implementation requires the definition of an additional parameter, f_0, which specifies a distance inward from the convective boundary (expressed as a fraction of the local pressure scale height, $f_0 \cdot H_p$) from which the overshooting extrapolation is actually initiated. This prescription ensures a smooth and physically consistent transition of the diffusion coefficient across the hydrodynamic boundary

(Calderón et al., 2025). Furthermore, the mixing length parameter, α_{MLT}, is a free dimensionless variable handled by the `mlt` module that determines the efficiency of convective energy transport by defining the mean free path of fluid elements in terms of the local pressure scale height (Paxton et al., 2011).

In `MESA`, the convective velocity (v_c) is computed through the `mlt` module, which implements the standard MLT formalism or its opacity dependent variants (Paxton et al., 2011). Physically, this quantity characterizes the average upward and downward motion of fluid elements driven by thermodynamic instabilities in superadiabatic regions, and it constitutes the central variable for the computation of Eulerian diffusion coefficients that govern chemical mixing and convective energy transport. In hydrodynamic evolutionary regimes, or during phases requiring extremely short timesteps, `MESA` incorporates analytic mechanisms to limit the acceleration of the convective velocity, in order to prevent the development of instantaneous, unphysically large gradients that could compromise the numerical stability of the model (Paxton et al., 2015).

Chapter 3

Analysis and results

3.1 The case of V1001 Cen

V1001 Cen, also known as HD 125104 and ASAS 141909-5552.9, has coordinates of $\alpha_{2000} = 14^{h}\,19^{m}\,09^{s}$, $\delta_{2000} = -55^{\circ}\,52'\,56''$, with an apparent visual magnitude of 7.30 ± 0.02 mag and a B-V color index of 0.066 ± 0.054 mag. Classified as an eclipsing binary, this little studied system has an orbital period of 6.736 ± 0.003 days according to the ASAS-3[1] catalog (Pojmański, 2002), and is located in a region close to Alpha Centauri. Furthermore, V1001 Cen exhibits a long photometric cycle of 247 ± 3 days, and was reported as a DPV by Mennickent et al. (2016a). V1001 Cen is mentioned in that work as part of a larger set of objects studied in the context of interactive W Serpentids[2] binaries and DPVs.

3.1.1 Photometric and spectroscopic studies

3.1.1.1 Photometric data

Photometry is the astronomical technique dedicated to measuring the flux or intensity of electromagnetic radiation from a celestial object, allowing the analysis of its

[1] https://www.astrouw.edu.pl/asas/?page=acvs

[2] W Serpentis-type stars constitute a class of interacting binary systems in an evolutionary phase of intense and non-conservative mass transfer, characterized by the presence of an optically thick accretion disk around the gaining star.

temporal variations in brightness. To perform the photometric analysis of the V1001 Cen system, we used data from the all sky automated survey ASAS-3 (V filter)[3]. The All Sky Automated Survey, conceived by Pojmański (2002), is an astronomical project that uses multi pixel CCD detectors and has been instrumental in monitoring variable objects in the sky, including red giants and variable stars (Pojmański, 2003). ASAS-3, in particular, is notable for its ability to observe the entire southern sky with two wide-field instruments and one narrow field one, collecting photometric data used for the study of binary systems and variable stars (Pojmański, 2001). Furthermore, ASAS is a useful tool in the automated classification of periodic variable stars (Eyer and Blake, 2002). This long term project has managed to discover 50,099 variables and 11,076 eclipsing binaries, contributing to the census of bright variable stars in the sky (Paczyński et al., 2006; Pigulski, 2013). The ASAS public database [4] has also been essential for the analysis of light curves of eclipsing binary systems, providing a good data source for research in this field (Ulaş and Ulusoy, 2015).

To determine the period of the system, we first disentangled the light curve using software developed by Zbigniew Kolaczkowski and described in Mennickent et al. (2012a). This algorithm is based on fitting the data to a Fourier series, incorporating fundamental frequencies and their respective harmonics, which are identified in advance. The choice of the number of harmonics to be used is intrinsically linked to the morphology of the light curve. For example, in curves with sinusoidal patterns, the use of a few harmonics may be sufficient. However, given the inherent complexity of the light curves of eclipsing binary systems, the inclusion of a greater number of harmonics, typically on the order of 12 or more, is required for an accurate fit. Following the adjustment of the main light curve and its harmonics, the algorithm provides a set of residuals. These residuals are analyzed in the search for secondary frequencies associated with a second period.

We then used the `Lomb scargle fast` algorithm from the Python[5] library `gatspy`

[3]The V (Visual) filter is part of the Johnson Cousins photometric system, centered at approximately 5500 Å. It is the primary standard in optical astronomy for measuring visual magnitudes.
[4]https://www.astrouw.edu.pl/asas/
[5]https://www.python.org/

`periodic` (VanderPlas and Ivezić, 2015), this library extends the single band multiharmonic analysis of variance algorithm to estimate periods in multiple bands, improving period recovery rates by up to 50% (Mondrik et al., 2015). Furthermore, `gatspy` aggregates multidimensional and sparsely sampled time series information, which significantly increases the period retrieval rate (Huijse et al., 2018). We used `gatspy` to estimate the orbital period and the long period. The method extracts a periodic component with a specified frequency and leaves a residue curve that could show a second periodic component.

The orbital period was found to be $P_o = 6.73 \pm 0.01$ d. In addition, a long cycle of $P_l = 247.19 \pm 10.0$ d was found, and is represented in Table 3.1.1. The light curves for each period reveal an orbital modulation typical of an ellipsoidal binary but with unequal maxima and a longer cycle characterized by quasi sinusoidal variability. Fig. 3.1.1 shows the light curve for the orbital period and the long period.

In the work of Mennickent et al. (2016a) the following ephemerides were reported for the light curve maxima of V1001 Cen:

$$\mathrm{HJD}_{\mathrm{long}} = 2452441.9293 + 6.736(3) \times \mathrm{E}, \tag{3.1.1}$$

$$\mathrm{HJD}_{\mathrm{long}} = 2452439.69 + 247(3) \times \mathrm{E}. \tag{3.1.2}$$

But in our case the epochs found for the minimum of the light curve are:

$$\mathrm{HJD}_{\mathrm{orb}} = 2453409.8424 + 6.73(1) \times \mathrm{E}, \tag{3.1.3}$$

$$\mathrm{HJD}_{\mathrm{long}} = 2454164.7747 + 247.19(1) \times \mathrm{E}. \tag{3.1.4}$$

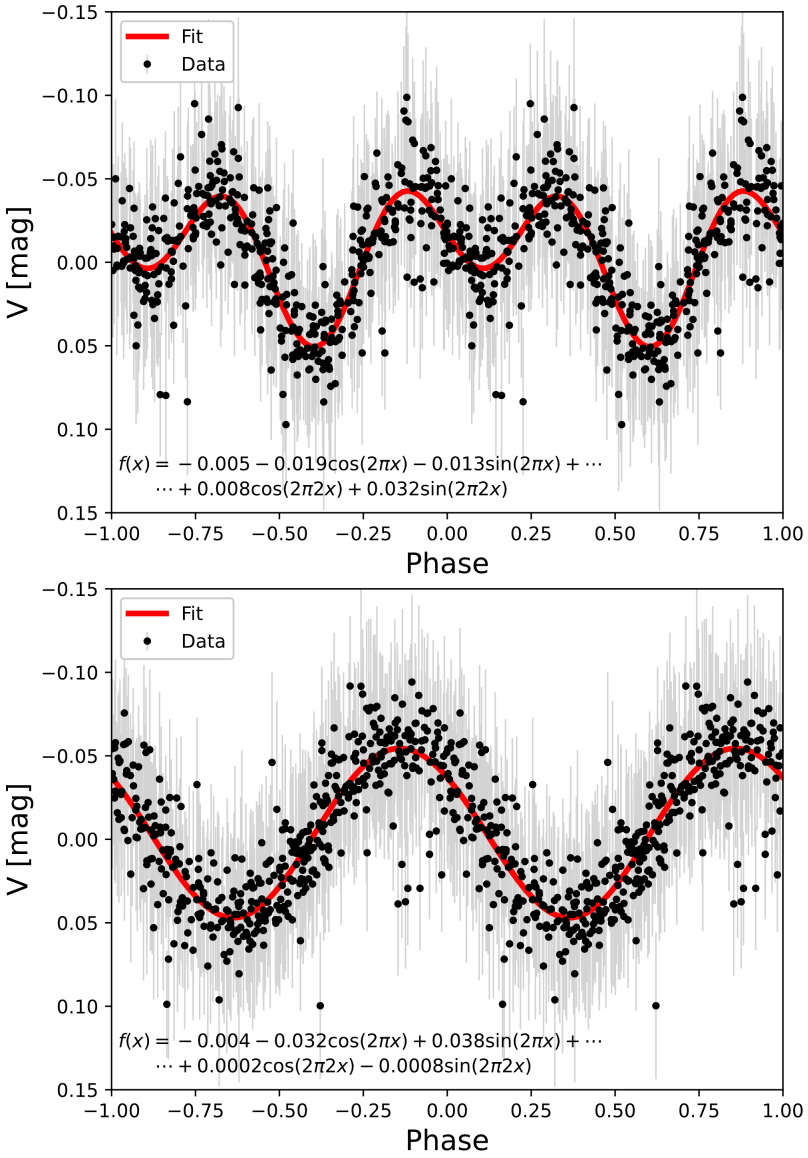

Figure 3.1.1: Disentangled light curves from the ASAS data for the orbital period (Top) and long period (Bottom), phased between -1.0 and 1.0. The solid red line represents the best-fit function f(x) shown in the plot, and the gray lines represent the error bars.

Table 3.1.1: Orbital parameters for the donor or gainer star of V1001 Cen.

Parameter	Value	error
P_o (d)	6.73	0.01
P_l (d)	247.28	10.00
q	0.151	0.003
$K_g\,(kms^{-1})$	21.70	0.38
$K_d\,(kms^{-1})$	142.33	0.34

Notes. These parameters were obtained through minimization of χ^2 . Calculated using `gatspy` library for the periods, and using `iraf` routines for the radial velocities.

In addition, from the photometric analysis to the ASAS data, we have determined other values, such as those in Table 3.1.2 showing the photometric aparent magnitudes in different filters extracted from the ExoFOP[6] database. In turn, Fig. 3.1.1 shows the fitting of the light curves for the orbital period and the long period using a Fourier series. For the orbital period, the maximum magnitude of the curve is 7.34 ± 0.04 mag, the minimum is 7.26 ± 0.04 mag, and the total amplitude of the curve is 0.043 ± 0.003 mag. The detailed values of the parameters of the fitting functions for each case are specified in the footnotes of the corresponding figures.

3.1.1.2 Spectroscopic data

Spectroscopy is the study of the interaction between electromagnetic radiation and matter through the decomposition of light into its different wavelengths. In astrophysics, this technique allows the analysis of absorption and emission lines to determine the chemical composition, temperature, density, and radial velocity of celestial objects. We obtained the spectra using the highly stable cross dispersion spectrometer CHIRON[7] on the 1.5 m SMART telescope. A total of ten spectra were

[6] https://exofop.ipac.caltech.edu/tess/
[7] http://exoplanets.astro.yale.edu/instrumentation/chiron.php

Table 3.1.2: Summary of photometric data for V1001 Cen.

Band	Magnitude (mag)	$\lambda_{\rm eff}$ (Å)	Filter ID	Reference
B	7.36 ± 0.02	4280	Tycho/Tycho.B	(Høg et al., 2000)
V	7.30 ± 0.03	5340	Tycho/Tycho.V	(Høg et al., 2000)
J	6.90 ± 0.01	12350	2MASS/2MASS.J	(Skrutskie et al., 2006)
H	6.81 ± 0.04	16620	2MASS/2MASS.H	(Skrutskie et al., 2006))
K	6.76 ± 0.02	21590	2MASS/2MASS.Ks	(Skrutskie et al., 2006)
Gaia	7.19 ± 0.01	6230	GAIA G, DR2	(Collaboration et al., 2018)
WISE 3.4	6.69 ± 0.06	33526	WISE/WISE.W1	(Wright et al., 2010)
WISE 4.6	6.59 ± 0.02	46028	WISE/WISE.W2	(Wright et al., 2010)
WISE 12	6.59 ± 0.01	115608	WISE/WISE.W3	(Wright et al., 2010)
WISE 22	6.45 ± 0.06	220883	WISE/WISE.W4	(Wright et al., 2010)

Notes. Photometric data at different band passes extracted from ExoFOP.

taken covering the orbital phase of the system. CHIRON is a fiber fed, Echelle type spectrometer with multiple observation modes that allow for spectral resolutions ranging from 28,000 to 120,000 (Schwab et al., 2012). This instrument is designed for high precision Doppler measurements using an iodine absorption cell and is optimized for monitoring the radial velocities of bright stars with high cadence and precision. For our observations, we used the high resolution mode, which provides a spectral resolution of $R = 80{,}000$, measured using a Thorium Argon calibration lamp. This mode delivers a broad spectral coverage from 410 to 870 nm, with an average signal to noise ratio (S/N) of ~ 59 in our data. Fig. 3.1.2 shows the set of nine spectra centered at Hβ (4861.332 Å).

3.1.1.3 Radial velocity and spectral disentangling

To determine the radial velocity of each component of V1001 Cen, we first identified characteristic absorption lines that represent the individual motion of each star. For the donor star, which exhibits a wider orbital motion reflected in its absorption lines, we selected the Fe I line at 6677.993 Å (see Fig.3.1.3, Table 3.1.3). For the other component, the accreting star, we used the Hα line at 6562.817 Å. Subsequently, we employed the deblending technique offered by `iraf` [8] and fit Gaussian functions to these lines. We selected lines that did not show significant broadening beyond the natural Gaussian profile, in order to avoid the accumulation of uncertainty caused

[8]Image Reduction and Analysis Facility

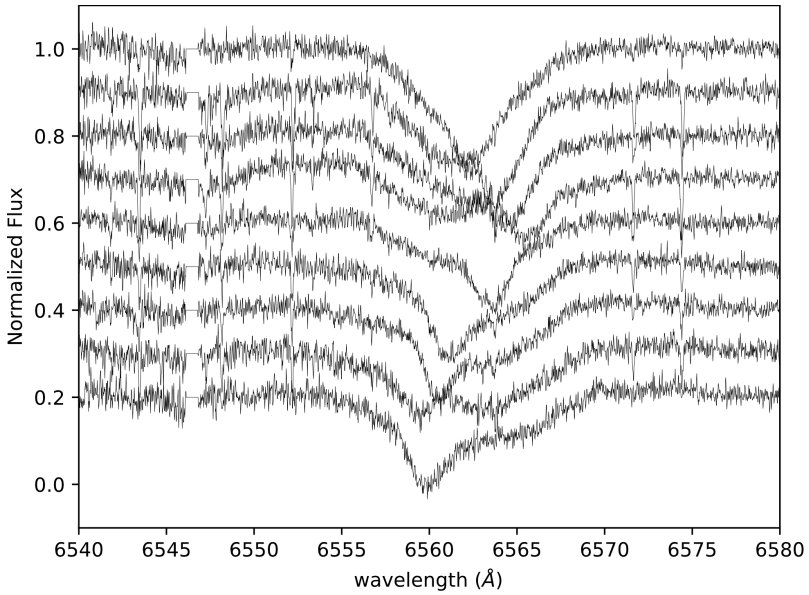

Figure 3.1.2: Spectral dataset centered on the spectral line 6562.8 Å, obtained from cross dispersion spectrometer CHIRON. The orbital phase values of the spectra from top to bottom are 0.14, 0.23, 0.26, 0.43, 0.58, 0.70, 0.73, 0.84, 0.99.

by inhomogeneous broadening, such as the macroscopic Doppler effect or statistical variations in the energies of the atomic levels. In this way, we ensured that we analyzed lines whose dominant broadening is due to natural processes, mainly collisions between atoms. The error associated with the Gaussian fit is provided by `iraf`, to which we subsequently incorporated the estimated precision of the instrument.

To analyze each stellar component independently, we used an iterative spectral disentangling method developed by Gonzalez and Levato (2006). The method consists of the following: an initial set of radial velocities is assumed for each star (see Table 3.1.3). Using these velocities, the observed spectra are shifted to their individual rest frames and then combined. This combination generates a template that represents the flux contribution of a single star, although still slightly contaminated by the light of its companion. This process is repeated for the other star, thus generating the first spectral templates for each stellar component. These first templates are subtracted from each original spectrum to remove the individual contribution of each star. In the next iteration, the previous steps are repeated, generating new templates and performing the subtractions successively until convergence is reached and a clean

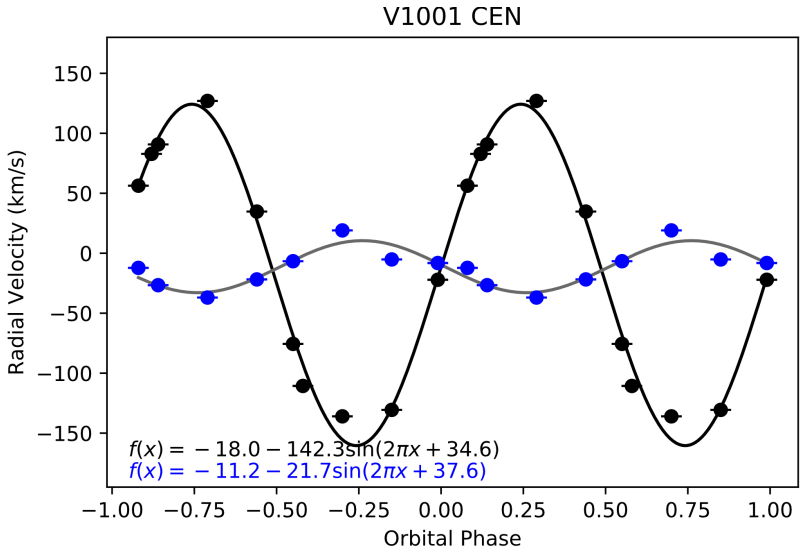

Figure 3.1.3: Radial velocities of the gainer and donor star with their respective errors, using the lines 6562.8 Å for gainer and 6677.9 Å for donor.

average spectrum is obtained for both components. However, it is important to note that the disentangling method will not allow us to separate the contribution of the accreting star from that of a possible accretion disk, as there are no models available for the spectral lines of accretion disks.

To date, no fully predictive theoretical or empirical models exist that can generally reproduce the emission lines of accretion disks in binary systems due to the intrinsic physical complexity of these environments. Accretion disks in interacting binaries are highly nonstationary, geometrically and optically complex systems where coupled processes of hydrodynamics, magnetohydrodynamics, radiative transfer out of local equilibrium, time dependent ionization, and feedback with the incoming mass flow from the Lagrange point coexist. Furthermore, the thermodynamic and kinematic conditions of the gas vary strongly with the radius, disk height, and orbital phase, and are modulated by phenomena such as shocks, impact currents, disk winds, and self occultation. These characteristics prevent the construction of universal and self consistent models that predict emission line profiles.

Table 3.1.3: Radial velocities of the gainer and donor star.

Epoch HJD (-2450000) (d)	Orbital phase	RV_{6562} (kms^{-1})	error (kms^{-1})	RV_{6677} (kms^{-1})	error (kms^{-1})
57212.6076	0.08	-12.206	1.004	56.297	1.009
57219.6001	0.12	——	——	82.838	1.006
57226.4706	0.14	-26.643	1.008	90.717	1.007
57227.4449	0.29	-36.962	1.004	126.980	1.006
57228.4592	0.44	-21.837	1.004	34.742	1.009
57222.5051	0.55	-6.662	1.003	-75.598	1.011
57229.4570	0.58	——	——	-110.657	1.004
57223.5049	0.70	19.032	1.003	-136.004	1.007
57224.5100	0.85	-5.183	1.004	-130.610	1.009
57225.4702	0.99	-8.163	1.004	-22.120	1.008

Notes. Radial velocities and their respective errors were calculated using the spectral lines 6562.8 Å for gainer and 6677.9 Å for donor.

3.1.1.4 Determination of stellar parameters by spectral fitting

In the case of V1001 CEN, the determination of the stellar parameters of each component was carried out by fitting synthetic spectra to previously unraveled observed spectra. To generate these synthetic spectra, we used the well known `Spectrum` [9] code (Gray et al., 2001; Gray and Corbally, 1994) which is based on stellar atmosphere models provided by `ATLAS9` [10] (Castelli and Kurucz, 2003), It is a recognized program in the field of astrophysics for spectral synthesis and analysis. It is used for generating synthetic spectra based on a range of stellar atmospheric parameters, including effective temperature (T_{eff}), surface gravity ($\log g$), and chemical composition. The incorporation of atomic and molecular data gives `spectrum` the ability to model the physical processes that allow the characteristics of stellar spectra to be recreated. This allows us to compare synthetic and observed spectra, thereby aiding in the determination of key stellar parameters such as temperature, metallicity, and rotational velocity. The versatility and adaptability of `spectrum` makes it a useful tool for probing chemical abundances and properties of astronomical objects in a spectral type range from B to M.

[9] http://www.appstate.edu/~grayro/spectrum/spectrum.html
[10] https://www.user.oats.inaf.it/fiorella.castelli/grids.html

Therefore, a grid was constructed for the donor star with different free parameters, such as the ($T_{\rm eff}$), the ($\log g$), the macroturbulence velocity ($v_{\rm mac}$), the microturbulence velocity ($v_{\rm mic}$), and the rotational velocity ($v \sin i$), and even the veiling factor (η). This last parameter corresponds to a proportionality constant between the theoretical and observed spectra due to the light contribution from its companion, which has veiled the absorption lines. All spectra were constructed using a metallicity index similar to that of the Sun (M/H = 0.0) and a fixed mixing length parameter $l/H = 1.25$ by default. In computational stellar physics, it is common practice to calibrate the mixing length parameter by reproducing the Sun's radius and luminosity at its current age. Therefore, we recommend using a mixing length parameter value close to the solar calibration value. A chi squared optimization algorithm was implemented, which consists of minimizing the deviation between the normalized theoretical spectrum and the observed average spectrum of the donor. The theoretical model was produced by varying the aforementioned parameters as follows: the $T_{\rm eff}$ varied from $3500 \leq T_{\rm d} \leq 10000$ K and $10,000 \leq T_{\rm d} \leq 30,000$ K for the gainer, with a step of 250 K; the log g varied from $0.0 \leq \log g \leq 5.0$ dex, with a step of 0.5 dex; the macroturbulence velocity varied from $0 \leq v_{\rm mac} \leq 10$ kms^{-1}, with steps of 1 kms^{-1}; while the microturbulence velocity took values of 0.0 and 2.0 kms^{-1}, the rotational velocity varied from $10 \leq v \sin i \leq 150$ kms^{-1}, with steps of 10 kms^{-1}, and the veiling factor $0.0 \leq \eta_{5400-5700} \leq 1.0$, with steps of 0.1. The implemented method successfully converged to a minimum. The adopted parameter ranges were selected to encompass the typical physical conditions expected for the stellar components of DPVs. The chosen intervals therefore ensure that the explored parameter space adequately covers the range of stellar properties inferred from previous observational and theoretical studies of DPVs, while avoiding unphysical configurations.

The synthetic spectrum that obtained the lowest chi square value $\chi^2 = 0.49$ relative to the donor spectrum was the one at $8,750 \pm 125$ K, $\log g = 3.5 \pm 0.25$ dex and $v \sin i = 40 \pm 5$ kms^{-1}. In the case of the gainer, several synthetic spectra achieved similar chi square values, so further checking is required. Fig. 3.1.4 and Fig. 3.1.5 show the disentangled spectra of the donor and gainer, along with the synthetic spectra that best achieved a fit.

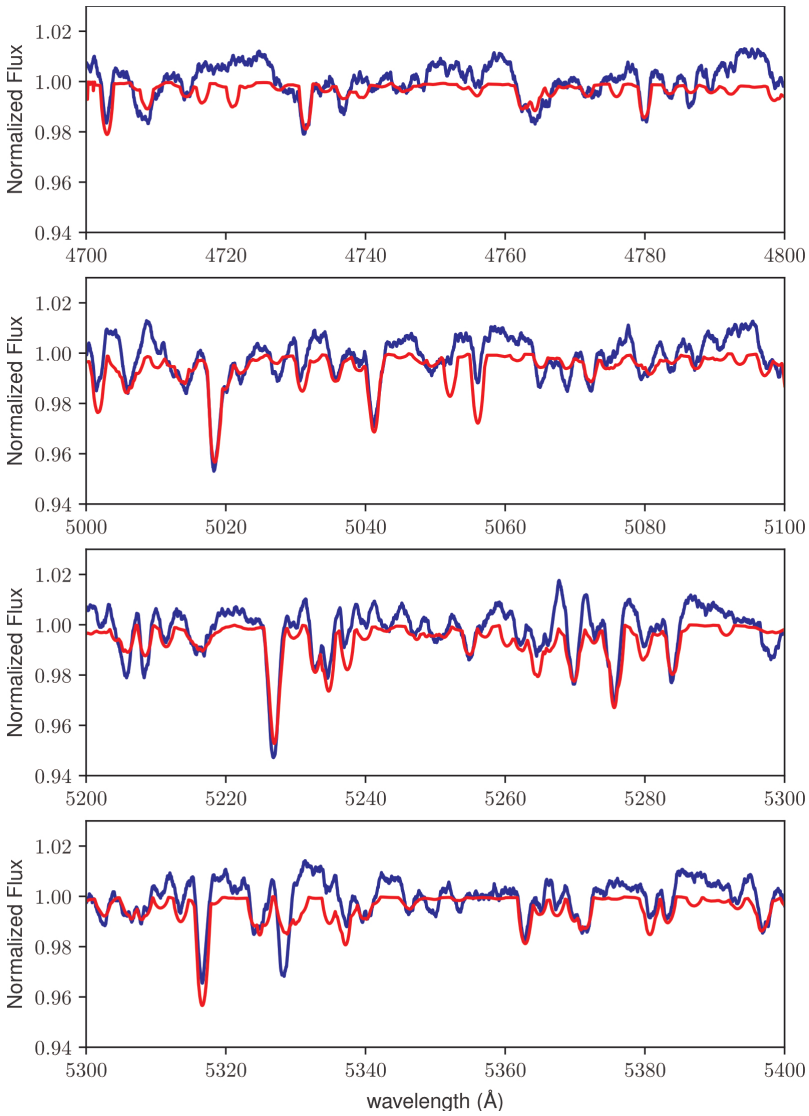

Figure 3.1.4: Comparison of synthetic spectra (red line) with the Donor disentangled spectrum (blue line). The windows show portions of the spectrum from 4700 Å to 5400 Å.

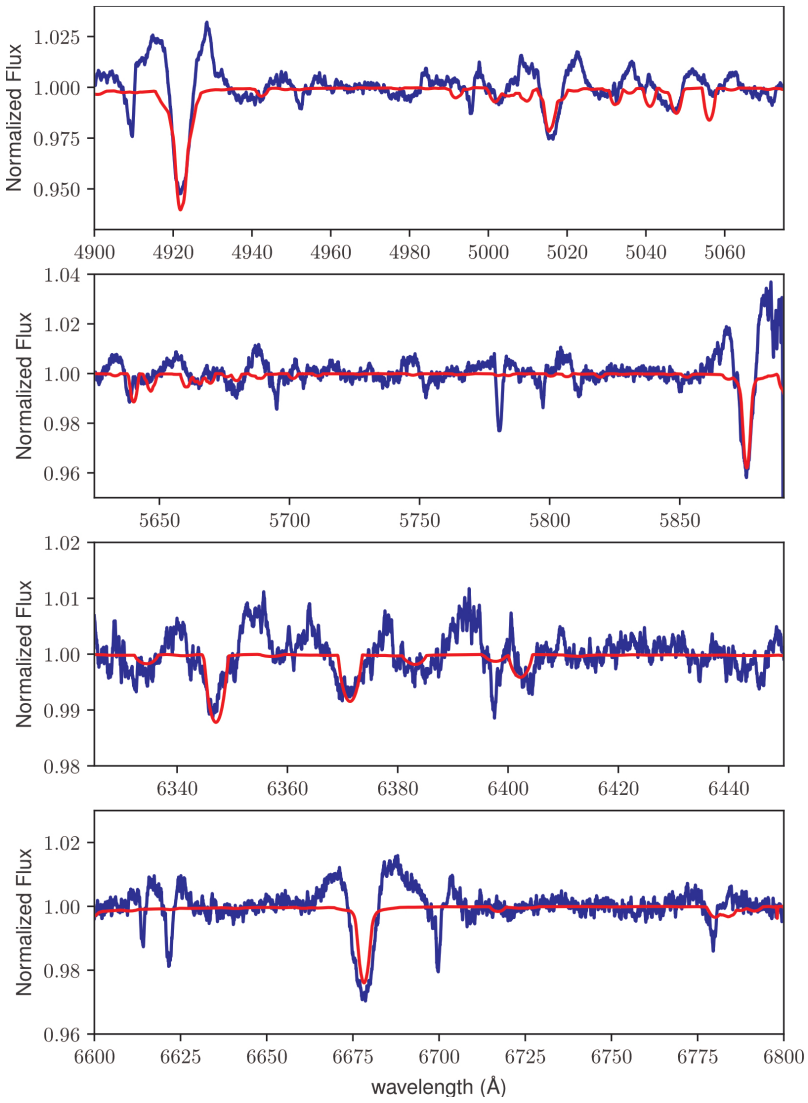

Figure 3.1.5: Comparison of synthetic spectra (red line) with the Gainer disentangled spectrum (blue line). The windows show portions of the spectrum from 4900 Å to 6750 Å.

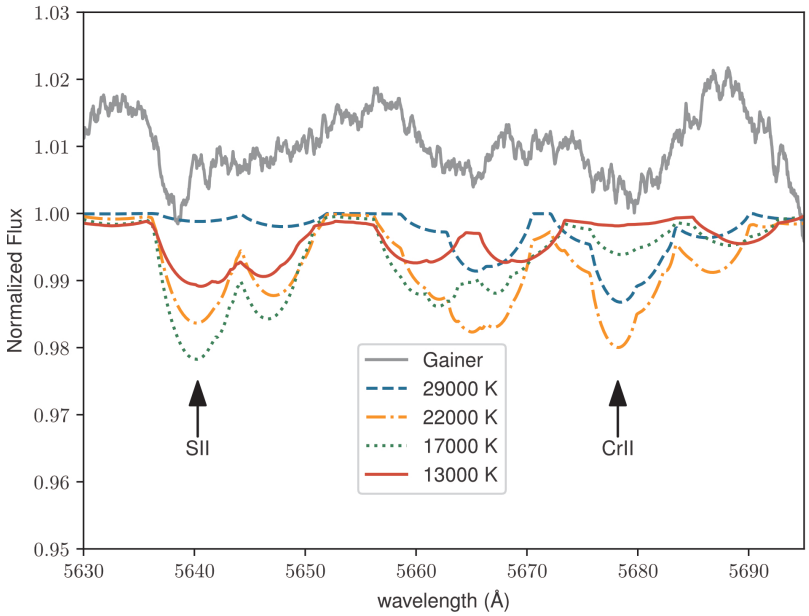

Figure 3.1.6: Comparison of lines S II 5640.32 Å and Cr II 5678.42 Å in the synthetic spectra generated with Spectrum. The variation in the depth of each line with changes in temperature can be seen in the synthetic spectra.

While the temperature of the donor star was effectively determined by fitting synthetic spectra generated with `spectrum` to its observed spectrum by minimizing the chi squared, the presence of an accretion disk around the accreting star complicates this direct approach. Therefore, to estimate the temperature of the accretor, spectral lines characteristic of B type stars were explored. The ratio between the equivalent widths of these lines could provide a valuable indication of the central star's temperature, minimizing the influence of the disk. Each calibrated equivalent width relationship provides a measure of the stellar temperature. To identify T_{eff} indicators, we conducted an exploratory survey across synthetic spectra generated by the `spectrum`. Our criteria for line selection required proximity for consistent continuum levels in observed spectra and distinct temperature dependent variations in line depths. From our analysis of lines between 4580 and 7590 Å in previously used synthetic spectra, only a pair of lines at S II 5640.32 Å and Cr II 5678.42 Å met these criteria (Fig. 3.1.6), which are located beyond telluric absorption lines.

We applied the χ^2 test to assess the equivalent width ratios from both synthetic and untangled spectra. Fig. 3.1.7 presents our adjustment of the values of χ^2 with

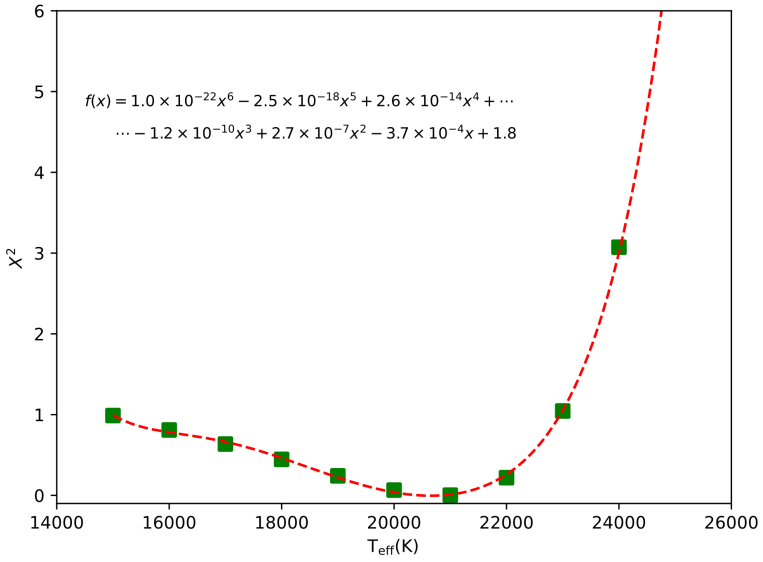

Figure 3.1.7: Adjustment of a function of the values of χ^2 from the comparison of theoretical and observed EW ratios vs. temperature.

the temperature, where a comparison is made between observed EW ratios and theoretical EW ratios. This statistic indicates the degree of alignment of the data with the regression line, with values close to 1 denoting a strong correlation. It is important to note that line depths can be influenced by the star's rotational velocity. To adapt this to the gainer, different speeds were tested in the synthetic spectra between $100\,\mathrm{kms}^{-1}$ and $250\,\mathrm{kms}^{-1}$, with $200\,\mathrm{kms}^{-1}$ being the one that gave the best fit. This analysis aimed to determine the temperature of the gainer by comparing the equivalent width ratio between its spectrum and the synthetic spectra. As can be seen in Fig. 3.1.7, the lowest value of χ^2 was found in the range of 20,000 to 22,000 K, for $\log g = 3.0 \pm 0.2$ being the value with the lowest χ^2, where a $\log g$ was varied between 2.5 and 4.0.

Using the untangled spectra, we deduced the probable spectral types for each component. The gainer star's spectral characteristics align with a B2 or B3 classification, while the donor's features suggest a A3 type. In the disentangled spectrum of the gainer (Fig. 3.1.5), emission wings are observed on either side of the main absorption lines, a feature that has also been reported in other DPV systems. Several studies have suggested that these wings could originate from circumstellar

material associated with mass flows or bipolar winds. In particular, Mennickent et al. (2012b) proposed the existence of a cyclic bipolar wind in V393 Scorpii, originating from the interaction between the mass transfer stream and the accretion disk, thereby generating extended structures that produce photon scattering and broad emission wings in Balmer lines such as $H\alpha$ and $H\beta$. Similarly, Rosales et al. (2023a) observed line profiles with emission shoulders in V4142 Sgr, which they interpreted as evidence of an extended atmosphere around the gainer's accretion disk, responsible for the formation of the wings. Additionally, Mennickent et al. (2010) and Mennickent et al. (2016b) highlighted that disk structures in DPVs, rather than being thin Keplerian disks, present irregular geometries and extended flows, all of these could be possible explanations for the wings detected in the disentangled spectra of V1001 Cen.

3.1.1.5 Light curve synthesis model

Djurašević (1992b) proposed a light curve synthesis model for W Ser type binaries. In these binary systems, which are in a phase of high matter exchange between the components, a gaseous disk usually forms around the primary star. The Roche model is used to approximate the maximum size of these star systems, taking into account the effect of asynchronous rotation. Djurašević (1992b) applies the inverse problem method to estimate the fundamental orbital and physical parameters of the binary system. This technique involves constructing a model that simulates the system's light curve behavior. By comparing the observed light curves with those predicted by the model, the parameters are iteratively adjusted to achieve the best fit. Certain parameters—such as the temperature of the gainer and the mass ratio—are held fixed, using values derived in earlier sections. Notably, the model does not incorporate the radial velocity data previously computed. The fitting procedure typically explores a range of values for key parameters, including mass, radius, and temperature. In particular, the radius of the accretion disk is estimated relative to the Roche lobe radius. For a detailed explanation of the methodology used to determine these physical parameters, refer to subsection 2.2.1 of the theoretical framework. Djurašević (1996) modified the model to include a white dwarf companion, allowing it to be applied to another group of binary systems.

Thus, based on the light curve synthesis model mentioned, we calculate the best fit,

the O-C residuals, along with the individual flux contributions of the donor, gainer, and disk of V1001 Cen, and include the view of the optimal model at orbital phases 0.05, 0.20, 0.50, and 0.80. From the residuals, we notice a scatter around $\Delta V \sim 0.92$ (mag) without dependencies related to orbital or long cycle phases. The best fitting model contains an optically and geometrically thick accretion disk surrounding a nonsynchronous gainer star with the presence of a bright and hot spot (see Fig. 3.1.8. Table 3.1.4).

In this study, the gainer star is assumed to be surrounded by an accretion disk, without considering other potential sources of emission, such as jets, stellar winds, or gas streams. However, the model allows for the inclusion of an azimuthally dependent variations in the emissivity of the disk by introducing two emitting spots in the disk (a bright spot and a hot spot). Bisikalo et al. (1998, 1999, 2003) studied the hydrodynamic simulations of mass transfer in close binaries, suggesting the possibility of forming hot and bright spots in the accretion disk. These spots may represent shock regions characterized by higher density and temperature than the surrounding medium. Although this simplification has certain limitations and despite excluding possible external contributions, previous investigations in Algol systems with disks suggest that this model adequately represents the main sources of emission in the light continuum.

Our findings indicate that the best fitting model of V1001 Cen contains an optically and geometrically thick disk surrounding the hottest and most massive gainer star (Table 3.1.4). The radius of the disk, $\mathrm{R_d} = 13.2 \pm 0.1\,\mathrm{R_\odot}$, It is approximately 5 times larger than that of the central star ($\mathrm{R_g} = 2.68 \pm 0.1\,\mathrm{R_\odot}$). The disk has a relatively flat shape, with a central thickness $\mathrm{d_c} = 1.32 \pm 0.1\,\mathrm{R_\odot}$ and an edge thickness of $1.25 \pm 0.1\,\mathrm{R_\odot}$. The temperature of the disk increases from $\mathrm{T_d} = 7,415 \pm 500\,\mathrm{K}$ at its edge to $\mathrm{T_g} = 18,310 \pm 500\,\mathrm{K}$ at the inner radius, where it is in physical and thermal contact with the gainer star. The disk temperature is the same as the gainer at its inner edge and decreases with a radial profile described by an exponent, a_T.

$$T(r) = T_g * (r/R_g)^{a_T}, \tag{3.1.5}$$

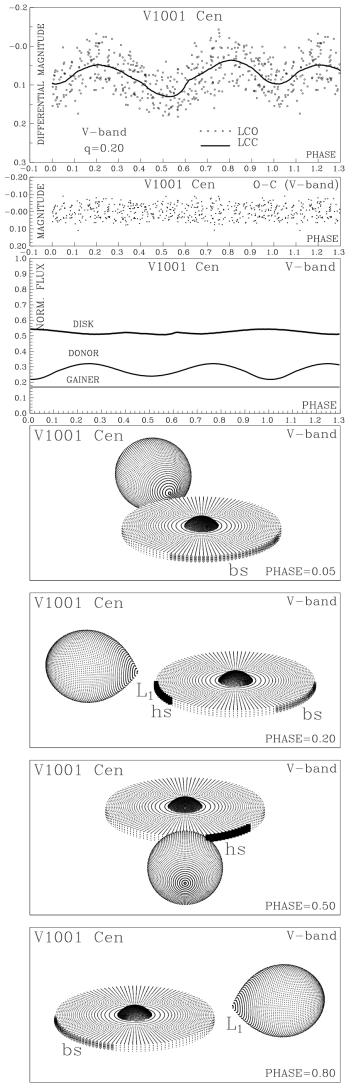

Figure 3.1.8: Observed (LCO) and synthetic (LCC) light curves of the system V1001 Cen obtained by analyzing ASAS V band photometric observations and final O-C residuals between the observed and optimum synthetic light curves; fluxes of donor, gainer and of the accretion disk, normalized to the donor flux at phase 0.25; the views of the optimal model at orbital phases 0.05, 0.20, 0.50 and 0.80, obtained with parameters estimated by the light curve analysis.

where T_g and R_g denote the temperature and radius of the donor star, respectively. The constraint $a_T < 0$ ensures that the temperature decreases radially outward from the star.

In the best model, we observe a hot spot with an angular radius of $21.^{\circ}6 \pm 1.^{\circ}2$, located at longitude $\lambda_{hs} = 326.^{\circ}9 \pm 3.^{\circ}0$, approximately between the components of the system. This is where the gas current falls on the disk (Lubow and Shu, 1975). The hotspot temperature is $9787 \pm 500\,\mathrm{K}$. Although including the hotspot region in the model improves the fit, it does not fully represent the asymmetry in the light curve. Hence, an additional bright spot is introduced, larger than the hotspot and located at $\lambda_{bs} = 172.^{\circ}7 \pm 8.^{\circ}0$ on the disk's edge, leading to a much better fit. This bright spot has $\mathrm{T_{bs}} = 10,232 \pm 500\,\mathrm{K}$ and an angular radius of $49.^{\circ}5 \pm 1.^{\circ}3$. The lambda angles are measured from a line that joins the center of the donor with the center of the gainer, in the opposite direction to the orbital motion, and the theta angle measures the angular extension of the spots. For a comprehensive treatment, the size, position, and temperature of the spots are calculated, for further details, see the work of (Djurašević, 1992a). Due to the inclination of the system ($68.^{\circ}3 \pm 0.^{\circ}3$), it was necessary to assume that it is the disk that is hidden during the eclipse, which can lead to the exposed errors being less than the possible real errors. The system exhibits active mass transfer, generating thermal irregularities in the disk. In this context, the hot spot is defined as the localized region of high temperature produced by the direct impact of the mass flow from the Lagrange point on the accretion disk, while the bright spot corresponds to an extended, luminous region associated with the redistribution and dissipation of energy along the disk's edge. The high temperature and large size of the bright spot suggest that the disk is not a uniform structure, but rather possesses zones of intense energy release, likely originating from complex hydrodynamic processes. The inclination of $68.^{\circ}3$ indicates that we are observing the system almost edge-on, allowing the disk to partially obscure the light from the stellar components.

Table 3.1.4: Results of the analysis of V1001 Cen ASAS V band light curves.

Quantity	Vband	Quantity	
n	578		
$\Sigma(\mathrm{O}-\mathrm{C})^2$	0.9197		
σ_{rms}	0.0399		
$q=\mathcal{M}_{\mathrm{c}}/\mathcal{M}_{\mathrm{h}}$	0.20		
$i[^\circ]$	68.3 ± 0.3		
$\mathrm{F_d}$	0.967 ± 0.01		
$\mathrm{T_d[K]}$	7415 ± 50		
$\mathrm{d_e}[a_{\mathrm{orb}}]$	0.048 ± 0.01		
$\mathrm{d_c}[a_{\mathrm{orb}}]$	0.051 ± 0.01		
$\mathrm{a_T}$	0.69 ± 0.02	$\mathcal{M}_{\mathrm{h}}[\mathcal{M}_\odot]$	4.25 ± 0.1
$\mathrm{F_c}$	1.000	$\mathcal{M}_{\mathrm{c}}[\mathcal{M}_\odot]$	0.85 ± 0.1
$\mathrm{T_h[K]}$	18310 ± 500	$\mathcal{R}_{\mathrm{h}}[\mathrm{R}_\odot]$	2.68 ± 0.1
$\mathrm{T_c[K]}$	8750	$\mathcal{R}_{\mathrm{c}}[\mathrm{R}_\odot]$	6.47 ± 0.1
$\mathrm{A_{hs}}=\mathrm{T_{hs}}/\mathrm{T_d}$	1.32 ± 0.04	$\log\ g_{\mathrm{h}}$	4.21 ± 0.1
$\theta_{\mathrm{hs}}[^\circ]$	21.6 ± 1.2	$\log\ g_{\mathrm{c}}$	2.75 ± 0.1
$\lambda_{\mathrm{hs}}[^\circ]$	326.9 ± 3.0	$M^{\mathrm{h}}_{\mathrm{bol}}$	-2.36 ± 0.1
$\theta_{\mathrm{rad}}[^\circ]$	27.2 ± 3.0	$M^{\mathrm{c}}_{\mathrm{bol}}$	-1.07 ± 0.1
$\mathrm{A_{bs1}}=\mathrm{T_{bs}}/\mathrm{T_d}$	1.38 ± 0.04	$a_{\mathrm{orb}}[\mathrm{R}_\odot]$	25.80 ± 0.2
$\theta_{\mathrm{bs}}[^\circ]$	49.5 ± 1.3	$\mathcal{R}_{\mathrm{d}}[\mathrm{R}_\odot]$	13.22 ± 0.1
$\lambda_{\mathrm{bs}}[^\circ]$	172.7 ± 8.0	$\mathrm{d_e}[\mathrm{R}_\odot]$	1.25 ± 0.1
Ω_{h}	11.948	$\mathrm{d_c}[\mathrm{R}_\odot]$	1.32 ± 0.1
Ω_{c}	2.233		

Notes. The results of the analysis were obtained from solving the inverse problem for the Roche model with an large accretion disk partially obscuring the more massive (hotter) gainer in critical nonsynchronous rotation regime.
FIXED PARAMETERS:

- $q=\mathcal{M}_{\mathrm{c}}/\mathcal{M}_{\mathrm{h}}=0.20$ - mass ratio of the components.
- $\mathrm{T_c}=8750\mathrm{K}$ - temperature of the less massive (cooler) donor.
- $\mathrm{F_c}=1.0$ - filling factor for the critical Roche lobe of the donor.
- $f_{\mathrm{h}}=20.0; f_{\mathrm{c}}=1.00$ - nonsynchronous rotation coefficients of the gainer and donor respectively.
- $\beta_{\mathrm{h}}=0.25; \beta_{\mathrm{c}}=0.25$ - gravity darkening coefficients of the gainer and donor.
- $\mathrm{A_h}=1.0; \mathrm{A_c}=1.0$ - albedo coefficients of the gainer and donor.

Quantities:

- n - number of observations.
- $\Sigma(\mathrm{O}-\mathrm{C})^2$ - final sum of squares of residuals between observed (LCO) and synthetic (LCC) light curves.
- σ_{rms} root mean square of the residuals.
- $q = \mathcal{M}_{\mathrm{c}}/\mathcal{M}_{\mathrm{h}}$ - mass ratio of the components.
- i - orbit inclination (in arc degrees).
- $\mathrm{F_d} = \mathrm{R_d}/\mathrm{R_{yc}}$ - disk dimension factor (ratio of the disk radius to the critical Roche lobe radius along y axis).
- $\mathrm{T_d}$ - disk edge temperature.
- $\mathrm{d_e}$, $\mathrm{d_c}$ - disk thicknesses (at the edge and at the center of the disk, respectively) in the units of the distance between the components.
- a_{T} - disk temperature distribution coefficient.
- $\mathrm{F_h} = R_h/R_{zc} = 1.0$ - filling factor for the critical nonsynchronous lobe of the hotter, more massive gainer (ratio of the stellar polar radius to the critical nonsynchronous lobe radius along z axis for a star in critical rotation regime).
- $\mathrm{T_h}$ - temperature of the more massive (hotter) gainer.
- $\mathrm{A_{hs,bs}} = \mathrm{T_{hs,bs}}/\mathrm{T_d}$ - hot and bright spots' temperature coefficients.
- $\theta_{\mathrm{hs,bs}}$ and $\lambda_{\mathrm{hs,bs}}$ - spots' angular dimensions and longitudes (in arc degrees).
- θ_{rad} - angle between the line perpendicular to the local disk edge surface and the direction of the hot spot maximum radiation.
- $\Omega_{\mathrm{h,c}}$ - dimensionless surface potentials of the hotter gainer and cooler donor.
- $\mathcal{M}_{\mathrm{h,c}}[\mathcal{M}_\odot]$, $\mathcal{R}_{\mathrm{h,c}}[\mathrm{R}_\odot]$ - stellar masses and mean radii of stars in solar units.
- $\log g_{\mathrm{h,c}}$ - logarithm (base 10) of the system components effective gravity.
- $M_{\mathrm{bol}}^{\mathrm{h,c}}$ - absolute stellar bolometric magnitudes.
- a_{orb} $[\mathrm{R}_\odot]$, $\mathcal{R}_{\mathrm{d}}[\mathrm{R}_\odot]$, $\mathrm{d_e}[\mathrm{R}_\odot]$, $\mathrm{d_c}[\mathrm{R}_\odot]$ - orbital semi major axis, disk radius and disk thicknesses at its edge and center, respectively, given in the solar radius units.

3.1.1.6 TESS photometric data and comparison with ASAS

The *TESS* satellite (Transiting Exoplanet Survey Satellite) performs a nearly all sky photometric survey in the near optical band, observing most of the sky in sectors of approximately 27-28 days, providing a temporal coverage of about one month for the V1001 Cen system. TESS photometry is of very high precision: according to Ricker et al. (2015), TESS is expected to achieve a photometric precision of 60 ppm on hourly timescales for bright stars. In fact, thousands of high quality light curves for eclipsing binary systems have been published thanks to TESS observations (Prša et al., 2022; Ricker et al., 2015).

In contrast, the ASAS instrumentation provides photometry in V and I bands to a relative accuracy of 0.01-0.02 mag. for stars brighter than 10th magnitude (Pojmański, 2001). Its cadence is one or two points per night, which allows one to trace light curves of long period systems, albeit with a significantly higher dispersion than TESS. Due to its limited temporal coverage ($\sim$ 27 days), TESS data do not allow for the derivation of long term parameters such as modulation cycles or long periods.

To assess the compatibility between both datasets, we fit a Fourier series to the ASAS light curve, as shown in Figure 3.1.9. This fit curve (red line) was then compared with the TESS data (blue points) for the same system. We find that the ASAS based fit reproduces the TESS light curve with very good agreement; the differences are minimal and limited primarily to slight variations in the depth of the secondary eclipse. In other words, the light curve models fit to ASAS data reproduce the main features also observed by TESS.

Therefore, it is not strictly necessary to recalibrate a new light curve synthesis model based solely on the TESS data. The photometric model derived from ASAS data is fully compatible with TESS photometry within the expected uncertainty, indicating that the fundamental eclipse properties (phase, shape, and duration) are preserved. Nevertheless, the higher photometric precision and continuous coverage of TESS could allow for refinement of some sensitive parameters, such as the depth of the secondary eclipse or the size of the accretion disk. However, these adjustments would not significantly affect the other physical parameters derived in the synthesis model discussed in (3.1.1.5).

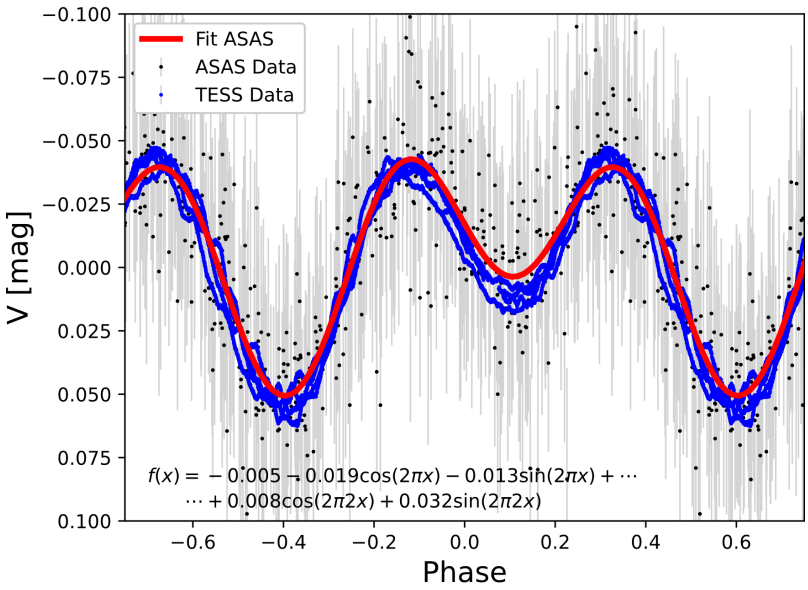

Figure 3.1.9: Light curve of V1001 Cen derived from ASAS data (black points) and TESS data (blue points). The red line corresponds to a Fourier series fit to the ASAS data. A good agreement is observed between the fit function and the TESS photometry, indicating consistency between both datasets.

Furthermore, using the TESS data, we plotted a periodogram using the Lomb Scargle method from the gatspy python library to investigate the possible presence of other significant periodicities in the TESS data, as shown in Figure 3.1.10. The resulting periodogram shows that the dominant periodicity corresponds to the known orbital period, previously derived from the ASAS dataset. No additional significant periods were detected within the time span covered by TESS. This result supports the consistency between the ASAS and TESS datasets, reinforcing the conclusion that the ASAS photometry captures the essential periodic features of the system, also observed in the high precision TESS data.

3.1.2 The spectral distribution of energy and the circumstellar disk for V1001 Cen

o construct the spectral energy distribution (SED) of V1001 Cen, we compiled the available photometric fluxes for this system. We extracted this information from the Vizier photometric viewer. We selected theoretical models of individual stars using

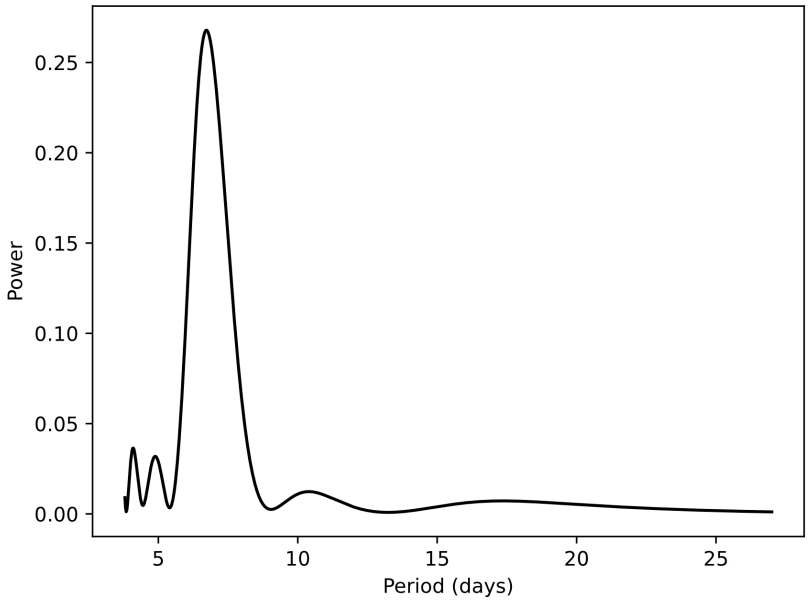

Figure 3.1.10: Periodogram of the TESS data for V1001 Cen. The periodogram reveals a dominant period consistent with the previously determined orbital period from ASAS data. No additional significant periodic signals are detected.

the Virtual Observatory SED Analyzer (VOSA; (Bayo et al., 2008)) to perform a fit to the SED. This fit allowed us to determine the albedo of the system's accretion disk. For this process, we kept the distances provided by Gaia DR3[11] fixed. Given the high accuracy of the Gaia satellite's distance measurements, this parameter is assumed to be a fixed value in our analysis. Our models were centered using parameters from (3.1.1.5), specifically: a cool star with an effective temperature ($T_{\rm eff,c}$) of 8750 K and a surface gravity ($\log g_{\rm c}$) of 3 dex, an $T_{\rm eff}$ for the hot star (T_h) of 18,000 K, and a ($\log g_{\rm h}$) of 4.0 dex. Furthermore, we considered an interstellar reddening value of $E(B-V) = 0.6351 \pm 0.0292$ (mag) ((Schlafly and Finkbeiner, 2011)) We consider this value as a constant in the model, taking advantage of the precision of these galactic dust maps to avoid degenerations with the effective temperature. The model that best fits our data is the one that minimizes the reduced χ^2, considering the composite flux described by the following equation (Fitzpatrick and Massa, 2005):

$$f_\lambda = f_{\lambda,0} 10^{-0.4E(B-V)[k(\lambda-V)+R(V)]}. \tag{3.1.6}$$

[11] https://gea.esac.esa.int/archive/

In this equation, $E(B-V)$ represents the color excess, which quantifies how much the star's light has been reddened due to interstellar dust. The term $k(\lambda - V) \equiv E(\lambda - V)/E(B-V)$ is the normalized extinction curve, which describes how extinction varies as a function of wavelength (λ) relative to the V band. On the other hand, $R(V) \equiv A(\lambda)/E(B-V)$ is the ratio between the total extinction ($A(\lambda)$) and the reddening in the V band. The term $f_{\lambda,0}$ corresponds to the sum of the intrinsic surface fluxes of both stars at wavelength λ, before being affected by interstellar reddening, and is calculated as:

$$f_{\lambda,0} = \left(\frac{R_c}{d}\right)^2 \left[\left(\frac{R_h}{R_c}\right)^2 f_{h,\lambda} + f_{c,\lambda}\right] + \left(\frac{R_{disk}}{d}\right)^2 f_{disk,\lambda}, \tag{3.1.7}$$

where $f_{h,\lambda}$ and $f_{c,\lambda}$ represent the fluxes of the hotter and cooler star, respectively, and $f_{disk,\lambda}$ the flux corresponding to the accretion disk. The normalized extinction curve $k(\lambda - V)$ was calculated using the prescriptions described in Martin and Whittet (1990) and Cardelli et al. (1989).

In essence, we analyzed the light reaching us from V1001 Cen in different colors (photometric fluxes) and compared it with the light predicted by theoretical models of two stars. To make this comparison accurately, we took into account the distance to the system, obtained from the high precision data of Gaia DR3. Furthermore, we corrected for the effects of interstellar dust, which alters the colors of starlight. The equation used to model the total flux considers the contribution of both stars, taking into account their relative sizes (R_c and R_h relative to the distance d) and their intrinsic fluxes at each wavelength. The best model is the one that, after applying the correction for interstellar reddening, most faithfully reproduces the observed fluxes, which is quantified by minimizing the reduced χ^2. This process allowed us to obtain valuable information about the system's properties, including the albedo of its accretion disk.

To define this contribution, we used expression (5.9) from (Frank et al., 2002):

$$F = \frac{L_\star}{4\pi R^2}(1-\beta)\cos\varphi, \tag{3.1.8}$$

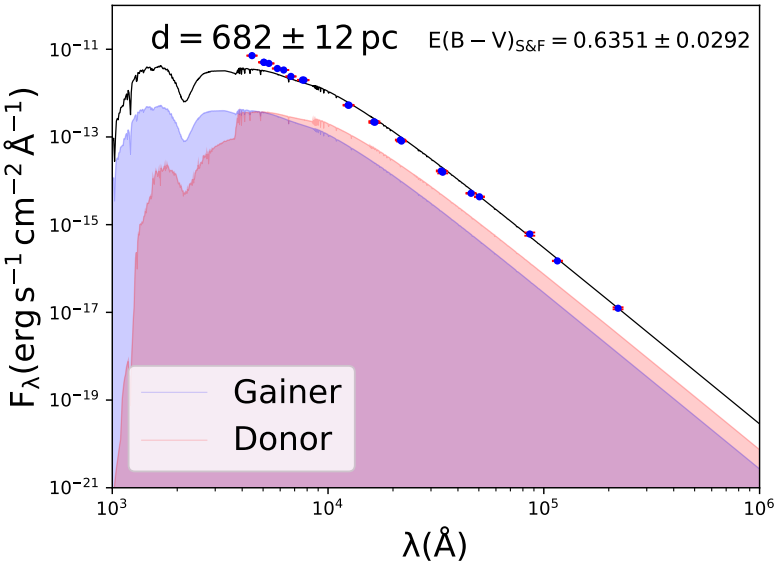

Figure 3.1.11: Spectral energy distribution and the best χ^2 minimization.

where

$$L_\star = 4\pi R_\star^2 \sigma T_\star^4. \tag{3.1.9}$$

combining the two previous expressions, we obtain.

$$F = 4\pi R^2 \frac{\sigma T_\star^4}{4\pi R_\star^2}(1-\beta)\cos(\varphi) = \sigma T_\star^4 \left(\frac{R}{R_\star}\right)^2 (1-\beta)\cos(\varphi), \tag{3.1.10}$$

which shows that the disk flux is directly related to $F \propto T_{star}^4$, with $T_\star$ being the temperature of the accretor. This allowed us to model the additional flux contribution in the theoretical equation of the spectral flux as a percentage of the accretor's flux. This percentage factor $(1-\beta)\cos\varphi$, which represents the disk albedo, is parameterized as part of Equation 7. From the disk thickness data extracted from Table 4, we can estimate the factor $\cos\varphi \approx 1$, whereby our albedo factor mainly depends on $(1-\beta)$. For our minimization of $(1-\beta)$, this factor was a free parameter that varied in the range of 0 to 1. And for our case, the best fit is $(1-\beta) = 0.34$. Fig. 3.1.11 shows the best χ^2 minimization found to represent the SED of V1001 Cen.

For the value of the fractional radius of the gaining object, $R_1/a = 0.1$, it has been found that there is enough space for the formation of an accretion disk, considering the mass ratio of the system. In this case, the star acting as a mass receiver is smaller than the circularization radius, where a particle released from the inner Lagrangian point can conserve its angular momentum (Lubow and Shu, 1975). This low fractional radius is attributed to the separation and orbital period of the system, which is consistent with the existence of an accretion disk inferred from the light curve model. Furthermore, the calculated value is similar to that obtained in long period systems such as V495 Cen (Rosales et al., 2019a, 2021). Note that the vertical height of the disk near the receiving object is approximately half the radius of the receiving object, causing partial occultation of the star.

Under hydrostatic equilibrium conditions, the vertical height, H, of a disk of radius R, in chapter 3 of the book (Kolb, 2010) it is defined as:

$$H = 10^4 \sqrt{\frac{T}{10^4\, K}} \sqrt{\frac{R^3}{GM_1}}\, [ms^{-1}] \tag{3.1.11}$$

The above equation predicts that for V1001 Cen, a disk in hydrodynamic equilibrium would have a relative thickness H/R of 0.10 and $H = 9.47 \times 10^8$ m, indicating a thin disk. The data in Table 3.1.4 confirm this prediction: the disk thickness at the edge ($d_e/R = 0.09$) is close to the theoretical value, suggesting a low thermal pressure disk in hydrodynamic equilibrium. However, in the immediate vicinity of the star, the disk widens significantly ($d_c/R = 0.49$), covering almost half of the stellar radius. This fivefold increase in thickness cannot be explained by a temperature rise alone, as the thermal conditions of the disk do not justify such a dramatic expansion. Instead, this behavior can be attributed to the presence of turbulent motions within the disk, which increase the velocities beyond those expected for a Keplerian disk in thermal equilibrium. These turbulent motions enhance the vertical support of the disk, leading to the observed increase in the H/R ratio near the star.

Theoretically, the disk could be stable until reaching the tidal radius (Paczynski, 1977; Warner, 2003), which defines the last nonintersecting orbit:

$$\frac{R_t}{a_{orb}} = \frac{0.6}{1+q} = 0.5. \tag{3.1.12}$$

We have compiled the outer disk radii and the primary star radii for the DPV systems from Table 12 of the Mennickent et al. (2016a) paper. These radii, relative to the binary separation, are plotted in Fig. 3.1.12. The plot R_1/a versus q has previously been used to differentiate between Algol systems with and without disks (Plavec, 1989; Vanbeveren, 2013), and the observation of V1001 Cen is highlighted in Fig. 3.1.12. Based on those authors, three theoretical radii that are widely used to understand disk dynamics and mass transfer in binary systems are included in this analysis.

The first radius is the critical radius, defined by Lubow and Shu (1975) and approximated by Hessman and Hopp (1990):

$$\frac{r_c}{a} = 0.0085 q^{-0.426}. \tag{3.1.13}$$

This critical radius represents the maximum limit for the size of the primary star that allows the formation of an accretion disk. At this point, the specific angular momentum of a particle orbiting the critical radius is equal to that of a particle released from the inner Lagrangian point, L_1. This implies that the critical radius marks the maximum extent of a ring of matter that can form due to the Roche lobe overflow just before viscosity begins to expand the material into a disk. If the radius of the primary star exceeds this limit ($R_1 > r_c$), the system is classified as an impact system, where the gas flow hits the star directly, significantly reducing the chances of formation of accretion disks.

In real systems, because of the finite size of the gas flow, it is still possible for some outer orbits of the gas stream to escape the direct impact. This phenomenon generates a maximum effective radius, r_{max}, which is slightly larger than r_c and depends on the mass ratio q of the system (Lubow and Shu, 1975). This limit is also included in Fig. 3.1.12 to provide a more complete representation.

The second key radius is the tidal radius, derived by Paczynski (1977) and Warner (2003):

$$\frac{r_{tidal}}{a} = \frac{0.6}{1+q}. \tag{3.1.14}$$

This radius defines the last nonintersecting orbit of the accretion disk. It is assumed that, as the disk grows, it begins to experience strong shear forces as a result of gravitational and viscous interactions. Therefore, the tidal radius sets an upper limit for the size of the disk, beyond which the disk material is significantly perturbed or redistributed.

The combination of these three theoretical radii (the critical radius, the maximum radius, and the tidal radius) provides a comprehensive view of the dynamical configurations possible in binary systems. These limits help characterize the mass transfer and accretion disk structure, key elements in the evolution of binary stellar systems.

For the case of the V1001 Cen gainer with a value of R_1/a slightly lower than r_c as seen in Fig. 3.1.12, it would indicate that the mass flow does not reach the star and collides with itself at a larger radius. The radial motion dissipates and the resulting ring of material spreads viscously to form an accretion disk. It should be noted that the disk has an extension comparable to the tidal radius, its maximum possible boundary.

The gainer star has a mass of 4.25 solar masses and a temperature of 18,310 K. This temperature is unusually high for a star with this mass. A plausible interpretation is that the elevated temperature is related to the effects of ongoing mass accretion. In particular, accretion may alter the thermal structure of the stellar envelope, leading to departures from thermal equilibrium and an apparent increase in the effective temperature. Additionally, variations in surface composition, such as a lower effective metallicity in the outer layers, could reduce atmospheric opacity and enhance the emergent flux.

An alternative, non-exclusive explanation is that the derived temperature does not correspond to a purely stellar photosphere, but instead reflects the presence of circumstellar material contributing to the observed spectrum. In this context, the formation of a pseudo-photosphere associated with the accretion flow or boundary

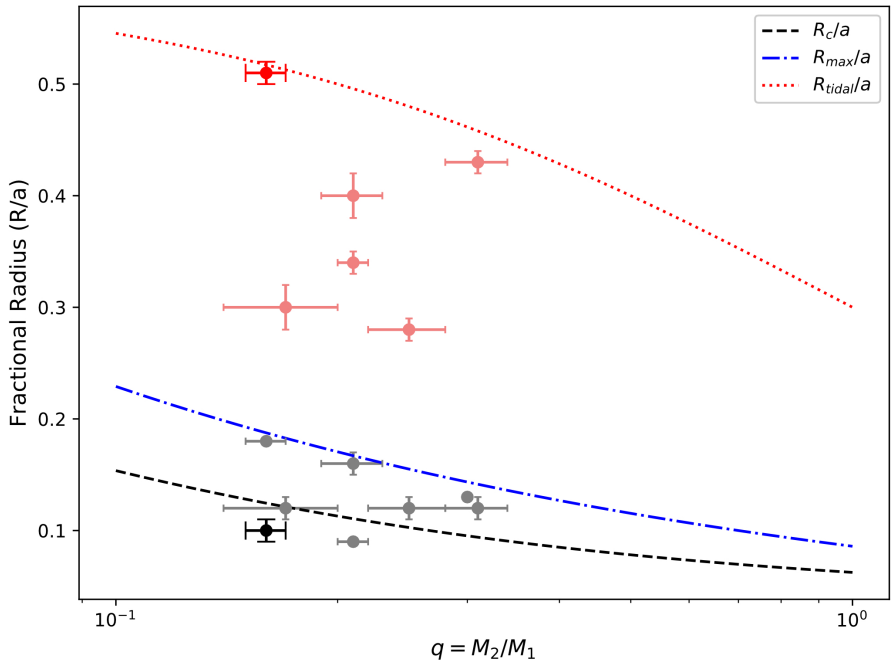

Figure 3.1.12: Relative radius for the Gainer R_1/a (black dot) and disk (R_d/a (red dot) of V1001 Cen, the gray dots are other DPVs extracted from Table 12 of Mennickent et al. (2016a), and the pink dots represent their disks. Below the circularization radius shown by the dashed black line a disk should form and below the dashed blue line a disk could form. The tidal radius indicates the maximum possible extent of the disk.

layer could lead to an overestimation of the stellar effective temperature.

Observational evidence for this type of configuration has been reported in other Double Periodic Variables, such as AU Monocerotis (Armeni and Shore, 2022). In that system, the analysis of ultraviolet and optical spectral lines indicates that several absorption features, including Balmer and Mg II 4481 Å lines, are not purely photospheric but have a significant circumstellar contribution, particularly during the weak states of the long cycle. Furthermore, UV resonance lines (e.g., Mg II, Al II, and Si II) are predominantly formed in the accretion disk. These results support the presence of a stratified circumstellar environment and an optically thick boundary layer around the gainer.

In this context, the high temperature derived for the gainer in V1001 Cen may be affected by similar processes. However, a quantitative assessment of these effects would require detailed spectroscopic modelling capable of disentangling the stellar and circumstellar contributions, which is beyond the scope of the present work.

3.1.3 Evolutionary modeling of V1001 Cen with `MESA`

Paxton et al. (2015) introduced a new module in `MESA` called `MESA`binary, which allows for the simultaneous evolution of pairs of stars that rotate differentially, greatly enhancing the model's ability to simulate binary evolution. The inclusion of this module in `MESA` expands the possibilities for exploration in the field of astrophysics, allowing researchers to model binary systems with greater precision and their complex interactions.

For further details, the reader is referred to the features and functionalities of `MESA`, see sections 2.2.2 of the theoretical framework and their cited references.

For our evolutionary models of binary systems, we use the `MESA` code version 22.11.1. Given that V1001 Cen is classified as a DPV system, we chose to use a formulation of the `MESA` code previously developed by Rosales et al. (2019a) to study the DPV V495 Cen, and in his most recent study of the V4142 Sgr ((Rosales et al., 2024)). In his most recent model, Rosales develops an intermediate mass binary system where the gainer star is constrained by the Eddington accretion rate, preventing high rate

Table 3.1.5: Evolutive stages from the donor star for DPV V1001 Cen.

Stage	Age (Myr)	M ($M_\odot$)	R ($R_\odot$)	log T (K)	$\dot{M}$ ($M_\odot yr^{-1}$)	Ev. Process
A	0.000	4.399	2.523	4.196	2.15E-11	Zero Age Main Sequence, Hydrogen burning.
B	30.000	4.399	2.759	4.183	1.79E-11	Terminal age main sequence
C	132.359	4.386	5.943	4.078	9.71E-07	Mass transfer.
D	132.393	4.064	4.435	3.838	3.07E-05	Central hydrogen depletion.
U_1	132.400	3.863	3.826	3.818	3.56E-05	Inversion masses.
E	132.552	1.467	3.399	3.787	3.93E-06	Minimun value Roche lobe.
F	147.785	1.193	4.137	3.883	1.37E-09	End of the first phase of mass transfer.
G	184.000	1.157	3.777	3.951	8.26E-11	Start of the secondphase of mass transfer.
X_2	190.675	0.806	6.563	3.931	1.13E-07	Present stage.
H	192.982	0.482	12.848	3.868	2.77E-08	End of the secondphase of mass transfer.

accretion. Eventually, the donor star fills the Roche lobe, triggering a significant mass transfer and the formation of an accretion disk. This approach aims to replicate the physical conditions under which these stellar systems are believed to exist.

The formalism proposed by Rosales et al. (2024, 2019a) introduces certain initial parameters that are modified compared to the default parameters used by `MESA`. Here, we succinctly outline these parameter adjustments. Our initialization of our `MESA` model incorporates a metallicity value of $Z = 0.02$, this metallicity value was used because V1001 Cen is located within the disk of our galaxy, and $Z = 0.02$ is usually the classical reference value to represent stars with solar metallicity. In turn, a initial surface rotation velocity of 26 kms^{-1} for the donor star, aimed at activating the magnetic dynamo mechanism defined by the Spruit Tayler paradigm, which we present in subsection 2.2.2.3, with a mixing diffusivity value of Spruit Tayler $D_{ST} = 0.1$.

Our models employ the mass transfer scheme of Kolb and Ritter (1990). In seeking a conservative approach, we explored a range of values for the mass loss fractions through winds. For the fraction of mass lost from the vicinity of the donor as a fast wind (α), we varied the values between $0.0005 \leq \alpha \leq 0.5$ with increments of 0.001. Similarly, for the fraction of mass lost from the vicinity of the accretor as a fast wind (β), we explored the range $0.0001 \leq \beta \leq 0.1$ with a step of 0.0001. Following this exploration, we determined that the values of $\alpha = 5 \times 10^{-3}$ and $\beta = 1 \times 10^{-4}$ were

the most suitable for maintaining a conservative system in our simulations, thereby minimizing mass loss during the transfer events and favoring the reproduction of a conservative system. Additionally, we incorporate Reimers prescription for mass loss during the RGB phase[12], utilizing the scale factors of $w_{c,R} = 0.8$ and Blocker's definition during the AGB phases with $w_{c,B} = 1.0$. Furthermore, the loss attributed to a hot wind employs a Dutch type scheme with $w_{h,D} = 0.8$.

For convection, we adopt the theory proposed by Henyey et al. (1965). Our models include the usage of Rosseland radiative opacity values for high temperatures, while the OPAL opacity tables[13] (Iglesias and Rogers, 1993, 1996), particularly Type 1, are integrated for temperatures exceeding 10^4 K. To extend capabilities, we enable the Type 2 OPAL tables essential for helium burn and beyond.

Overshooting in `MESA` depends on the classification of the convective zone, with variability at the top and bottom of the zone. The parameters for exponential diffusive overshoot are elucidated by Herwig (2000) in his paper "The Evolution of Convective Overshoot AGB Stars".

A critical aspect of overshooting control involves aligning the convective zone and the convection limit criteria. This necessitates defining the "overshoot_zone_type," "overshoot_zone_loc," and "overshoot_bdy_loc" for each convective boundary, along with relevant overshoot parameter values. In the Rosales model, the types of overshoot zone are specified for H, He, and Z, accompanied by the location of the overshoot zone for the shell and core, and the location of the overshoot boundary for both the upper and lower limits. The transition from convective mixing to overshooting occurs at a distance of $(\mathrm{f0} \cdot \mathrm{Hp})$ within the convection zone from the estimated position, with Hp signifying the height of the pressure scale at that location.

In `MESA`, overshooting is achieved by extrapolating the diffusion mixing coefficient beyond the edge of the convection zone. However, precisely at the edge of the zone,

[12]The Red Giant Branch (RGB) is the evolutionary stage following the main sequence for low-to-intermediate-mass stars. The Asymptotic Giant Branch (AGB) is a late evolutionary stage of all low-to-intermediate-mass stars (0.6 to 10 $M_\odot$).

[13]The OPAL opacity tables, developed by the Lawrence Livermore National Laboratory (LLNL), provide Rosseland mean opacity coefficients calculated from a detailed physical equation of state. https://opalopacity.llnl.gov/existing.html

the mixing coefficient drops to zero, which is suboptimal. To address this concern, the parameter $f0$ designates the distance from the edge where the overshooting begins. In addition, the code accommodates the specification of how far back into the zone the overshooting should extend, denoted in terms of scale height. Essentially, the overshooting starts at a location determined by $f0$, some distance before the edge of the actual convection zone. For this study, "$f0$" was established at 0.0005, and "f" was established at 0.001. Readers interested in a more comprehensive explanation of the `MESA` formalism used in this study are encouraged to review subsection 2.2.2 and the papers (Rosales et al., 2024, 2019a)

We conducted tests on initial masses ranging from 1.0 to 5.0 solar masses, and mass ratios (q) ranging from 0.9 to 0.3. The initial periods ranged from 1.0 to 3.0 days. The initial eccentricities were set to zero. All models were initiated from the main sequence and stopped when the donor star depleted its core helium ($X_{^4He_c}$) or until the end of the evolutionary time step.

Following Mennickent et al. (2012b), a multiparametric fit was performed with the synthetic stellar parameters ($S_{i,j,k}$) and observed (O_k), including mass, temperature, luminosity, radii and orbital period. The parameters were derived from `MESA` models, where i (ranging from one to n) indicates the model number, j (ranging from one to m) represents the step number within each model, and k (ranging from one to nine) denotes the stellar or orbital parameter.

$$\chi^2_{i,j} \equiv (1/N) \sum_k \omega_k [(S_{i,j,k} - O_k)/O_k]^2, \tag{3.1.15}$$

where N is the number of observations (9) and ω_k is the statistical weight of the parameter O_k, calculated as

$$\omega_k = \sqrt{O_k/\epsilon(O_k)}. \tag{3.1.16}$$

The error associated with the observable O_k is represented by the variable $\epsilon(O_k)$. From the light curve synthesis study, we observed that the gainer has an accretion disk that dominates its luminosity. This causes the observed brightness of the gainer

Table 3.1.6: Values for the conditions of the long period for the V1001 Cen.

Evolutionary state in the model	CV (ms^{-1})	D	Ro	α	P_l (d)	P_o (d)
Minimum value Roche lobe	6330.99	1774.19	0.02	0.48	50.30	1.37
Current evolutionary state	7884.74	153.06	0.08	0.71	248.03	6.75

Notes. The factor CV is the convective velocity, D is the number of dynamo, Ro is the Rossby number and α is a power law index.

to be much higher than predicted by the `MESA` models. Therefore, for the parametric adjustment, we consider the observed physical values of the donor and the gainer.

Our model aims to identify the best fit, and we calculate the value of χ^2 for each model. In the case of conservative models (without mass loss during the transfer phase) with the lowest $\chi^2 = 0.29$, the best fit suggests that the initial parameters of the binary system are an orbital period of $P_{i,o} = 2.1$ days, donor star mass of $M_{d,i} = 4.4\,M_\odot$, and gainer star mass of $M_{g,i} = 1.4\,M_\odot$. The system is found in the rapid mass transfer phase, in an almost conservative mass transfer stage with $\dot{M} = 1.13 \times 10^{-7}\,M_\odot yr^{-1}$, and an age of 190 Myr.

The HR diagram for the conservative model is shown in Fig. 3.1.13. The evolution of stars in the V1001 Cen system begins in the initial main sequence (ZAMS), with hydrogen burning, marked as point A. During this phase, the donor star maintains a mass of 4.399 $M_\odot$ and a radius of $2.523\,R_\odot$ while its core burns hydrogen and produces helium. This initial process allows the star to retain its stellar parameters without significant changes until it reaches an age of 132.359 Myr, at which point the mass transfer process (point C) begins. In this phase, the donor star begins to expand and transfer mass to its companion, causing a gradual decrease in its central hydrogen.

When the central hydrogen of the star reaches low values (point D), its mass is reduced to 4.064 $M_\odot$. At this stage, the mass transfer process intensifies, allowing the system to reach a mass reversal state (point U1) at an age of 132,400 Myr, when the donor mass drops to 3.863 $M_\odot$. Consequently, the system undergoes a rapid evolution in luminosity and temperature. Subsequently, the donor star reaches the minimum value of its Roche lobe (point E) at 132.552 Myr, with a mass of 1.467 $M_\odot$. This marks the beginning of a further expansion phase, which finally culminates at

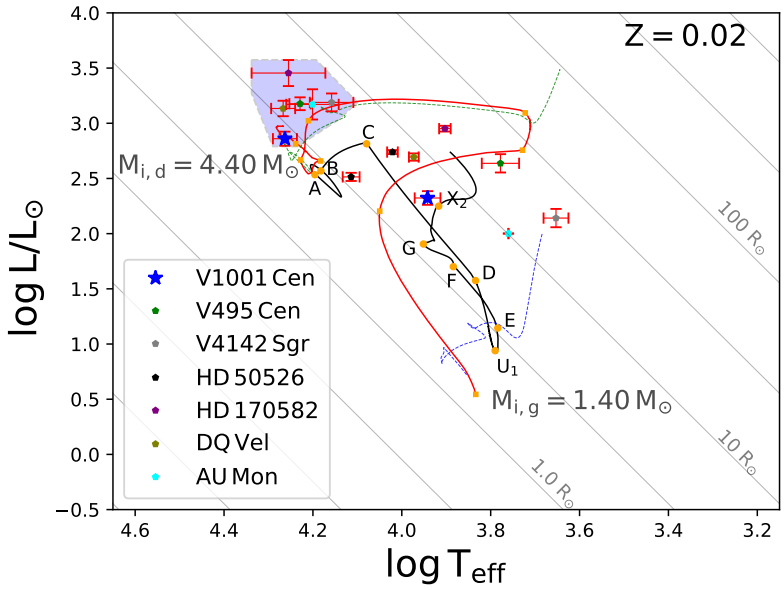

Figure 3.1.13: Evolutionary model with conservative mass transfer for V1001 Cen. Initial orbital period of 2.1 days, initial masses of 4.4 and 1.4 $M_\odot$. The dashed lines represent the evolutionary paths of single stars with initial masses equal to those of the binary model, the other points represent other known DPVs.

the end of the first mass transfer phase (point F), at 147,785 Myr.

Upon reaching 184 Myr (point G), the donor star enters a second phase of mass transfer, and its mass decreases even further, reaching a value of 1.157 $M_\odot$, while its radius contracts to 3.777 $R_\odot$. Finally, in the current stage (point X2) at 190.675 Myr, the donor star maintains a mass of 0.806 $M_\odot$ and an extended radius of 6.563 $R_\odot$, evidencing the advanced structural change in its core and envelope. The system reaches the end of its second mass transfer phase (H point) at 192.982 Myr, with a minimum mass of 0.482 $M_\odot$ and an expanded radius at 12.848 $R_\odot$.

The adjustment of the radius, mass, and period of the V1001 Cen system is best represented by this model, allowing for a detailed analysis of these fundamental properties of the system (see Fig. 3.1.14 for period vs. mass, Fig. 3.1.15 for mass vs. radius and Fig. 3.1.16 for mass transfer vs. mass). Furthermore, the distribution of helium and hydrogen in the H-R diagram of V1001 Cen reflects how the transfer of material from the donor star rejuvenates the gainer star (see Fig. 3.1.17).

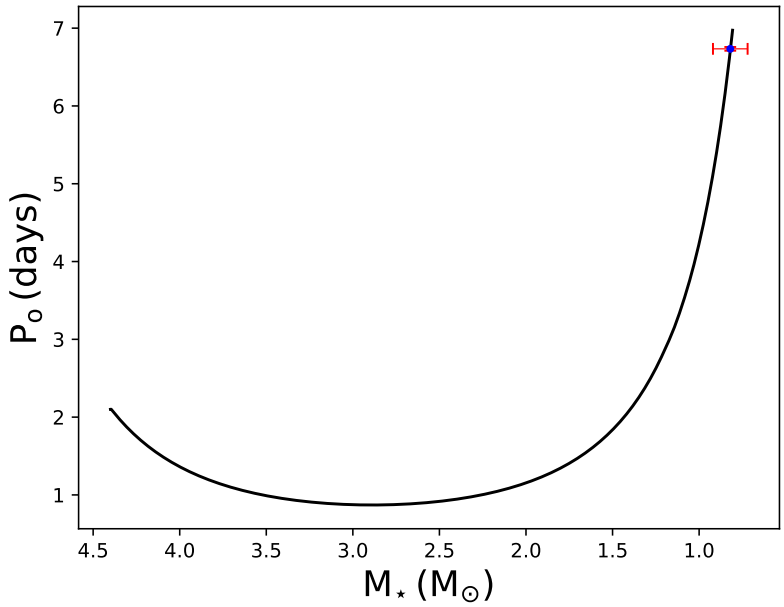

Figure 3.1.14: Evolution of the orbital period as a function of the mass of the donor star of V1001 Cen.

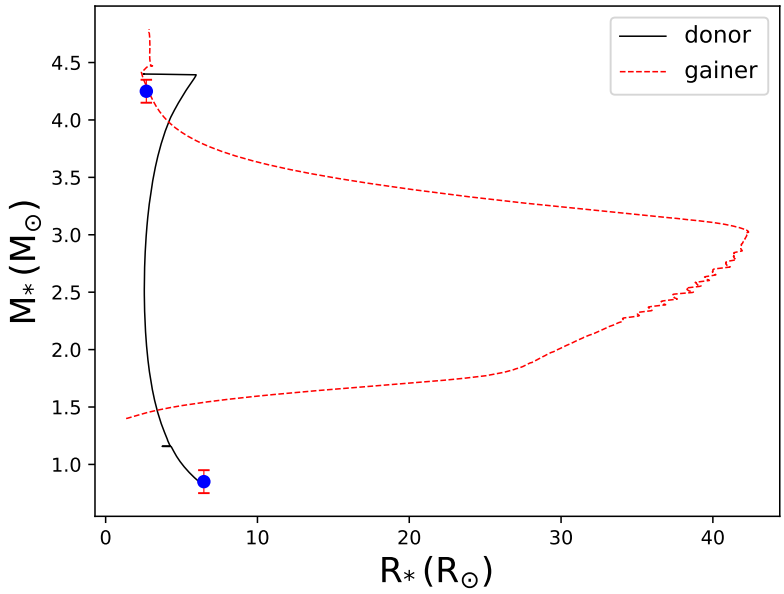

Figure 3.1.15: Schematic behavior of radius and mass for both stars. The gainer star decreases its radius, while the donor star expands to fill the Roche lobe.

The internal structure and evolution of each star in the V1001 Cen system for the conservative model can be visualized using the Kippenhahn diagrams (see Fig. 3.1.18).

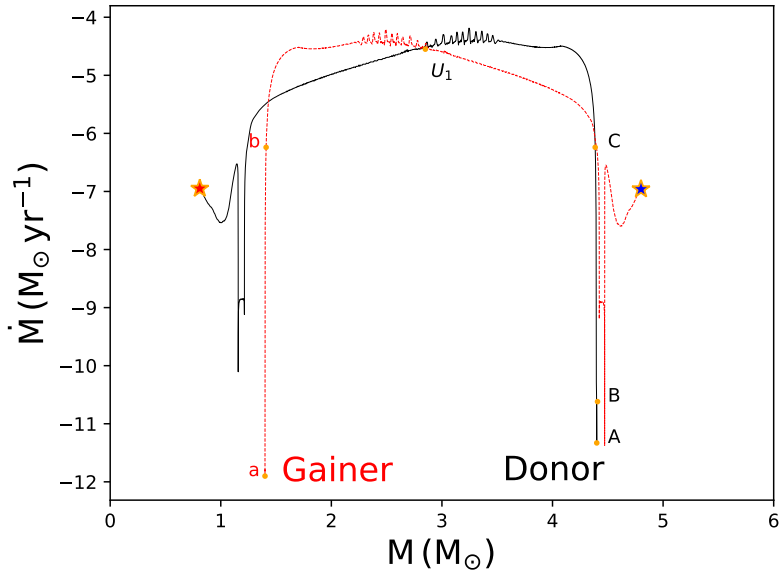

Figure 3.1.16: Theoretical variation in mass transfer until reaching the helium depletion for initial masses of 4.4 and 1.4 $M_\odot$.

The upper diagram represents the evolution of the donor star with an initial mass of $M_{d,i} = 4.4\,M_\odot$, while the bottom one shows the evolution of the gainer star with an initial mass of $M_{g,i} = 1.4\,M_\odot$. Both models are limited to the point where the donor star reaches helium core depletion, with $X_{He_c} < 0,1$. The x axis represents the star's age in units of millions of years.

The different layers are characterized by their $M/M_\odot$ values, with convective mixing shown in dashed green, semiconvective mixing in red, overshooting mixing in dashed violet, thermohaline mixing in dashed yellow, and the continuous black line indicating the surface of each star.

A key objective of this work is to evaluate the magnetic nature of the long cycle observed in DPVs by establishing a physical relationship between the donor's internal dynamics and its period of activity. As previously stated, this relationship is quantified by the equation (2.1.7).

This model helps to understand how the dynamo cycle is intrinsically linked to the orbital period in DPV systems. The convective velocity v_c and the radius of the secondary star are parameters extracted from fit `MESA` models, where v_c is determined

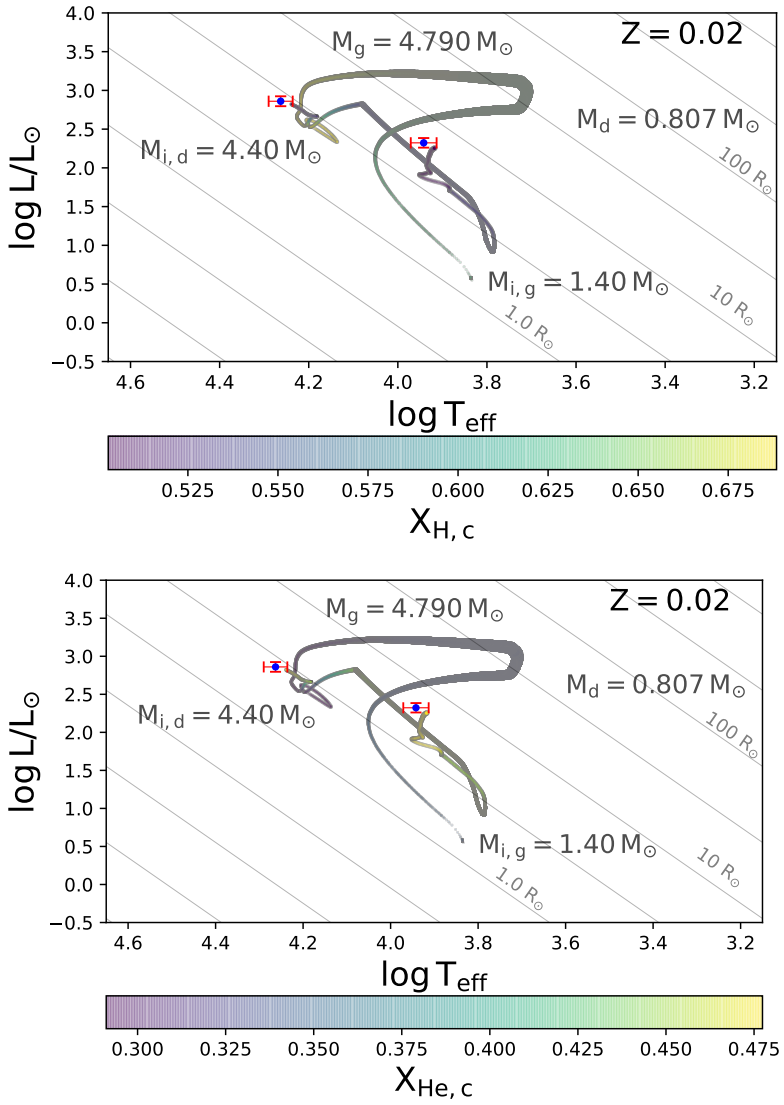

Figure 3.1.17: Hertzsprung Russel (H-R) diagrams illustrate the evolution of binary stars. The color bar indicates the proportion of hydrogen and helium in the core of each star.

as the maximum value in the possible convective regions within the donor star modeled with `MESA`. The Kepler period $P_{\rm Kep}$ is calculated using expression 6 from Schleicher and Mennickent (2017):

$$P_{Kep} = \frac{2\pi}{\omega_{Kep}} = 0.31 \times 2\pi \sqrt{\frac{a^3}{G(M_1 + M_2)}}* \tag{3.1.17}$$

To estimate the value of the dynamo number and therefore the coefficient α, we used the orbital and long periods obtained from photometry. These periods are inserted into equation (2.1.7) to estimate α, whose value, according to Schleicher and Mennickent (2017), should oscillate between 0.33 and 0.83. Table 3.1.6 of the study presents the calculated values of the dynamo number and α for the best fit `MESA` model. In Table 3.1.6, the theoretical values of the short and long periods, estimated using the calculated dynamo number, are also included.

3.2 The case of HD 170582

HD 170582 (ASAS ID 183048-1447.5) is a significant system among Galactic DPVs, notable for possessing an orbital period intermediate in value among those known, with $P_o = 16.87177 \pm 0.02084$ days, and an associated long cycle of $P_l \approx 587$ days. The system operates in a semi-detached Algol type configuration, and its fundamental parameters have been well constrained through detailed photometric and spectroscopic studies (Mennickent et al., 2015).

The system is composed by a donor star (d), cold and evolved of A-giant/supergiant type that fills its Roche lobe. Its key parameters are: $M_2 = 1.9 \pm 0.1$ $M_\odot$, $R_2 = 15.6 \pm 0.2$ $R_\odot$, and $T_2 = 8,000 \pm 100$ K. In addition, the gainer star (g) is a rejuvenated and hot star. This is an early B-type dwarf, with the following parameters $M_1 = 9.0 \pm 0.2$ $M_\odot$, $R_1 = 5.5 \pm 0.2$ $R_\odot$, and $T_1 = 18,000 \pm 1,500$ K, surrounded by an accretion disk. The mass ratio is low, $q = 0.21$. The accretion disk is optically and geometrically thick, and is highly luminous, contributing approximately 35% of the total luminosity in the V band. Its radial extent is considerable, $R_d \approx 20.8 \pm 0.3$ $R_\odot$ (Mennickent et al., 2015).

3.2.1 The fitting procedure of the `MESA` model

Based on the classification of HD 170582 as a DPV system, we adopted the specific `MESA` configuration framework established by Rosales et al. (2019b) for the analysis of V495 Cen, which was also recently applied to V4142 Sgr (Rosales et al., 2024). The grid of evolutionary models covered initial masses between 1.0 and 4.0 solar masses,

with mass ratios (q) ranging from 0.3 to 0.9. We explored initial orbital periods from 1.0 to 5.0 days. Evolution commenced at the zero-age main sequence (ZAMS) and terminated either upon the 8.22 Myr in the donor star or when the simulation reached the end of the time step.

Following the methodology of Mennickent et al. (2012b), we performed a multi-parametric minimization comparing synthetic stellar parameters ($S_{i,j,k}$) against the observed data (O_k). This adjustment is specifically designed to optimize the fundamental properties of the system, namely the mass, temperature, luminosity, radii, and orbital period. In this notation, derived from the `MESA` output, i $(1 \ldots n)$ denotes the specific model track, j $(1 \ldots m)$ represents the time step within the model, and k $(1 \ldots 9)$ identifies the specific physical parameter. The goodness-of-fit statistic is defined as:

$$\chi^2_{i,j} \equiv (1/N) \sum_k \omega_k [(S_{i,j,k} - O_k)/O_k]^2, \tag{3.2.1}$$

where $N = 9$ represents the total number of observations. The statistical weights, ω_k, are inversely proportional to the observational errors, calculated as:

$$\omega_k = \sqrt{O_k/\epsilon(O_k)}. \tag{3.2.2}$$

Here, $\epsilon(O_k)$ represents the uncertainty associated with the observable O_k. Notably, results from light curve synthesis indicate that the gainer's luminosity is dominated by an optically and geometrically thick accretion disk that acts as an extended pseudo-photosphere. This structure reprocesses a significant fraction of the stellar radiation and contributes its own thermal flux, resulting in an observed brightness that significantly exceeds the hydrostatic photospheric predictions from standard `MESA` models (Calderón et al., 2025). Consequently, to avoid systematic errors, our parametric adjustment focuses on the physical properties of the donor and the fundamental parameters of the gainer, without considering the luminosity of the

gainer, thus explaining this luminosity discrepancy.

3.2.2 The evolution of HD 170582

We evaluated the χ^2 value for each simulation to identify the optimal evolutionary scenario. Within the conservative regime (assuming no systemic mass loss), the best-fit solution yielded a minimum $\chi^2 = 0.05$. This model corresponds to a binary system with initial parameters: orbital period $P_{i,o} = 3.0$ days, donor mass $M_{d,i} = 6.0\,M_\odot$, and gainer mass $M_{g,i} = 5.0\,M_\odot$. The system is currently determined to be 81.7 Myr old, undergoing a phase of rapid, quasi-conservative mass transfer with a rate of $\dot{M} = 9.57 \times 10^{-7}\,M_\odot yr^{-1}$.

Figures 3.2.2and 3.2.1 presents the Hertzsprung-Russell (HR) diagram corresponding to the conservative evolutionary model. Table 3.2.1 shows the evolution of HD 170582 commences at the Zero Age Main Sequence (ZAMS), designated as point A (The sequence of alphabetical labels used in Table 3.2.1 follows the convention used by Rosales et al. (2019b, 2024).), where the core hydrogen burning phase begins. During this stage, the donor star retains a mass of $6.0\,M_\odot$ and a radius of $2.99\,R_\odot$. The stellar parameters remain relatively stable until the system reaches an age of 67.9 Myr, marking the onset of mass transfer (point E). At this juncture, the donor initiates expansion and transfers material to the companion, coinciding with a gradual depletion of central hydrogen.

The mass transfer rate subsequently accelerates, driving the system to a mass reversal configuration (point U_1) at 68.1 Myr, at which point the donor mass is $5.17\,M_\odot$. This phase is characterized by rapid evolution in both luminosity and effective temperature. The donor subsequently reaches its minimum Roche lobe filling factor (point F) at 68.2 Myr with a reduced mass of $4.44\,M_\odot$. This expansion phase persists until the cessation of the first mass transfer episode (point U_2) at 80.7 Myr.

A second phase of mass transfer initiates at 81.5 Myr (point G), where the donor contracts to a radius of $12.13\,R_\odot$ and its mass is further reduced to $2.29\,M_\odot$. The

Table 3.2.1: Evolutive stages from the donor star for DPV HD 170582.

Stage	Age (Myr)	M ($M_\odot$)	R ($R_\odot$)	log T (K)	$\dot{M}$ ($M_\odot yr^{-1}$)	Ev. Process
A	0.000	6.00	2.99	4.275	1.774E-10	Zero Age Main Sequence, Hydrogen burning.
B	67.789	5.97	7.62	4.168	7.396E-10	Terminal age main sequence
E	67.901	5.97	7.66	4.167	1.318E-07	Mass transfer.
U_1	68.166	5.17	7.32	4.088	2.460E-05	Mass inversion.
F	68.194	4.44	7.36	4.019	2.648E-05	Minimun value Roche lobe.
U_2	80.775	2.29	11.77	3.929	1.355E-09	End of the first phase of mass transfer.
G	81.550	2.29	12.13	3.951	1.049E-06	Start of the second phase of mass transfer.
X_2	81.785	1.84	15.70	3.959	9.571E-07	Present stage.

system's current evolutionary status is identified at point X_2 (81.7 Myr), where the donor possesses a mass of 1.84 $M_\odot$ and a significantly expanded radius of 15.7 $R_\odot$, indicative of advanced structural evolution in the core and envelope. We identify this point as the current evolutionary stage since it corresponds to the best fit solution, where the theoretical parameters converge with the observational values minimizing the statistical error. The second mass transfer phase concludes at point H (82.1 Myr), resulting in a donor with a minimum mass of 1.15 $M_\odot$ and a radius of 29.2 $R_\odot$, this transfer phase occurs in a short time interval of only 0.49 Myr.

The conservative model described herein provides the optimal fit for the observed mass, radius, and orbital period of HD 170582, enabling a rigorous analysis of the system's fundamental properties. Detailed comparisons of the period versus mass, mass versus radius, and mass transfer rate versus mass are provided in Figures. 3.2.2 and 3.2.1 respectively. Furthermore, Figure. 3.2.4 illustrates the distribution of helium and hydrogen on the HR diagram, highlighting the rejuvenation of the gainer star resulting from the accretion of material from the donor. Figure. 3.2.3 shows the variation of mass transfer with respect to the variation of the orbital period.

The internal structure and evolutionary history of both components of HD 170582 are visualized via Kippenhahn's diagrams in Figure. 3.2.5. Based on Kippenhahn diagrams, the internal evolution of HD 170582 reveals contrasting dynamics driven by quasi-conservative mass transfer. While the donor star (left panel) experiences drastic erosion of its envelope and contraction of its convective core due to mass loss

(dropping from 6.0 $M_\odot$ to 1.84 $M_\odot$), the recipient star (right panel) shows a clear rejuvenation process characterized by a substantial increase in its mass (reaching 9.1 $M_\odot$) and the revitalization of its convective core (dashed green), which expands as it processes the accreted hydrogen rich material, thus extending its stay on the main sequence.

3.2.3 Stellar dynamo in the donor star

In the case of the ST dynamo, Figure. 3.2.6 shows how the differential rotation (represented by the angular velocity and angular momentum profiles) curls the magnetic field lines, resulting in amplification where the toroidal component (B_ϕ, green line) significantly dominates over the poloidal component (B_r, black line), as predicted by theory ($B_\phi > B_r$). Furthermore, it is observed that the diffusivity associated with the ST dynamo (D_{ST}) operates efficiently outside the overshooting zones, facilitating angular momentum transport and confirming that the model reproduces the conditions necessary to maintain magnetic activity in the stellar interior.

To evaluate the effect of the magnetic field on the mass transfer rate in the HD 170582 system, we followed and reproduced the calculations performed by Mennickent et al. (2025) for the OGLE-LMC-ECL-14413 system, where they compute the relation between magnetic energy and the structural variations of the donor star. A fluctuation in the magnetic field B induces a fractional change in the radius of the donor star ($\Delta R/R_2$), which can be approximated by:

$$\frac{\Delta R}{R_2} \approx \frac{2}{3}\frac{R_2^4}{GM_2^2}B^2, \tag{3.2.3}$$

where G is the universal gravitational constant, and R_2 and M_2 are the radius and mass of the donor star, respectively.

According to the parametric prescription for mass transfer through the Roche lobe described by Ritter (1988), the mass transfer rate ($\dot{M}$) is highly sensitive to changes in the stellar radius and is defined exponentially as:

$$\dot{M} = \dot{M}_0 \exp\left(\frac{\Delta R}{H_2}\right), \tag{3.2.4}$$

where $\dot{M}_0$ represents the unperturbed secular mass transfer rate and H_2 is the pressure scale height in the atmosphere of the donor star. This thermodynamic parameter can be expressed analytically as:

$$H_2 = \frac{kT_2}{\mu m_p g}, \tag{3.2.5}$$

where k is the Boltzmann constant, T_2 is the effective temperature, μ is the mean molecular weight of the atmosphere, m_p is the proton mass, and g is the local surface gravity of the donor star.

By combining the previous equations, we obtain the modulation of the mass transfer rate as a function of the subsurface magnetic field strength:

$$\dot{M} = \dot{M}_0 \exp\left(\frac{2}{3}\frac{R_2^5}{H_2 G M_2^2} B^2\right). \tag{3.2.6}$$

For the specific case of the HD 170582 system, we adopt the physical parameters derived for the donor star: $M_2 = 1.9\,M_\odot$, $R_2 = 15.6\,R_\odot$, and $T_2 = 8,000$ K. With these values, the resulting surface gravity is $g \approx 214.1\,\mathrm{cm\ s^{-2}}$. By applying Equation 3.2.5 and assuming a mean molecular weight $\mu \approx 1.23$, we obtain a pressure scale height of $H_2 \approx 2.51 \times 10^9$ cm (equivalent to $0.036\,R_\odot$). The ratio $R_2/H_2 \approx 433$ indicates the presence of an extremely thin and concentrated stellar atmosphere, which is characteristic of evolved components filling their Roche lobes.

Considering a radial surface magnetic field $B_r \approx 10^3$ G, consistent with the behavior of the dynamo model profiles at an age of 81.7 Myr, Equation 3.2.3 yields a fractional radius variation of $\Delta R/R_2 \approx 9.7 \times 10^{-7}$. This corresponds to an absolute radial perturbation of $\Delta R \approx 1.05 \times 10^6$ cm. Evaluating the ratio $\Delta R/H_2 \approx 4.2 \times 10^{-4}$ in the exponent of Equation 3.2.6, the enhancement factor for the mass transfer rate becomes $\exp(4.2 \times 10^{-4}) \approx 1.00042$. Mathematically, this represents a marginal increase of 0.042% relative to the secular regime $\dot{M}_0$. Consequently, a purely surface

magnetic field is physically insufficient to produce the drastic variations in mass transfer required to sustain the strong photometric variability observed during the long cycle of the system. This limitation supports the idea that a magnetic prescription beyond the Tayler–Spruit framework may be operating in the donor, allowing the subsurface magnetic field strength to become sufficiently large to drive substantial changes in the mass-transfer rate.

To establish a physical basis for the long-period variability characteristic of DPVs, we investigated the magnetic activity cycles generated within the donor star's convective envelope by a dynamo magnetic mechanism other than the ST dynamo. The physical plausibility of this dynamo-driven mechanism is reinforced by its capacity to quantitatively relate the activity period (P_{cycle}) to the orbital period through a functional dependence on the dynamo number (D) and the power-law index α (Rosales et al., 2024). Following the stellar dynamo theory proposed by Schleicher and Mennickent (2017), the theoretical relationship linking P_{cycle} to the hydrodynamic and geometric properties derived in chapter 2 is used:

$$P_{cycle} = \left(\frac{11.5\, v_c P_{Kep} R_\odot}{\epsilon_H R_2 [\ \mathrm{kms}^{-1}\ \mathrm{yr}]} \right)^{-2\alpha} P_{rot}. \tag{3.2.7}$$

This intrinsic link between the donor's magnetic dynamo cycle and the system's orbital period is used for model validation. The observed orbital (P_o) and long (P_l) periods from photometry are utilized in the theoretical relation (analogous to Equation 2.1.7 described in the theoretical framework) to estimate the coefficient α and the dynamo number (D) (Calderón et al., 2025; Schleicher and Mennickent, 2017). The calculated α is constrained to a theoretically coherent range, typically between 1/3 and 5/6. The consistency of the MESA evolutionary models is validated when they successfully reproduce the observed long period using the calculated α and D for the system's current evolutionary state, as demonstrated for systems such as V1001 Cen, DQ Velorum, and V4142 Sgr (Calderón et al., 2025; Rosales et al., 2024).

Table 3.2.2: Mixing length parameter ($\alpha_{\rm MLT}$) values adopted from the dynamos table.

$\alpha_{\rm MLT}$ (Dimensionless)	Evolutionary stage	V_c (ms^{-1})	D (Dimensionless)	R_0 (Dimensionless)	α (Dimensionless)
0.5	U_1	167.661	1965014.744	0.0007	0.244
	F	152.736	2130768.237	0.0006	0.243
	X_2	1725.024	2731.788	0.019	0.448
1.0	U_1	211.785	1232139.599	0.001	0.253
	F	191.849	1344168.395	0.001	0.251
	X_2	2802.027	1111.042	0.03	0.506
2.0	U_1	266.509	778582.892	0.001	0.261
	F	464.410	231504.538	0.002	0.287
	X_2	3639.066	660.324	0.039	0.547
3.0	U_1	858.585	75010.534	0.004	0.316
	F	2032.324	12137.226	0.009	0.377
	X_2	6593.823	202.708	0.070	0.668
4.0	U_1	2955.234	6300.077	0.013	0.406
	F	6886.118	1058.007	0.031	0.510
	X_2	14869.657	39.480	0.159	0.965

Notes. The factor V_c is the convective velocity, D is the number of dynamo, R_0 is the Rossby number and α is a power law index.

3.2.4 The α mixing length parameter in Stellar Convection for HD 170582

The variation of the $\alpha_{\rm MLT}$ parameter significantly influences the evolutionary tracks of binary systems, particularly DPVs, within the Hertzsprung-Russell Diagram. This effect is especially pronounced in the mass-accreting star (gainer). $\alpha_{\rm MLT}$ modulates the rejuvenation process experienced by the gainer due to mass transfer (Rosales et al., 2024). For lower values of $\alpha_{\rm MLT}$, the gainer star tends to remain attached to the main sequence for a longer period in the HR diagram. Conversely, if high $\alpha_{\rm MLT}$ values are employed, the rejuvenation process becomes more abrupt and transient (Rosales et al., 2024). Regarding the donor star, the variation of $\alpha_{\rm MLT}$ affects the duration of the mass transfer phase, prolonging it significantly until the star reaches the minimum limit of its Roche Lobe. Furthermore, it was observed that the modeled system evolves faster with a higher $\alpha_{\rm MLT}$ value (Rosales et al., 2024).

To assess the impact of the convection efficiency on the dynamo mechanism, we generated a group of evolutionary models based on the best-fit solution found for HD 170582. While keeping the initial system parameters fixed, we only varied the $\alpha_{\rm MLT}$ across a broad range of values: 0.5, 1.0, 2.0, 3.0, and 4.0. Although values as high as $\alpha_{\rm MLT} \geq 3.0$ are generally considered physically unlikely for this type of star, they were included to amplify and better visualize the sensitivity of the stellar structure to extreme variations in convective efficiency. For each model, we extracted the physical properties of the donor star specifically the stellar radius and the maximum convective velocity (v_c), at three critical evolutionary stages: the mass inversion point (U_1), the minimum Roche lobe filling factor (F), and the current evolutionary state of the system (X_2). Using these hydrodynamic variables, we computed the dynamo number (D), the Rossby number (R_o), and the power-law index (α) following the dynamo formalism established by Schleicher and Mennickent (2017). These results are summarized in Table 3.2.2.

3.2.5 The Mixing-Length Parameter and Its Influence on Dynamo Dynamics

The analysis of the parameter Table 3.2.2 and Figure 3.2.7 shows that the $\alpha_{\rm MLT}$ acts as a key regulator of the thermal and dynamical structure of the donor star. A positive correlation is identified between the value of $\alpha_{\rm MLT}$ and the maximum convective velocity (v_c) across all evolutionary stages considered (U_1, F, and X_2). From a physical standpoint, an increase in $\alpha_{\rm MLT}$ translates into a higher efficiency of convective energy transport in the superadiabatic regions of the stellar envelope in the analyzed models.

For low values of the parameter ($\alpha_{\rm MLT} = 0.5$), the convective velocities remain within moderate ranges, from $\sim$ 167 m/s during U_1 up to $\sim$ 1725 m/s in the X_2. This behavior suggests a relatively inefficient energy transport regime in which radiative processes still play a significant role. In contrast, for an extreme value of $\alpha_{\rm MLT} = 4.0$, the convective velocity in the X_2 stage reaches 14869.657 m/s. This pronounced increase indicates that a larger mixing length promotes a more substantial temperature excess in fluid parcels, thereby enhancing buoyancy forces and, consequently, the convective rise velocity. Nevertheless, it is important to note that a value of $\alpha_{\rm MLT} = 4.0$ is not physically realistic within the context of standard stellar models.

The parameter α corresponds to the power-law index in the relation proposed by Schleicher and Mennickent (2017), which links the activity cycle period to the physical properties of the system. For the considered dynamo mechanism to be physically consistent within the framework of stellar dynamo theory, the value of α should preferably lie within the interval $0.33 \leq \alpha \leq 0.83$.

Variations in $\alpha_{\rm MLT}$ directly affect the viability of the dynamo throughout the different evolutionary stages. In the low to standard regime ($0.5 \leq \alpha_{\rm MLT} \leq 2.0$), the system fails to activate a consistent dynamo during the early phases of mass transfer (U_1 and F), yielding α values in the range 0.24–0.28. Only upon reaching the current stage, associated with stellar radius expansion and significant structural changes, does the parameter α enter the validity range, for example $\alpha = 0.547$ for $\alpha_{\rm MLT} = 2.0$.

In the intermediate regime ($\alpha_{\rm MLT} = 3.0$), the model favors an earlier activation of the dynamo. Although in the U_1 stage the value of α remains slightly below the threshold ($\alpha = 0.316$), during the minimum Roche lobe phase it reaches a consistent value ($\alpha = 0.377$) and remains within the acceptable range in the current stage ($\alpha = 0.668$). This indicates that moderately enhanced convective efficiencies can extend the evolutionary window in which the dynamo operates, even if such values exceed the typical solar calibrated regime.

For high values of the parameter ($\alpha_{\rm MLT} = 4.0$), while the dynamo can be activated at early stages such as U_1 ($\alpha = 0.406$) and F ($\alpha = 0.510$), a value of $\alpha = 0.965$ is obtained in the X_2 stage, exceeding the theoretical upper limit of 0.83. This behavior indicates that excessively large values of $\alpha_{\rm MLT}$ drive the system into a regime that is incompatible with the theoretical constraints of the dynamo model and, therefore, unlikely to represent physically realistic configurations for DPV systems.

Overall, these results indicate that the choice of $\alpha_{\rm MLT}$ not only modifies the efficiency of thermal transport but also determines the evolutionary windows in which magnetic activity can develop. The analysis suggests that values of $\alpha_{\rm MLT}$ of the order of the solar calibration, and not significantly exceeding ~ 2, provide a more consistent and physically motivated description of the dynamo behaviour proposed by Schleicher and Mennickent (2017), as they reproduce the long cycle properties without driving the system into non physical regimes.

At the same time, the results obtained for $\alpha_{\rm MLT} = 3.0$ show that moderately higher values can still yield internally consistent dynamo solutions over relevant evolutionary stages, particularly near and after the onset of Roche lobe overflow. This suggests that the acceptable range of convective efficiency may not be sharply bounded, but rather that there exists a transitional regime in which the dynamo remains viable, albeit with increasing tension with standard stellar calibrations.

Finally, it is worth noting that deviations from solar-calibrated values of $\alpha_{\rm MLT}$ could be associated with the non-equilibrium conditions imposed by ongoing mass transfer. This process may alter the thermal structure and convective properties of the donor envelope, leading to effective convective efficiencies that differ from those of isolated stars. However, this interpretation remains speculative and requires further

investigation in order to establish a robust physical connection between mass loss and modifications of convective transport.

It is crucial to emphasize that the fulfillment of the dynamo condition, namely that the power-law index α lies within the physically admissible range, constitutes a necessary but not sufficient requirement for the manifestation of the DPV phenomenon. In addition to satisfying the magnetic constraint, the binary system must have reached a semidetached configuration in which the donor star fills its Roche lobe and sustains an active mass-transfer phase. Only under these circumstances can magnetic activity in the donor effectively translate into a modulation of the mass-transfer rate through the L_1 point and, consequently, into a detectable long photometric cycle.

The analysis of the viability of the dynamo mechanism was carried out through the construction of a diagnostic diagram Figure 3.2.8 based on the analytical formulation proposed by Schleicher and Mennickent (2017), which relates the long-cycle period to stellar magnetism and to a set of parameters associated with the internal structure of the donor star. Assuming the observed period relation characteristic of DPV systems, this expression was used to determine the required value of the exponent α over a continuous domain of theoretical parameters, spanning a wide range of donor radii and maximum convective velocities. The resulting diagram provides a graphical representation of the α-level surfaces, allowing one to visualize how this parameter of interest varies as a function of the hydrodynamical and geometrical properties of the star, independently of any specific evolutionary track.

From this theoretical projection (Figure 3.2.8), it is possible to constrain the physical regime in which the mechanism proposed by Schleicher and Mennickent (2017) is most likely to operate. Since the model assumes that the exponent α must remain confined within a previously established approximate physical range for the dynamo to be capable of modulating the observed long period, the isolines corresponding to these limiting values delineate the so called activation zone in the R-v_c plane. Consequently, this diagram allows for a direct assessment of which combinations of stellar radius and convective velocity are compatible with the generation of the magnetic cycle, thereby helping to identify the evolutionary stages in which the structural conditions of the donor star favor the operation of the dynamo. In the diagram, the position

corresponding to HD,170582 is indicated by a star, defined by the values of R and v_c extracted from the best-fitting model obtained with `MESA` for this system.

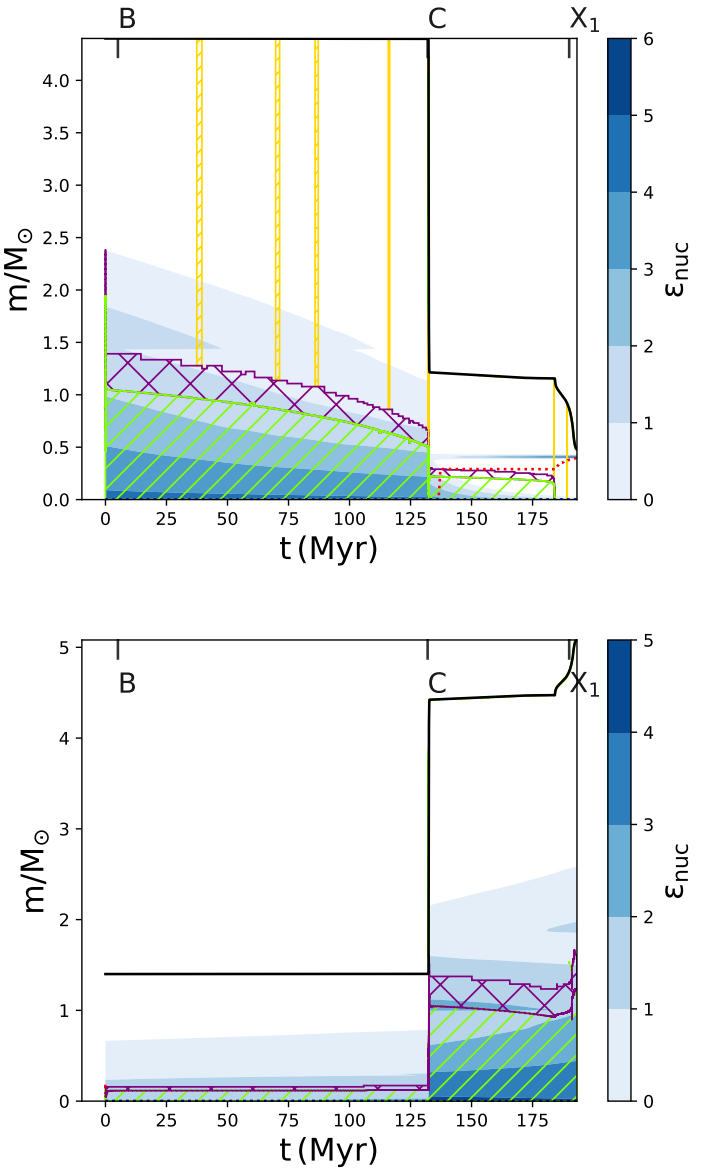

Figure 3.1.18: Kippenhahn plots derived from the MESA model with conservative mass transfer for V1001 Cen. At the top we see graph donor star and below gainer star for a conservative model of initial mass of 4.4 and 1.4 $M/M_{\odot}$ and initial orbital period of 2.1 days. In the graphical representation, the x axis displays the age since hydrogen ignition in units of million years (Myr), and the different stellar layers are identified by their mass proportions ($M/M_{\odot}$). Each mixing process is illustrated with specific colors and patterns: convective mixing is represented in green with a hatching pattern, semi convective mixing in red, convective overshooting mixing with a crosshatched pattern in purple, and thermohaline mixing in yellow with a hatching pattern. The solid black line indicates the surface of each star.

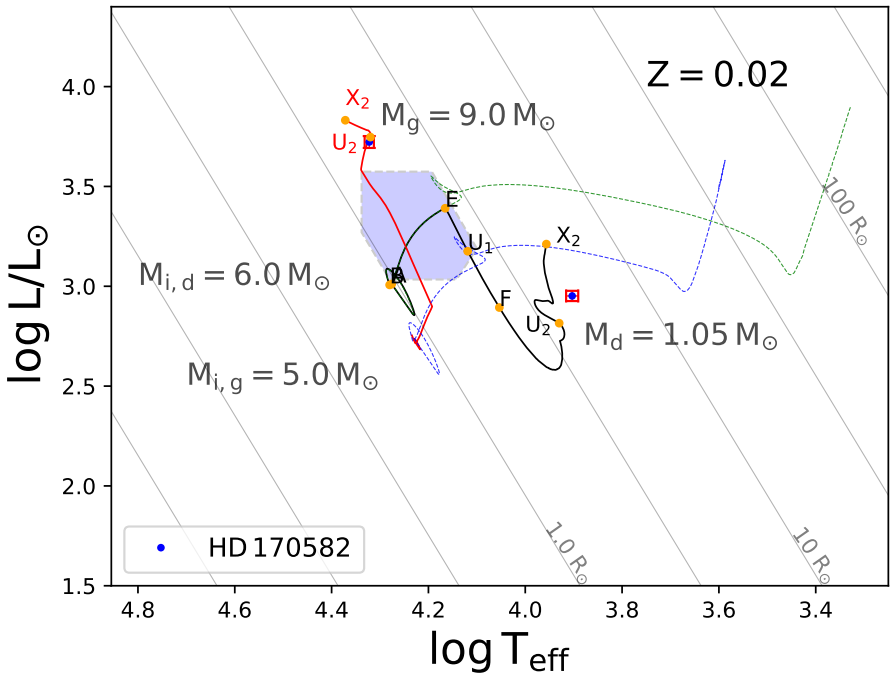

Figure 3.2.1: Evolutionary model with conservative mass transfer for HD 170582. Initial orbital period of 3.0 days, initial masses of 6.0 and 5.0 $M_\odot$. The simulation covers the evolution up to the current stage of the system, corresponding to an age of 81.78 Myr. The solid black line corresponds to the evolutionary track of the donor, while the solid red line corresponds to the gainer. The dashed blue and green lines represent the evolutionary trajectories of single stars with the same initial mass as the donor and gainer, respectively.

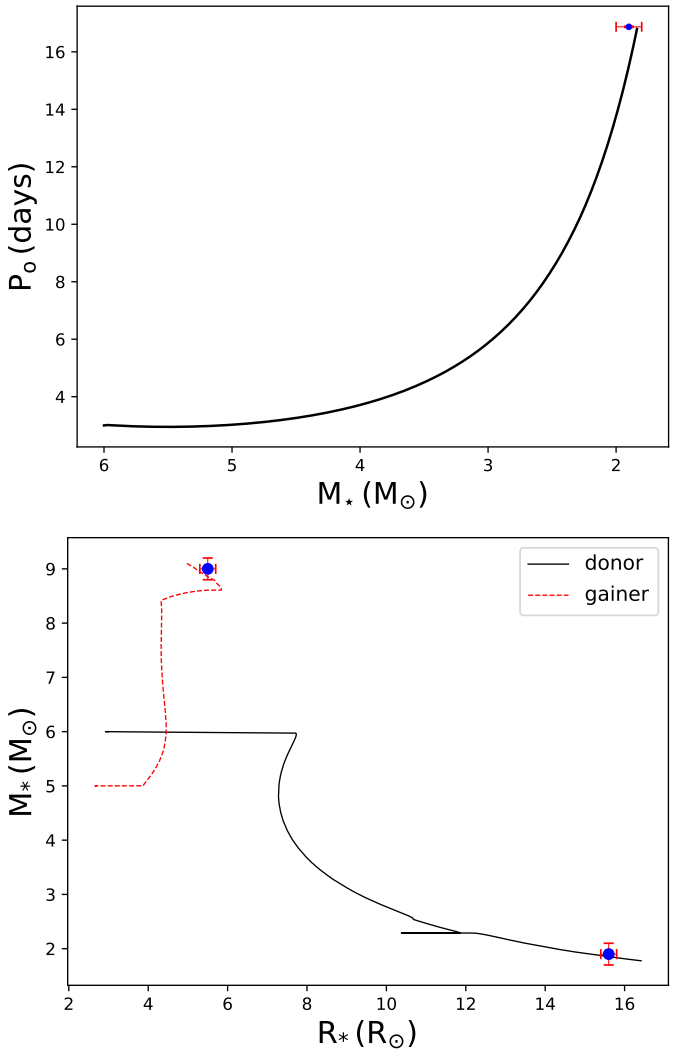

Figure 3.2.2: (Top) Evolution of the orbital period as a function of the mass of the donor star. (Bottom) Schematic behavior of the radius and mass of both stars, the solid black line corresponds to the donor's path, while the dashed red line corresponds to the gainer.

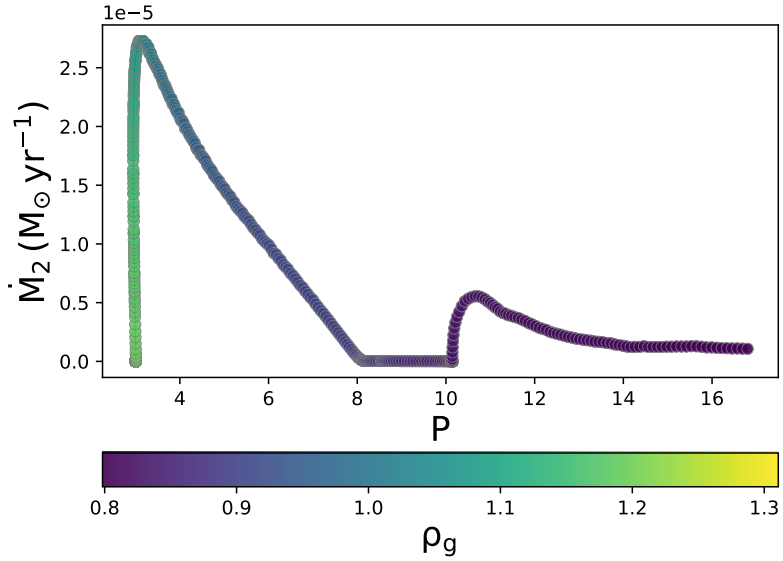

Figure 3.2.3: Evolution of mass transfer as a function of the orbital period of the donor star.

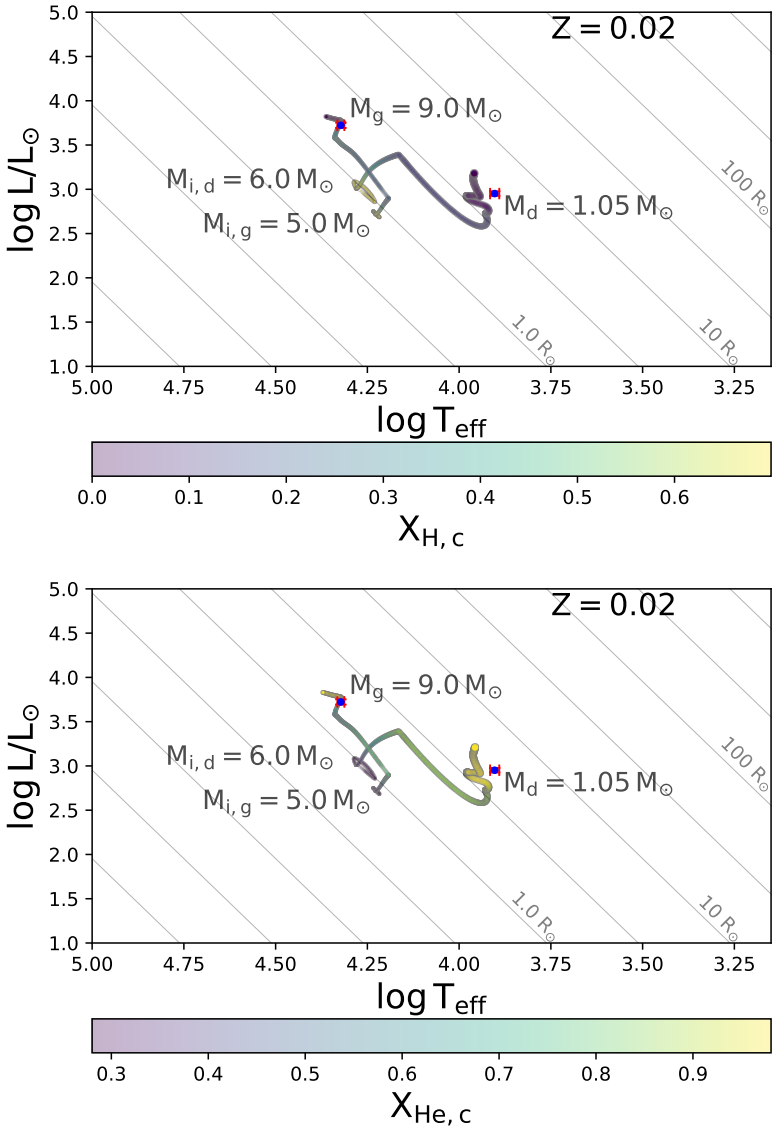

Figure 3.2.4: Hertzsprung Russel (H-R) diagrams illustrate the evolution of binary stars. The color bar indicates the proportion of hydrogen and helium in the core of each star.

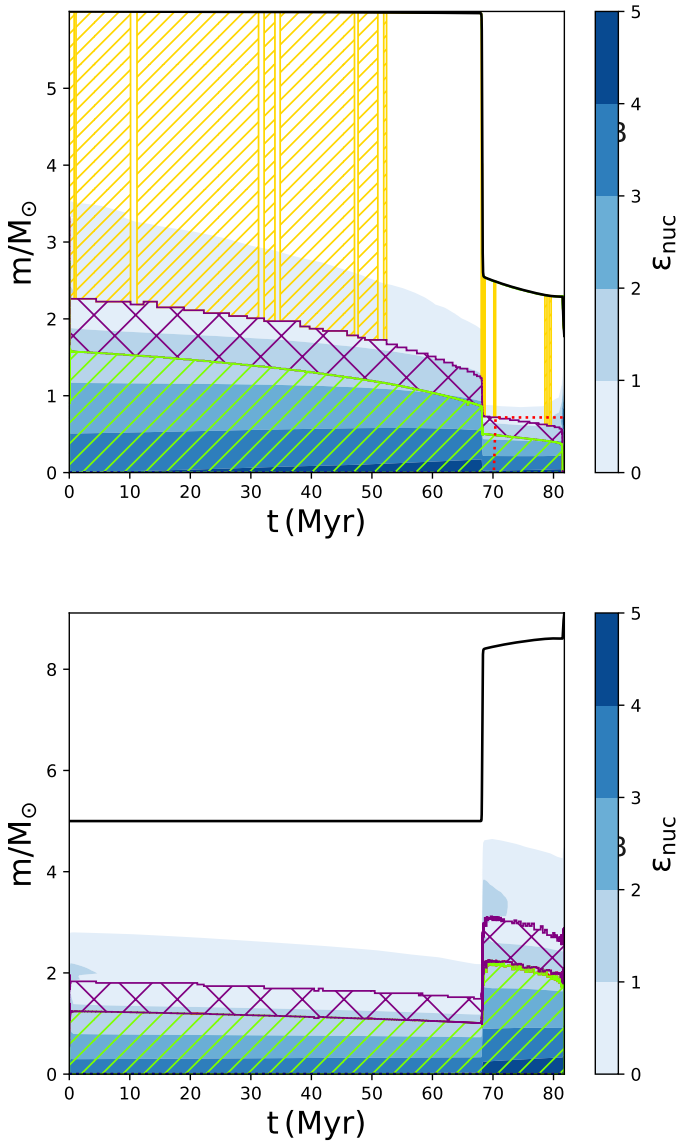

Figure 3.2.5: Kippenhahn plots derived from the MESA model with conservative mass transfer for HD 170582. On the left we see graph donor star and on the right gainer star for a conservative model of initial mass of 6.0 and 5.0 $M/M_{\odot}$ and initial orbital period of 3.0 days. In the graphical representation, the x axis displays the age since hydrogen ignition in units of million years (Myr), and the different stellar layers are identified by their mass proportions ($M/M_{\odot}$). Each mixing process is illustrated with specific colors and patterns: convective mixing is represented in green with a hatching pattern, semi convective mixing in red, convective overshooting mixing with a crosshatched pattern in purple, and thermohaline mixing in yellow with a hatching pattern. The solid black line indicates the surface of each star.

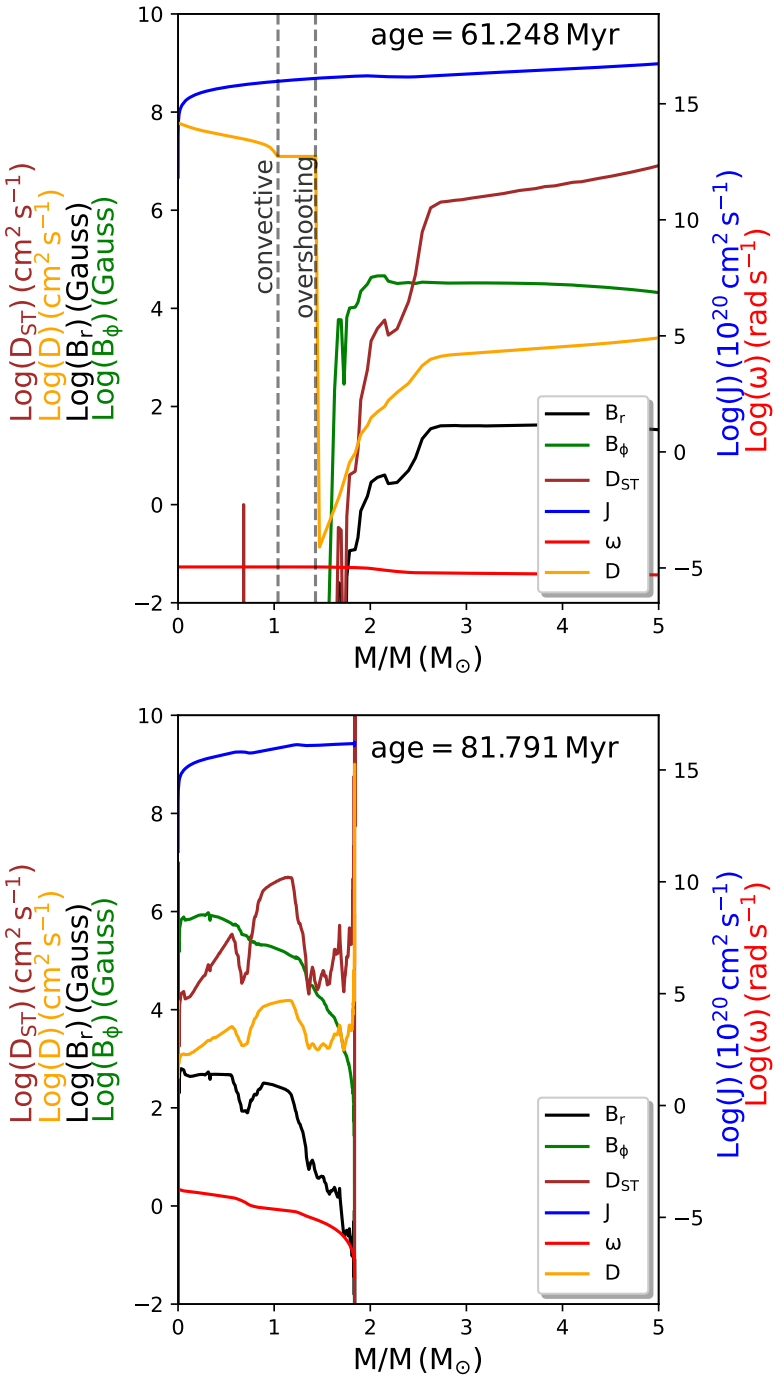

Figure 3.2.6: Profiles of the poloidal magnetic field, B_r, and the toroidal magnetic field, B_ϕ, generated by the ST dynamo in the donor star. The Eulerian diffusion coefficient for mixing is shown in orange, the ST diffusion coefficient as a brown line, the poloidal magnetic field in black, the toroidal magnetic field in green, the angular momentum in blue, and the angular velocity in red.

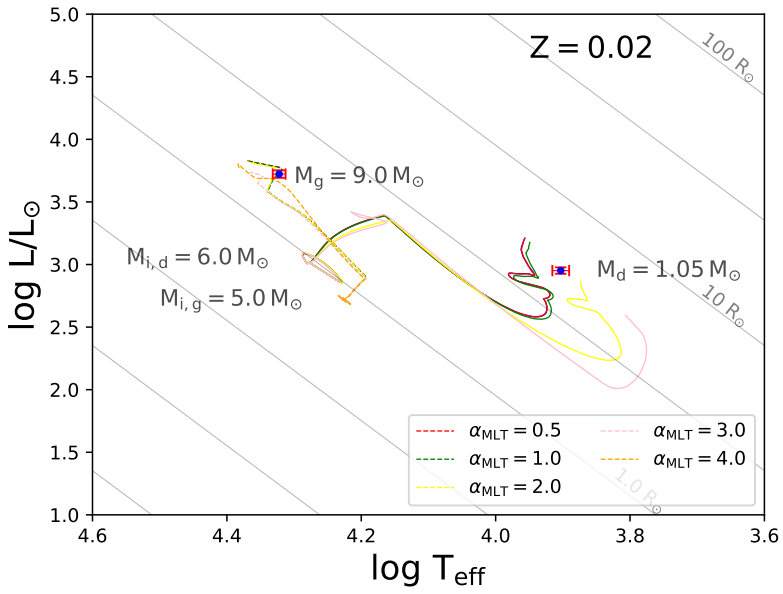

Figure 3.2.7: Schematic representation of the behavior of the mixing length parameter ($\alpha_{\rm MLT}$) for different values. This parameter governs the so-called rejuvenation process of the gainer star. While it does not affect the mass transfer evolution, the stellar masses, or the binary orbital period, it plays a crucial role in shaping the evolutionary track of the secondary star during mass transfer. In particular, up to the end of the optically thick mass transfer phase, lower values of $\alpha_{\rm MLT}$ lead to a more advanced evolutionary state of the secondary star, in contrast to the behavior observed in the gainer star.

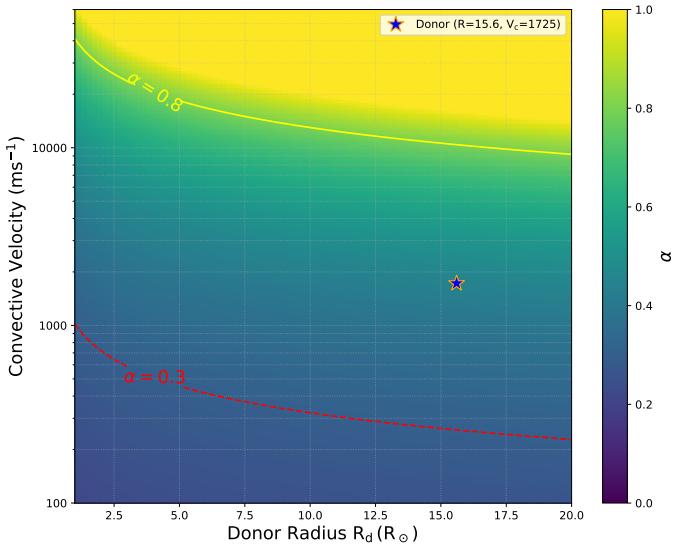

Figure 3.2.8: Relationship between the maximum convective velocity (v_c) and the donor star radius (R_2). The color scale represents the mixing length parameter ($\alpha_{\rm MLT}$), ranging from 0 to 1. The lines demarcate the theoretical region favorable for dynamo activation: the red dashed line indicates the lower limit of $\alpha_{\rm MLT}$, while the solid yellow line indicates the upper limit. The area between these two lines corresponds to the parameter space where the combination of radius and convective velocity favors dynamo operation.

Chapter 4

Conclusions

4.1 Conclusions

In this thesis, we developed a unified observational evolutionary framework to investigate the nature of Double Periodic Variables (DPVs), linking their photometric and spectroscopic properties with accretion disk phenomenology and binary evolutionary modelling using `MESA`. Within this framework, we quantitatively assessed the central hypothesis that a magnetic dynamo operating in the donor star is responsible for the long photometric cycle, and tested its internal consistency across systems at different evolutionary and interaction stages. By applying this approach to the Galactic DPVs V1001 Cen and HD 170582, we obtained a coherent picture of their present configuration, evolutionary history, and the internal stellar conditions required for long cycle modulation.

4.1.1 Observational results

A detailed photometric and spectroscopic characterization of V1001 Cen confirms its nature as an interacting DPV composed of a Roche-lobe filling donor with approximately solar chemical composition and an effective temperature $T \simeq 8750$ K, and an early type B gainer with $T \simeq 20000 \pm 2000$ K. The radial velocity analysis yields a precise mass ratio of $q = 0.151 \pm 0.003$, providing a robust dynamical

foundation for the subsequent geometric and evolutionary modelling.

The orbital light curve of V1001 Cen is consistently reproduced by a configuration that includes an optically thick accretion disk around the gainer. The best fit solution requires two bright regions located on the disk rim at longitudes $\lambda = 172^\circ \pm 8$ and $326^\circ \pm 3$, with temperatures approximately 32–38% higher than that of the disk outer edge. These features support an interpretation in terms of stream disk interaction and localized shock heating, in agreement with current hydrodynamic scenarios for interacting Algol like systems.

The inferred accretion disk properties are consistent with those expected for stable disk formation in DPVs. In particular, for V1001 Cen the system lies within the parameter space where a persistent disk can form around the gainer, and an accretion disk albedo of $(1 - \beta) = 0.34$ is obtained, a value relevant for understanding disk heating, energy redistribution, and the contribution of the disk to the observed flux.

4.1.2 Evolutionary results

The evolutionary history of V1001 Cen was reconstructed under a conservative mass-transfer scenario. The preferred solution places the system at an age of ~ 190 Myr, currently undergoing a second phase of mass transfer at a rate of $\dot{M} \simeq 1.13 \times 10^{-7}\,\mathrm{M}_\odot\,\mathrm{yr}^{-1}$. The system originates from initial masses $\mathrm{M_{i,d}} = 4.4\,M_\odot$ and $\mathrm{M_{i,g}} = 1.4\,M_\odot$, with an initial orbital period of 2.1 days. The present day configuration corresponds to a Roche lobe filling donor and a gainer that has been significantly rejuvenated by accretion.

For HD 170582, a multiparametric minimization strategy yields a consistent evolutionary solution beginning with initial masses $\mathrm{M_{d,i}} = 6.0\,M_\odot$ and $\mathrm{M_{g,i}} = 5.0\,M_\odot$, and an initial orbital period of 3.0 days. The system is currently at an age of ~ 81.8 Myr and undergoing rapid mass transfer at $\dot{M} \approx 9.6 \times 10^{-7}\,\mathrm{M}_\odot\,\mathrm{yr}^{-1}$. The donor presently has $\sim 1.84\,M_\odot$ and $15.70\,R_\odot$, while the gainer has accreted up to $\sim 9.1\,M_\odot$, illustrating a clear case of mass ratio inversion and thermal timescale interaction.

These evolutionary reconstructions demonstrate that both systems can be consistently

reproduced from ZAMS under conservative or quasi conservative mass transfer, providing a physically grounded basis for extracting internal stellar quantities relevant to the long cycle mechanism.

4.1.3 Physical results: dynamo convection connection

A central objective of this thesis was to test the dynamo interpretation of the long photometric cycle in a physically consistent manner. In V1001 Cen, the observed long cycle can be reproduced by adopting a dynamo number D = 7884.74 and a power-law index $\alpha = 0.71$, following the system through key evolutionary stages, including the Roche lobe minimum and the current configuration. This result supports the emergence of donor magnetic activity not only at the present epoch, but potentially already near the onset of strong interaction, naturally linking binary evolution with long cycle modulation.

In HD 170582, the application of the Schleicher & Mennickent dynamo formalism combined with internal stellar quantities extracted from `MESA` shows that the long cycle can be reproduced under standard convective assumptions. The models yield a dynamo index $\alpha \approx 0.5$ during the evolutionary interval extending from the mass inversion phase to the current stage, consistent with dynamo driven long cycle behaviour operating in the donor star.

A key thesis level result is that the dynamo hypothesis provides a quantitative diagnostic of the donor's convective regime. In HD 170582, we find a strong dependence of the maximum convective velocity v_c on the mixing-length parameter $\alpha_{\rm MLT}$. At the current evolutionary stage, v_c increases from ~ 1.7 km, s^{-1} for $\alpha_{\rm MLT} = 0.5$ to ~ 14.8 km, s^{-1} for $\alpha_{\rm MLT} = 4.0$. By requiring the dynamo power law index to remain within the theoretically admissible range ($1/3 \leq \alpha \leq 5/6$), we obtain a physically motivated constraint on the convective efficiency. In this context, moderate values of $\alpha_{\rm MLT}$, comparable to the solar calibrated regime and not significantly exceeding ~ 2, are preferred, as they yield dynamo solutions compatible with the observed DPV phenomenology. While intermediate values (e.g. $\alpha_{\rm MLT} \sim 3.0$) may still allow dynamo operation during certain evolutionary phases, they tend to approach the limits of the admissible parameter space. In contrast, larger values (e.g. $\alpha_{\rm MLT} \gtrsim 4.0$) lead to

convective velocities that drive the dynamo index into non-physical regimes, and are therefore disfavoured.

4.1.4 Implications for the population of DPVs

The combined analysis of V1001 Cen and HD 170582 demonstrates that DPVs can be understood as a single astrophysical phenomenon emerging from the coupled evolution of mass transfer, accretion disk formation, and donor star magnetism. Within the unified framework developed in this thesis, the long photometric cycle is not an ad hoc feature, but a measurable manifestation of the donor's internal convective conditions operating within an interacting binary.

These results suggest that the dynamo consistency requirement can be used as an independent physical constraint on the internal structure of donor stars in DPVs, complementing traditional observational and evolutionary diagnostics. Extending this methodology to larger samples of Galactic and extragalactic DPVs offers a promising avenue to assess the universality of the dynamo mechanism, explore its dependence on mass and evolutionary stage, and refine our understanding of the interplay between stellar convection, magnetic activity, and mass transfer in interacting binary systems.

4.1.5 Assessment of the central hypothesis

The central hypothesis of this thesis states that the long photometric cycle observed in Double Periodic Variables is produced by a cyclic magnetic dynamo operating in the donor star, which modulates the mass-transfer rate and, consequently, the structure and emission of the accretion disk. The results obtained for V1001 Cen and HD 170582 allow this hypothesis to be tested in complementary physical regimes.

In the case of V1001 Cen, the hypothesis is supported at the level of global consistency between observations and evolutionary modelling. The system admits a simultaneous reproduction of its photometric, spectroscopic, and geometric properties, while also yielding dynamo parameters compatible with the observed long cycle. This indicates that the proposed mechanism can operate self-consistently in a system undergoing relatively stable mass transfer, where the disk structure and variability can be

naturally linked to cyclic modulation of the donor star.

In contrast, HD 170582 provides a more stringent test of the internal physical conditions required by the hypothesis. The detailed exploration of the donor structure, particularly the dependence on the mixing-length parameter $\alpha_{\rm MLT}$, shows that only a restricted range of convective efficiencies leads to physically consistent dynamo indices. In this sense, this system primarily constrains the internal viability of the dynamo mechanism and its sensitivity to stellar structure, rather than only its global observational consistency.

Despite these results, an important limitation remains. The present analysis relies on the dynamo formalism proposed by Schleicher and Mennickent, which is primarily grounded in empirical scaling relations combined with simplified physical assumptions. As a consequence, alternative prescriptions such as the Tayler–Spruit mechanism are not explored in detail, since they are based on fundamentally different assumptions regarding angular momentum transport and magnetic field generation, and therefore are not directly comparable within the same framework.

Bibliography

Applegate, J. H. (1992). A mechanism for orbital period modulation in close binaries. *ApJ*, 385:621.

Armeni, A. and Shore, S. N. (2022). Revisiting the high-mass transfer close binary star system AU Monocerotis. *A&A*, 664:A103.

Baliunas, S. L., Nesme-Ribes, E., Sokoloff, D., and Soon, W. H. (1996). A dynamo interpretation of stellar activity cycles. *ApJ*, 460:848.

Bayo, A., Rodrigo, C., Barrado Y Navascués, D., Solano, E., Gutiérrez, R., Morales-Calderón, M., and Allard, F. (2008). VOSA: virtual observatory SED analyzer. An application to the Collinder 69 open cluster. *A&A*, 492(1):277–287.

Bisikalo, D. V., Boyarchuk, A. A., Chechetkin, V. M., Kuznetsov, O. A., and Molteni, D. (1998). Three-dimensional numerical simulation of gaseous flows structure in semidetached binaries. *MNRAS*, 300(1):39–48.

Bisikalo, D. V., Boyarchuk, A. A., Chechetkin, V. M., Kuznetsov, O. A., and Molteni, D. (1999). Comparison of 2d and 3d models of flow structure in semidetached binaries. *Astron. Rep.*, 43:797. Astron. Zh. 76, 905 (1999) [Astron. Rep. 43, 797 (1999)].

Bisikalo, D. V., Boyarchuk, A. A., Kaigorodov, P. V., and Kuznetsov, O. A. (2003). Morphology of the interaction between the stream and cool accretion disk in a semidetached binary system. *Astron. Rep.*, 47:809–820.

Blöcker, T. (1995). Stellar evolution of low and intermediate-mass stars. i. evolutionary tracks for progenitor stars of planetary nebulae. *A&A*, 297:727.

Calderón, P. A., Mennickent, R. E., Rosales, J. A., Schleicher, D. R. G., Djurašević, G., and Castro-Toledo, N. (2025). V1001 Cen: A dual approach of spectroscopy and numerical modeling to understand stellar evolution and dynamo mechanisms. *A&A*, 703:A293.

Cardelli, J. A., Clayton, G. C., and Mathis, J. S. (1989). The relationship between

IR, optical, and UV extinction. In Allamandola, L. J. and Tielens, A. G. G. M., editors, *Interstellar Dust*, volume 135 of *IAU Symposium*, pages 5–10.

Castelli, F. and Kurucz, R. (2003). New grids of atlas9 model atmospheres. *MSA, IAU Symposium*, 210:A20.

Celedón, L., Mennickent, R. E., Barría, D., Garcés, J., and Jurković, M. (2025). The vanishing of the long photometric cycle in au monocerotis. *A&A*, 700:A217.

Collaboration, G. et al. (2018). Vizier online data catalog: Gaia dr2 (gaia collaboration, 2018). *VizieR*, pages I–345.

de Jager, C., Nieuwenhuijzen, H., and van der Hucht, K. A. (1988). Mass loss rates in the hertzsprung-russell diagram. *A&AS*, 72:259.

Djurašević, G. (1992a). An analysis of active close binaries (cb) based on photometric measurements: Ii. active cb with accretion discs. *Ap&SS*, 196:267–282.

Djurašević, G. (1992b). An analysis of active close binaries (cb) based on photometric measurements: Iii. the inverse-problem method—an interpretation of cb light curves. *Ap&SS*, 197:17–34.

Djurašević, G. (1996). A model of light-curve synthesizing for dwarf novae and the analysis of the oy car observations by application of the inverse-problem method. *Ap&SS*, 240:317–329.

Eggleton, P. (2006). *Evolutionary Processes in Binary and Multiple Stars*. Cambridge University Press.

Eggleton, P. P. (1983). Aproximations to the radii of roche lobes. *ApJ*, 268:368.

Eyer, L. and Blake, C. (2002). Automated classification of variable stars for asas data. In *Radial and Nonradial Pulsationsn as Probes of Stellar Physics*, volume 259 of *ASPCS*, pages 160–164.

Fitzpatrick, E. L. and Massa, D. (2005). An Analysis of the Shapes of Ultraviolet Extinction Curves. IV. Extinction without Standards. *AJ*, 130(3):1127–1140.

Frank, J., King, A., and Raine, D. J. (2002). *Accretion Power in Astrophysics: Third Edition*. Cambridge University Press.

Garcés, J., Mennickent, R. E., Petrović, J., Barría, D., Celedón, L., Cortés, C. C., and Djurašević, G. (2025). Photometric study of hot algol-type binaries with long cycles. *A&A*, 701:A90.

Garcés, L. J., Mennickent, R. E., Djurašević, G., Poleski, R., and Soszyński, I. (2018). Asymmetric ejecta of cool supergiants and hypergiants in the massive cluster westerlund 1 free. *MNRAS*, 477:L11.

García, G. R., Mennickent, R., Iwanek, P., Gorrini, P., Garcés, J., Soszyński, I., and Astudillo-Defru, N. (2021). New galactic β lyrae-type binaries showing superorbital photometric cycles. *ApJ*, 922(1):30.

Gonzalez, J. F. and Levato, H. (2006). Separation of composite spectra: the spectroscopic detection of an eclipsing binary star. *A&A*, 448(1):283–292.

Gray, R., Napier, M., and Winkler, L. (2001). The physical basis of luminosity classification in the late a-, f-, and early g-type stars. i. precise spectral types for 372 stars. *AJ*, 121(4):2148.

Gray, R. O. and Corbally, C. J. (1994). The calibration of mk spectral classes using spectral synthesis. 1: The effective temperature calibration of dwarf stars. *AJ*, 107:742–746.

Henyey, L., Vardya, M., and Bodenheimer, P. (1965). Studies in stellar evolution. iii. the calculation of model envelopes. *ApJ*, 142(3):841–854.

Herwig, F. (2000). The evolution of agb stars with convective overshoot. *A&A*, 360:952–968.

Hessman, F. V. and Hopp, U. (1990). The massive, nearly face-on cataclysmic variable gd 552. *A&A*, 228:387–398.

Hilditch, R. W. (2001). *An Introduction to Close Binary Stars*. Cambridge University Press.

Høg, E., Fabricius, C., Makarov, V., Urban, S., Corbin, T., Wycoff, G., Bastian, U., Schwekendiek, P., and Wicenec, A. (2000). The tycho-2 catalogue of the 2.5 million brightest stars. *A&A*, 355:L27–L30.

Huijse, P., Estévez, P. A., Förster, F., Daniel, S. F., Connolly, A. J., Protopapas, P., Carrasco, R., and Príncipe, J. C. (2018). Robust period estimation using mutual information for multiband light curves in the synoptic survey era. *ApJS*, 236(1):12.

Iglesias, C. A. and Rogers, F. J. (1993). Radiative opacities for carbon-and oxygen-rich mixtures. *ApJ*, 412:752–760.

Iglesias, C. A. and Rogers, F. J. (1996). Updated opal opacities. *ApJ*, 464:943.

Jermyn, A. S., Bauer, E. B., Schwab, J., Farmer, R., Ball, W. H., Bellinger, E. P., Dotter, A., Joyce, M., Marchant, P., Mombarg, J. S. G., et al. (2023). Modules for experiments in stellar astrophysics (mesa): Time-dependent convection, energy conservation, automatic differentiation, and infrastructure. *ApJS*, 265(1):15.

Jiao, C.-L., Zhao, E.-g., Zhu, L., and Matekov, A. (2026). Long Photometric Cycles in Double Periodic Variables from Nodal Precession of a Tilted Accretion Disk. *arXiv*, page arXiv:2602.19460.

Kolb, U. (2010). *Extreme environment astrophysics*. Cambridge University Press.

Kolb, U. and Ritter, H. (1990). A comparative study of the evolution of a close binary using a standard and an improved technique for computing mass transfer. *A&A*, 236:385–392.

Lubow, S. H. and Shu, F. H. (1975). Gas dynamics of semidetached binaries. *ApJ*, 198:383–405.

Martin, P. G. and Whittet, D. C. B. (1990). Interstellar Extinction and Polarization in the Infrared. *ApJ*, 357:113.

Mennickent, R. (2022). Accretion disks and long cycles in β lyrae-type binaries. *Galaxies*, 10(1):15.

Mennickent, R., Djurašević, G., Kołaczkowski, Z., and Michalska, G. (2012a). The evolution stage and massive disc of the interacting binary v 393 scorpii. *MNRAS*, 421(1):862–871.

Mennickent, R. and Kolaczkowski, Z. (2010). A class of interacting binaries: Double periodic variables. In *Binaries-Key to Comprehension of the Universe*, volume 435, page 283.

Mennickent, R., Kołaczkowski, Z., Djurasevic, G., Niemczura, E., Diaz, M., Curé, M., Araya, I., and Peters, G. (2012b). A cyclic bipolar wind in the interacting binary v 393 scorpii. *MNRAS*, 427(1):607–624.

Mennickent, R., Kołaczkowski, Z., Graczyk, D., and Ojeda, J. (2010). A study of the interacting binary v393 scorpii. *MNRAS*, 405(3):1947–1959.

Mennickent, R. E. (2017). *SAJ*, 194:1.

Mennickent, R. E., Cabezas, M., Djurašević, G., Rivinius, T., Hadrava, P., Poleski, R., Soszyński, I., Celedón, L., Astudillo-Defru, N., Raj, A., and Fernández-Trincado, J. G. (2019). On the long-cycle variability of the algol ogle-lmc-dpv-065 and its stellar, orbital, and disc parameters. *MNRAS*, 487:4169.

Mennickent, R. E. and Djurašević, G. (2021). Model for the long and orbital brightness variability of the lyrae type binary ogle-blg-ecl-157529. *A&A*, 653:A89.

Mennickent, R. E. and Djurašević, G. (2025). Cyclic variability of the accretion disk in the eclipsing binary ogle-lmc-dpv-065. *A&A*, 698:A56.

Mennickent, R. E., Djurašević, G., Cabezas, M., Cséki, A., Rosales, J. G., Niemczura, E., and Araya, I. (2015). Fundamental parameters of the close interacting binary hd 170582 and its luminous accretion disc free. *MNRAS*, 448:1137.

Mennickent, R. E., Djurašević, G., Rosales, J. A., Garcés, J., Petrović, J., Schleicher, D. R. G., Jurkovic, M., Soszyński, I., and Fernández-Trincado, J. G. (2025).

Examining the brightness variability, accretion disk, and evolutionary stage of the binary ogle-lmc-ecl-14413. *A&A*, 693:A217.

Mennickent, R. E., Garcés, J., Djurašević, G., Iwanek, P., Schleicher, D., Poleski, R., and Soszyński, I. (2020). Long photometric cycle and disk evolution in the lyrae-type binary ogle-blg-ecl-157529. *A&A*, 641:A91.

Mennickent, R. E., Otero, S., and Kołaczkowski, Z. (2016a). Interacting binaries w serpentids and double periodic variables. *MNRAS*, 455:1728.

Mennickent, R. E., Pietrzyński, G., Diaz, M., and Gieren, W. (2003a). Double-periodic blue variables in the magellanic clouds. *A&A*, 399(3):L47–L50.

Mennickent, R. E., Pietrzyński, G., Diaz, M., and Gieren, W. (2003b). Long photometric cycles in hot algols. *A&A*, 399:L47.

Mennickent, R. E., Schleicher, D. R. G., and San Martin-Perez, R. (2018). Evidence of active regions in the donor of the algol-type binary v393 scorpii and test for the dynamo model of its long cycle. *PASP*, 130:094203.

Mennickent, R. E., Zharikov, S., Cabezas, M., and Djurašević, G. (2016b). Doppler tomography of the double periodic variable hd 170582 at low and high stage. *MNRAS*, 461:1674.

Michalska, G., Mennickent, R. E., Kołaczkowski, Z., and Djurašević, G. (2010). Light curves of galactic eclipsing double periodic variables. In *ASP Conference Series*, volume 435, page 357. Astronomical Society of the Pacific.

Mondrik, N., Long, J., and Marshall, J. (2015). A multiband generalization of the multiharmonic analysis of variance period estimation algorithm and the effect of inter-band observing cadence on period recovery rate. *ApJL*, 811(2):L34.

Nelder, J. A. and Mead, R. (1965). *CompJ*, 7:308.

Nugis, T. and Lamers, H. J. G. L. M. (2000). Mass-loss rates of wolf-rayet stars as a function of stellar parameters. *A&A*, 360:227.

Paczynski, B. (1977). A model of accretion disks in close binaries. *ApJ*, 216:822–826.

Paczyński, B., Szczygieł, D., Pilecki, B., and Pojmański, G. (2006). Eclipsing binaries in the all sky automated survey catalogue. *MNRAS*, 368(3):1311–1318.

Paxton, B., Bildsten, L., Dotter, A., Herwig, F., Lesaffre, P., and Timmes, F. (2011). Modules for experiments in stellar astrophysics (mesa). *ApJS*, 192:3.

Paxton, B., Cantiello, M., Arras, P., Bildsten, L., Brown, E. F., Dotter, A., and Mankovich, C. (2013). Modules for experiments in stellar astrophysics (mesa): Planets, oscillations, rotation, and massive stars. *ApJS*, 208:4.

Paxton, B., Marchant, P., Schwab, J., Bauer, E. B., Bildsten, L., Cantiello, M., and Dessart, L. (2015). Modules for experiments in stellar astrophysics (mesa): Binaries, pulsations, and explosions. *ApJS*, 220:15.

Paxton, B., Schwab, J., Bauer, E. B., Bildsten, L., Blinnikov, S., Duffell, P., and Farmer, R. (2018a). Modules for experiments in stellar astrophysics (mesa): Convective boundaries, element diffusion, and massive star explosions. *ApJS*, 234:34.

Paxton, B., Schwab, J., Bauer, E. B., Bildsten, L., Blinnikov, S., Duffell, P., Farmer, R., Goldberg, J. A., Marchant, P., Sorokina, E., et al. (2018b). Modules for experiments in stellar astrophysics (): Convective boundaries, element diffusion, and massive star explosions. *ApJS*, 234(2):34.

Pigulski, A. (2013). A review of pulsating stars from the asas data. *IAU Proceedings*, 9(S301):31–38.

Plavec, M. J. (1989). Circumstellar matter in algols and serpentids. In *International Astronomical Union Colloquium*, volume 107, pages 95–105. CUP.

Pojmański, G. (2001). The all sky automated survey (asas-3) system–its operation and preliminary data. In *International Astronomical Union Colloquium*, volume 183, pages 53–58. Cambridge University Press.

Pojmański, G. (2002). The all sky automated survey. variable stars in the 0h–6h quarter of the southern hemisphere. *AcA*, 52:397–427.

Pojmański, G. (2003). *The All Sky Automated Survey*, pages 337–347. Springer Netherlands, Dordrecht.

Poleski, R., Soszyński, I., Udalski, A., Szymański, M. K., Kubiak, M., Pietrzyński, G., Wyrzykowski, , and Ulaczyk, K. (2010). The optical gravitational lensing experiment. the ogle-iii catalog of variable stars. x. enigmatic class of double periodic variables in the large magellanic cloud. *AcA*, 60:179.

Prša, A., Conroy, K., Windemuth, D., et al. (2022). The tess input catalog and candidate target list. *ApJS*, 258(2):33.

Reimers, D. (1975). Circumstellar envelopes and mass loss of red giant stars. *MSRSL*, 8:369.

Ricker, G. R. et al. (2015). Transiting exoplanet survey satellite (tess). *JATIS*, 1(1):014003.

Rosales, J., Mennickent, R., Djurašević, G., Araya, I., Curé, M., Schleicher, D., and Petrović, J. (2023a). V4142 sgr: Double periodic variable with an accretor surrounded by the accretion disk's atmosphere. *A&A*, 670:A94.

Rosales, J., Mennickent, R., Schleicher, D., and Senhadji, A. (2019a). Evolutionary process of the interacting binary v495 centauri. *MNRAS*, 483(1):862–872.

Rosales, J. A., Mennickent, R. E., Djurašević, G., Araya, I., Curé, M., Schleicher, D. R. G., and Petrović, J. (2023b). "v4142 sgr: Double periodic variable with an accretor surrounded by the accretion disk's atmosphere" 670 a94 rosales 2023. *A&A*, 670:A94.

Rosales, J. A., Mennickent, R. E., Djurašević, G., Schleicher, D. R. G., Zharikov, S., Araya, I., and Celedón, L. (2021). Stellar and accretion disk parameters of the close binary hd 50526. *AJ*, 162:66.

Rosales, J. A., Mennickent, R. E., Schleicher, D. R. G., and Senhadji, A. A. (2019b). Evolutionary process of the interacting binary v495 centauri. *MNRAS*, 483:862.

Rosales, J. A., Petrović, J., Mennickent, R. E., Schleicher, D. R. G., Djurašević, G., and Leigh, N. W. C. (2024). Double periodic variable v4142 sgr: A key to approaching the stellar dynamo. *A&A*, 689:A154.

Rosales Guzmán, J. A., Mennickent, R. E., Djurašević, G., Araya, I., and Curé, M. (2018). Spectroscopic and photometric study of the eclipsing interacting binary v495 centauri. *MNRAS*, 476:3039.

Schlafly, E. F. and Finkbeiner, D. P. (2011). Measuring reddening with sloan digital sky survey stellar spectra and recalibrating sfd. *ApJ*, 737(2):103.

Schleicher, D. R. G. and Mennickent, R. E. (2017). A dynamo mechanism as the potential origin of the long cycle in double periodic variables. *A&A*, 602:A109.

Schwab, C., Spronck, J. F., Tokovinin, A., Szymkowiak, A., Giguere, M., and Fischer, D. A. (2012). Performance of the chiron high-resolution echelle spectrograph. In *Ground-based and Airborne Instrumentation for Astronomy IV*, volume 8446, pages 77–92. SPIE.

Skrutskie, M., Cutri, R., Stiening, R., Weinberg, M., Schneider, S., Carpenter, J., Beichman, C., Capps, R., Chester, T., Elias, J., et al. (2006). The two micron all sky survey (2mass). *AJ*, 131(2):1163.

Soberman, G. E., Phinney, E. S., and van den Heuvel, E. P. J. (1997). Stability of binary systems undergoing mass transfer. *A&A*, 327:620.

Soker, N. (2000). A solar-like cycle in asymptotic giant branch stars. *ApJ*, 540:436.

Soon, W. H., Baliunas, S. L., and Zhang, Q. (1993). An interpretation of cycle periods of stellar chromospheric activity. *ApJL*, 414:L33.

Spruit, H. C. (2002). Stellar dynamos by magnetic instabilities in differential rotation. *A&A*, 381:923.

Tauris, T. M. and van den Heuvel, E. P. J. (2023). *Physics of Binary Star Evolution: From Stars to X-ray Binaries and Gravitational Wave Sources*. Princeton University Press, Princeton.

Ulaş, B. and Ulusoy, C. (2015). First light curve analyses of binary systems ao aqr, cw aqr and asas 012206-4924.7. *NewA*, 41:1–4.

Vanbeveren, D. (2013). *The Influence of Binaries on Stellar Population Studies*, volume 264. Springer.

VanderPlas, J. T. and Ivezić, Ž. (2015). Periodograms for multiband astronomical time series. *ApJ*, 812:18.

Vink, J. S., de Koter, A., and Lamers, H. J. G. L. M. (2001). Mass-loss predictions for o and b stars as a function of metallicity. *A&A*, 369:574.

Warner, B. (2003). *Cataclysmic Variable Stars*. Cambridge University Press.

Wright, E. L., Eisenhardt, P. R., Mainzer, A. K., Ressler, M. E., Cutri, R. M., Jarrett, T., Kirkpatrick, J. D., Padgett, D., McMillan, R. S., Skrutskie, M., et al. (2010). The wide-field infrared survey explorer (wise): mission description and initial on-orbit performance. *AJ*, 140(6):1868.